

**Self-organized cyclic patterns in muscles
and microscopic swimming**
STEFAN GÜNTHER

Self-organized cyclic patterns in muscles and microscopic swimming

Dissertation

zur Erlangung des Grades des Doktors der Naturwissenschaften
der Naturwissenschaftlich-Technischen Fakultät II
– Physik und Mechatronik –
der Universität des Saarlandes

vorgelegt von

STEFAN GÜNTHER

Saarbrücken, 2009

Tag des Kolloquiums

19. November 2009

Dekan der Fakultät Physik und Mechatronik

UNIV.-PROF. DR. RER. NAT. CHRISTOPH BECHER

Mitglieder des Prüfungsausschusses

UNIV.-PROF. DR. RER. NAT. ALBRECHT OTT (Vorsitzender)

UNIV.-PROF. DR. PHIL. NAT. DR. RER. NAT. KARSTEN KRUSE

UNIV.-PROF. DR. RER. NAT. HEIKO RIEGER

PRIV.-DOZ. DR. RER. NAT. PATRICK HUBER

Abstract

Living cells are self-sustained units of organisms. Within cells the complex interplay of a high amount of proteins and other molecules relies on information that is encoded in the DNA. The self-organisation of cellular constituents might play an important role in cellular activity. There is evidence for self-organization in the cytoskeleton of cells where small numbers of interacting proteins create patterns of a higher order. The cytoskeleton of muscles has been shown to exhibit cyclic behaviour and wave patterns in absence of regulatory mechanisms. This thesis provides evidence that the experimental results can be accounted for by the self-organization of cytoskeletal filaments and motor proteins. A microscopic model exposes that the dynamics is excitable. Continuous descriptions of muscles reveal a non-hydrodynamic mode that accounts for wave generation. The phenomenological coefficients can directly be related to microscopic parameters. For this study, the principles that underly spontaneous muscle oscillations are used in a conceptual design of a simple self-driven swimmer at low REYNOLDS number. The swimmer's motion can self-organize into directed movement by dynamically breaking the swimmer's symmetries.

Kurzfassung

Lebende Zellen sind selbständige Untereinheiten von Organismen. Innerhalb von Zellen beruht das komplexe Wechselspiel einer großen Menge verschiedener Proteinarten und anderer Moleküle auf Informationen die in der DNA kodiert sind. Dabei könnte die Selbstorganisation der Bestandteile von Zellen eine wichtige Rolle in der zellulären Aktivität spielen. Es gibt Hinweise auf selbstorganisierte Prozesse im Zytoskelett von Zellen wobei wenige verschiedenartige Proteine miteinander wechselwirken und Ordnungsstrukturen erzeugen. Im Zytoskelett von Muskeln werden oszillatorische Aktivitäten und Wellenmuster beobachtet, ohne regulatorische Mechanismen. Diese Arbeit findet Hinweise, dass die Selbstorganisation von Filamenten und Motorproteinen des Zytoskeletts die experimentellen Ergebnisse erklären kann. Ein mikroskopisches Model zeigt zudem die Anregbarkeit der Dynamik. In Beschreibungen von Muskeln als kontinuierliches Medium kann eine nicht hydrodynamische Mode identifiziert werden, die für die Wellenphänomene von essentieller Bedeutung ist. Dabei können phänomenologische Koeffizienten mikroskopischen Parametern zugeordnet werden. Die Prinzipien, die zu spontanen Muskeloszillationen führen, werden in einer Konzeptstudie eines einfachen Schwimmers bei kleinen REYNOLDS-Zahlen genutzt. Die Bewegung des Schwimmers kann sich von selbst in einen Zustand gerichteter Bewegung organisieren indem sie die Symmetrien des Schwimmers dynamisch bricht.

Preface

This thesis was produced at the Max Planck Institute for the Physics of Complex Systems in Dresden and at the Saarland University in Saarbrücken. My scientific way was accompanied by the Biological Physics groups in Dresden and in Saarbrücken and I am grateful for the possibility I was given to be part of both groups. In particular I want to thank my advisor PROF. DR. DR. KARSTEN KRUSE for scientific and personal accompany during that last years.

I want express my deepest gratitude to J. MÜLLER and F. BÖRRNERT for who they are. My thanks also goes to P. BORN and M. K. AUGUSTIN for carefully reading the manuscripts.

Saarbrücken, 21. Juli 2009

S. G.

Contents

1	Introduction	1
2	What is life?	3
3	Self-organized filament–motor assemblies	7
3.1	The cytoskeleton	7
3.1.1	Filaments	8
3.1.2	Molecular motors	8
3.1.3	Motor descriptions	9
3.1.4	Self-organized cytoskeletal structures <i>in vitro</i>	10
3.2	Muscles	12
3.3	Spontaneous muscle oscillations	16
3.3.1	Cyclic contractions and waves	16
3.3.2	Available models	21
4	Phenomenological description of muscle fibres	23
4.1	Active polar gels	24
4.2	Hydrodynamic theory of muscle fibrils	26
5	Microscopic description	31
5.1	Simple homogeneous chain	32
5.2	Half-sarcomeres	33
5.2.1	Collective motor force	35
5.2.2	Ensemble average	38
5.2.3	Spontaneous oscillations	39
5.2.4	Stochastic simulations	44
5.2.5	Stretch activation	46
5.2.6	Shortening deactivation	47
5.3	Chains of half-sarcomeres	48
5.3.1	Single sarcomere element	48
5.3.2	Short chains	50
5.4	Continuum limit	54

Contents

6	Advanced nonlinear dynamics	57
6.1	Half-sarcomeres reloaded	57
6.1.1	Canard phenomenon	58
6.1.2	Generic canard phenomenon	60
6.1.3	Global bifurcations	66
6.2	Sarcomeres reloaded	69
6.2.1	Mode interactions	71
6.2.2	Pulse-coupled oscillators	72
6.2.3	Gluing-like bifurcations	73
6.2.4	Period doubling and chaotic behaviour	76
6.2.5	Generalized canard phenomenon	77
6.3	Chain of half-sarcomeres	77
7	Self-organized microscopic swimmer	79
7.1	Low REYNOLDS number swimming	80
7.2	Swimming strategies	81
7.3	Hydrodynamic interactions	82
7.4	Geometry of locomotion	84
7.5	Simple swimmer driven by molecular motors	86
8	Conclusions and perspectives	91
A	Parameter	95
A.1	Parameter set I	95
A.2	Parameter set II	96
B	Half-sarcomere element	97
B.1	FOKKER-PLANCK dynamics	97
B.2	Reduced equations of motion	98
B.3	Oscillatory instability	99
B.4	Critical frequency	99
B.5	Stochastic simulations	99
C	Chain of elements	101
C.1	Simple homogeneous chain	101
C.2	Reduced equations of motion	102
C.3	Stationary states of a chain	105
C.4	Continuum limit	105
C.5	Stochastic simulations	106
D	Swimmer displacement	107

List of Figures

3.1	Myosin-II motor proteins	9
3.2	Myosin-II cycle	10
3.3	Pattern formation in a filament–motor assay	11
3.4	Striated muscles	12
3.5	Myofibrils	13
3.6	Sarcomere scheme	14
3.7	Force–extension curve of titin	15
3.8	Spontaneous oscillations of sarcomere length	18
3.9	Muscle relaxation waves I	19
3.10	Muscle relaxation waves II	20
4.1	Linear response of muscles.	28
5.1	Chain of identical subunits	33
5.2	Schematic representation of the half-sarcomere model	34
5.3	Spontaneous oscillations	40
5.4	Phase diagram of half-sarcomere states I	42
5.5	Phase diagram of half-sarcomere states II	43
5.6	Frequency and amplitude behaviour	44
5.7	Stochastic simulations of length oscillations	45
5.8	Distribution of the motor spring tension	45
5.9	Stretch activation	46
5.10	Shortening deactivation	47
5.11	Chain of half-sarcomeres	48
5.12	Cyclic sarcomere contractions	49
5.13	Relaxation waves	50
5.14	Wave nucleation	51
5.15	Emergence of spontaneous waves	53
5.16	Dispersion relation	55
6.1	Canard explosion	59
6.2	Excitability of half-sarcomeres I	60

List of Figures

6.3	Excitability of half-sarcomeres II	61
6.4	Canard explosion in the VAN DER POL oscillator	62
6.5	Canards in phase space	63
6.6	Fixed points emergence and period scaling	66
6.7	Homoclinic bifurcations	67
6.8	Fixed points behaviour	69
6.9	Oscillatory modes of sarcomeres	71
6.10	Generic gluing bifurcation	74
6.11	Gluing bifurcation in sarcomeres	75
6.12	Period scaling for gluing bifurcations	75
6.13	Ghost dynamics	76
6.14	Mixed-mode oscillations	77
7.1	Three-sphere swimmer	81
7.2	Swimming and non advancing orbits	85
7.3	Self-propelled swimmer	87
7.4	Swimming velocity as a function of ζ	88
7.5	Swimming via the gluing of cycles	89
7.6	Stochastic switching of swimming directions	90

Glossary

Acronyms

ADP	Adenosine-5'-diphosphate. Regenerates ATP via endotherm phosphorylation. Thereby chemical energy is absorbed.
ATP	Adenosine-5'-triphosphate. Carrier of chemical energy. ATP hydrolyses into ADP via an exotherm dephosphorylation, which releases free energy.
DNA	Desoxyribonucleic acid. Carrier of information that allows cellular units to harbour life.
pH	Measure for the acidity or basicity of a chemical solution. It is defined as the negative logarithm of the effective concentration of dissolved hydrogen ions H^+ in a solution.
P_i	Phosphate group of the $ATP \rightleftharpoons ADP + P_i$ reaction.
RNA	Ribonucleic acid. Transfer molecule for information that is encoded through DNA.
SPOC	<i>Spontaneous oscillatory contraction of sarcomeres.</i>

Names

actin	Actin is an abundant protein in eucaryotic cells, which forms polar polymeric filaments. Actin's polymeric form is called F-actin.
auxotonic	Myofibrils are subject to an external load that increases with decreasing myofibril length.
cilia	Hairlike extensions of eucaryotic cells. A cilium contains a bundle of microtubules.
contraction	Process of force generation in muscles. Shortening and lengthening depends on the external mechanical conditions on the muscle.

Glossary

cytoskeleton	Network of protein filaments that are transiently cross-linked by proteins. Eucaryotic cells owe this network shape, stability and cell movements.
desmin	Highly elastic protein in the Z-disc of sarcomeres.
dynein	Family of motor proteins, which advance along microtubules using ATP hydrolysis.
eucaryote	Organism whose cells have a distinct nucleus.
flagella	Protrusions of cells used for swimming in fluids.
<i>in vitro</i>	Processes are taking place outside of an intact cell or organism in an isolated environment.
<i>in vivo</i>	Processes are taking place inside of an intact cell or organism.
isometric	The total length of myofibrils is maintained constant.
isotonic	Myofibrils bear a constant external load.
kinesin	Family of motor proteins, which use microtubules for advancement and force-exertion.
M-line	Disc of proteins that connects myosin filaments in their bare zone within sarcomeres.
micro-organisms	Organisms that are very small. First observed by A. VAN LEEUWENHOEK in 1675.
Min	Min proteins presumably self-organize into patterns in Escherichia coli bacteria.
myofibrils	Chains of sarcomeres in series. Bundles of myofibrils form muscle fibres.
myosin	Family of motor proteins advancing on actin-filaments (usually) towards the plus-end.
non-processive	Molecular motors detach after each power-stroke from the binding filament.
power-stroke	Step of a molecular motor. Sometimes only related to the mechanical work performing substep.

procaryote	Organism whose cells have no distinct nucleus.
processive	Molecular motors perform several steps on their binding filament before detachment.
reciprocal	Cyclic motion that consists of a forward and a backward stroke, whereas the backward stroke is identical to the forward stroke but time reversed and possibly faster or slower.
relaxing solution	In relaxing solution muscles' elasticities are at rest and myosin motors are not bound to actin.
rigor solution	In rigor solution muscles are stiff like in rigor mortis. The solution is ATP depleted, hence myosin motors remain bound to actin.
sarcomeres	Elementary structural units in striated muscles that can contract.
sarcoplasmic reticulum	Special type of an endoplasmic reticulum, which contains high levels of Ca^{2+} . During muscle contraction Ca^{2+} is released and during relaxation Ca^{2+} is absorbed.
sliding-filament	The sliding-filament theory of muscle contraction: Filaments composed of different proteins slide along each other while exerting contractile forces.
titin	Muscle constitutive giant protein, which elastically connects the Z-discs.
Z-disc	Disc of proteins that anchors the plus ends of actin filaments within sarcomeres.

Parameters

a	Microscopic length scale of the order of the step size of molecular motors.
d	Distance between adjacent motors on a motor filament.
$\Delta\mu$	Difference in chemical potential of the $\text{ATP} \rightleftharpoons \text{ADP} + \text{P}_i$ reaction. $\Delta\mu = \mu_{\text{ATP}} - \mu_{\text{ADP}} - \mu_{\text{P}_i}$.
E	Elastic modulus of muscles.
η	Viscosity of the swimmer's surrounding fluid.

Glossary

η_e	Friction coefficient of the gel's surrounding fluid.
f_0	Force exerted by a single unloaded motor.
\tilde{f}_{ext}	Dimensionless parameter with $\tilde{f}_{\text{ext}} = \omega_b f_{\text{ext}} / (k v_0)$.
γ	Dimensionless parameter with $\gamma = f_0 \omega_b / (K v_0)$.
K	Elasticity constant of motors.
k	Elasticity constant of half-sarcomeric elements.
κ	Dimensionless parameter with $\kappa = dk / f_0$.
$k_B T$	BOLTZMANN factor. At room temperature $k_B T \approx 4$ pN nm with temperature $T = 290$ K and the BOLTZMANN constant, $k_B = 1.38 \cdot 10^{-23}$ J K ⁻¹ .
L	Dimensionless parameter with $L = \omega_b (\ell_m + \ell_p - \ell_0) / v_0$.
ℓ_0	Resting length of passive half-sarcomere elements.
L_0	Dimensionless parameter with $L_0 = \omega_b \ell_0 / v_0$.
ℓ_p	Length of actin filaments.
$L_{r\mu}$	ATP hydrolysis rate for a given $\Delta\mu$.
ℓ_m	Half of the length of bipolar myosin filaments.
M	Number of non-processive motors that form an effective motor.
ω_{off}^0	Unbinding rate of single force free motors.
ω_{on}	Binding rate of single motors.
$L_{\sigma v}$	Friction coefficient accounting for a gel's dissipative stress.
$L_{\sigma\mu}$	Measure of the contribution of active elements to a gel's stress.
R	Radius of the swimmer's spheres.
R_l	Dimensionless parameter with $R_l = R / \ell_0$.
v_0	Velocity of unloaded motors.
ζ	Effective friction coefficient in half-sarcomere elements.
ζ	Dimensionless parameter with $\zeta = \zeta \omega_b / k$.

Symbols

Ca^{2+}	Ionized calcium is of major importance for signalling transduction in cellular life. Cells use the ability of Ca^{2+} to induce changes in protein conformations. For review, see [6].
i	Imaginary unit.
\Im	Imaginary part of a complex number.
\Re	Real part of a complex number.
*	Quantities carrying a star are in steady state and not evolving in time anymore.

Variables

H	Oseen tensor.
J	Jacobian.
\mathcal{M}	Mobility tensor.
Q	Fraction of bound motors.
r	ATP hydrolysis rate per unit volume and time.
ρ	Density of a gel.
σ	Inner stress of a gel.
v	Local velocity of the gel's constituents.
x	Length of half-sarcomeres.
y	Motor spring elongation.

Glossary

Chapter 1 Introduction

At the beginning of human progress stands the satisfaction of curiosity. Life has been a subject of human curiosity at all times. Is life only a logical consequence of physical laws? Does life follow general principles? Principles that are as yet undiscovered? There is at least one principle that nourishes the hope of becoming a general principle of life: Self-organization—through the interaction of a small number of distinct proteins new dynamical patterns form spontaneously. This concept is well known from the physics of non-living matter. There is evidence that self-organization plays an important role in living matter. In particular the cytoskeleton of cells is believed to incorporate such principles. The cytoskeleton is a network of protein filaments that are transiently cross-linked by proteins and is responsible for the cellular shape, shape changes and cell movements. Cytoskeletal structures like cilia and flagella allow cellular organisms to swim autonomously. In muscles the cytoskeleton generates the force through the collective interaction of filaments and motor proteins. Muscles are activated by external signals that result in an influx of calcium into the contractile apparatus.

Muscle cells have been found to exhibit cyclic activity that is not triggered by external signals and that is independent of calcium. Skinned cells show regular sustained oscillations in length in environments that contain no calcium but provide energy for the action of the muscles' motor proteins. Under these conditions regular wave patterns are observed. Waves appear at random, travel some distance and disappear.

The study at hand explores the dynamic phenomena in muscles with distinct approaches. Can spontaneously broken symmetries through self-organized processes of a small number of proteins with distinct properties account for the observed oscillatory and the wave behaviour?

Dynamically broken symmetries in the cytoskeleton presumably lead to the swimming strokes of the cilia and flagella of micro-organisms. In a conceptual design study a simple microscopic swimmer is presented. The swimmer is self-sustained and has structural similarities to muscle components. Its composition

Chapter 1 Introduction

is much simpler than the composition of cilia and flagella, yet the swimmer can self-organize into directed motion.

This theses begins with an introduction into the concept of self-organization in nature in chapter 2. The strong evidence for self-organization principles in the case of the cellular cytoskeleton is worked out in chapter 3. In particular the experimental evidence for spontaneous muscle oscillations and wave phenomena is introduced. In chapter 4 muscle fibres are described through symmetry considerations and conservation laws as active gels. The basic dynamics of a microscopic model of muscle fibres in comparison with the experimental results are analysed in chapter 5. In chapter 6 predictions for all the possible dynamics of the microscopic model are made. Chapter 7 introduces a conceptual design of a self-propelled microscopic swimmer.

Chapter 2 What is life?

Natural sciences are a marvellous foundation for the satisfaction of curiosity of the human mind. Life has attracted human curiosity for a long time in history. Observations about nature are already a matter in the oldest document of the occidental culture, in HOMER's epic in which a difference between living and non-living matter is recognized. However, it was ARISTOTELES who made living matter to a subject of *scientific* discourse. He is regarded as the father of the science of biology [1]. Not until 1855 the concept of spontaneous generation of life from non-living matter is rejected by R. VIRCHOW in the work *omnis cellula e cellula*. VIRCHOW makes a fundamental point about living matter in his work: Life is confined to cells and cells only originate from other cells like it. Cells are units that are irritable and have a metabolism.

This attempt to define life points to an important issue: Cells cannot have existed for all times. Cells must have developed at sometime in history from simple constituents. Life is a changing process. Any definition of life changes over time. A distinction of living and non-living matter nowadays does not necessarily account for life forms that had existed a long time ago. The time dependence is only one part of the problem of finding a clear definition what life is: The differentiation of living from non-living matter blurs. Physiochemical processes that are important for life are likewise found in non-living systems. In order to bypass these problems I will not give a definition of life but rather a set of properties of living matter. The properties are nonexclusive, i.e. a system that lacks a property cannot be denied containing life.

These days life is confined to cells, which form a thermodynamically open system. Cells are self-sustained and self-organized units. They process information from the extracellular world and have a metabolism. Single cells and multicellular organisms reproduce and adapt themselves according to the DARWINIAN theory of evolution.

From a physical perspective, life self-organizes into patterns that obey a certain function in the living system [2]. The formation of patterns corresponds to a higher orderliness in comparison to disordered systems. For the formation

of patterns the orderliness of living systems has to increase at the expense of a decreased orderliness of the environment [3]. In systems that are subject to a flux of matter and energy and that have the ability to reproduce with a low error rate M . EIGEN showed that the imbalance of orderliness and disorder becomes maximal [4]. In this case dissipative structures can form [5].

In essence, life self-organizes into complex patterns. Natur's principle of self-organization will be subject in the following part.

Self-organization in nature

Self-organization is usually defined as the emergence of stable dynamical patterns out of the collective behaviour of *agents*. Interactions of the agents lead to structures of higher orderliness without externally provided information or control. The behaviour and the properties of the agents does not straightforwardly imply the emerging patterns. Self-assembly occurs in thermal equilibrium without dissipation of energy, while self-organization dissipates energy. In self-sustained open systems such as living organisms presumably a complex interaction of self-assembly and self-organization processes create dynamic patterns. Many agents such as proteins, nucleic acids and lipids interact and form dynamical structures, which single molecule interactions cannot account for. For review see [2, and references therein].

For example, the formation of crystals and lipid bilayers are typical self-assembled processes at thermal equilibrium. In open systems dissipative structures emerge by the usage of energy that flows through the system. Liquids in temperature gradients give rise for RAYLEIGH-BÉNARD rolls [7, 8]. Beyond a critical temperature, collective cyclic motion of particles emerges. In a mixture of four chemicals, BELOUSOV discovered in 1900 spontaneous spiral wave patterns. Chemical kinetics and diffusion behave nonlinear and drive the BELOUSOV-ZHABOTINSKY reaction [9, 10]. The dynamic patterns are sustained only in open systems [11] with a continuous flux of matter and energy through the system. TURING suggested in 1952 the same spatial-temporal pattern forming principles for the morphogenesis of organisms [12]. On the highly complex level of cells and organisms the genotype cannot directly be mapped to one phenotype and vice versa. The interaction of agents derived from the genom with agents delivering environmental signals can self-organize into distinct higher level structures, i.e. distinct phenotypes.

In order to identify principles of self-organization in biology it is convenient to concentrate on small subsystems, which are composed of a tiny number of agent types. An entire cell's interactions of agents are far too complex for a direct analysis. Consider for example the Min system of bacteria, which presumably plays a role in determining the middle of E.Coli cells. At least *in vitro* it was shown that three Min protein types are capable of self-organizing into dynamical structures [13]. Within the bacterium the same organizing principles can initiate cell division at the right location [14]. The cytoskeleton of cells provides another subsystem. There is evidence that ensembles of filamentous structures and motor proteins exhibit self-organized behaviour *in vitro* and *in vivo*. Such structures will be discussed in the following chapter.

Chapter 3 Self-organized filament–motor assemblies

Cellular organization is reminiscent of small chemical plants. Understanding their organization principles is a major challenge. In order to support the foundations of the assumption of self-organizing principles underlying cellular orderliness this chapter concentrates on the cytoskeleton of cells. Components of the cytoskeleton will be introduced and experimental evidence for cytoskeletal self-organization will be provided. In particular I will concentrate on spontaneous cyclic activity of muscle cells.

3.1 The cytoskeleton

Prokaryotic as well as eukaryotic cells have a cytoskeleton. The cytoskeleton is a highly preserved concept of cellular life [15, 16]. Nature established a scaffold within cells. Intracellular transport and structures rely on this skeleton. Cells owe the cytoskeleton shape and the ability for shape changes, including cell division and motion of cells. Any cell motion is mediated by the cytoskeleton. Interaction of cells with the extracellular world is unthinkable without a cytoskeleton. Very likely it also participates in signaling. Flexibility in compliance of entirely different duties demands for a high degree of complexity. A network of filamentous protein structures remodels ceaselessly through other proteins, which bind to filaments. The filaments can dynamically assemble and disassemble.

Numerous filament binding proteins have plenty of different properties and therefore enable the cytoskeleton to form complex dynamical structures. Motor proteins are a special class of these proteins and are able to convert chemical energy into mechanical work along filaments. Distinct kinds of eukaryotic filaments and some of the motor proteins will be introduced in the following section.

3.1.1 Filaments

Eucaryotic cells are composed of four major types of filaments. *Microtubules* are hollow cylinders with a high bending rigidity. Microtubules are responsible for rigid plant cell walls, participate in mitotic cell division and cell movements: Cilia and flagella are composed of microtubules. Furthermore, motors transporting cell organelles often use microtubules as tracks. *Intermediate* filaments are composed of two antiparallel helical strands with an overall smaller bending rigidity in comparison to microtubules. Intermediate filaments can bear tension and participate in cell shape maintenance. *Actin* filaments consist of a double helix and have a low bending rigidity, for review see [17]. These filaments resist tension and can also maintain shape. Most prominently, actin filaments are jointly responsible for muscular force generation. The fourth filament type is DNA. As a carrier of information DNA enables cells to synthesize cell constitutive components. Motor proteins move along DNA and translate the information into compounds of specific molecules.

3.1.2 Molecular motors

Motor proteins convert chemical energy into mechanical work. Proton gradients induce rotations in *ATP-synthases*. Cytoskeletal motors bind to polar filaments and hydrolyse energy carrier such as ATP to gain chemical energy. Motors use the power to propel themselves along filaments through large scale conformational changes. Distinct types of motors use different types of filaments for binding and walk in varying directions with respect to the filaments' polarities. RNA-polymerases serve as an example of the many motors that bind to DNA. They are an executive part of the central dogma¹ in biology. Polymerases bind to and move along DNA, thereby initiating the transcription process. The cytoskeletal motors dynein and kinesin are microtubule associated. Dynein motors inter alia are responsible for the beating of cilia and flagella, while kinesin motors are important for cell division. Both motors are important players for the transport of cargos. Actin associated motors are summarized as myosins. In cell motility and presumably human hearing myosin plays a role. Most prominently, the first discovered molecular motor myosin-II provides the driving force of muscle contraction.

Myosin-II is a plus-end directed motor. A coiled-coil tail is attached to myosin's two heads, see figure 3.1. The motor's cycle is explained in figure 3.2. In a state where the motor is bound to actin, the hydrolysis of ATP changes

¹All known life nowadays relies on DNA, which is transcribed into RNA. The RNA is partially translated into proteins.

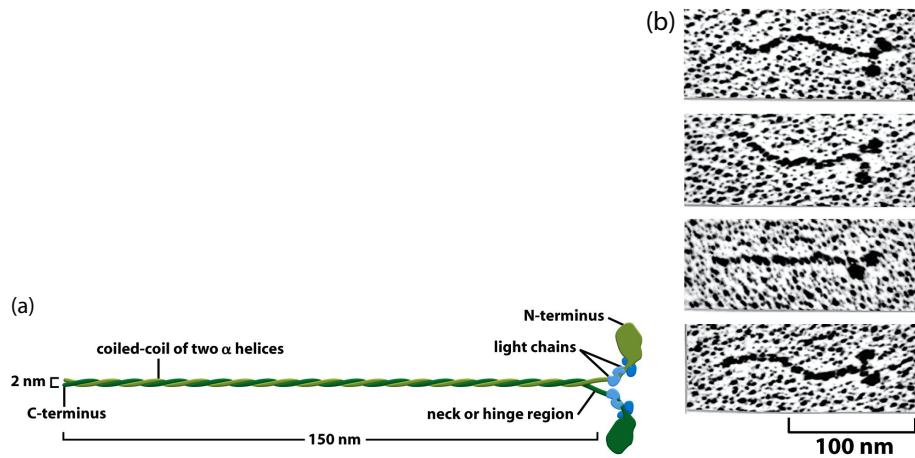


Figure 3.1 Myosin-II motor proteins. (a) Scheme of a myosin motor. The coiled-coil is composed of two light chains that form the tail, which is attached to two globular heads. (b) Electron micrographs of myosin-II motor proteins. Taken from [15].

the motor's conformation. This power-stroke yields to a relative displacement of motor and filament. According to the motor's cycle, the whole myosin-II molecule unbinds from the filament before the next power stroke can proceed. Such behaviour is called non-processive, opposed to processive motors, which perform several steps on a filament before unbinding. Two-headed motors can hand over the task alternately between each head. Processive motors can individually work effective, while non-processive motors usually operate in ensembles. More information on myosin motors can be found in [18].

3.1.3 Motor descriptions

Early attempts to understand how nanometer sized objects can undergo directed motion treat molecular motors as BROWNIAN motors. Such objects rectify their BROWNIAN motion, for review see [21, 22]. According to the motors' different states as depicted in figure 3.2 for myosin-II, motor motion is also regarded as a multiple state process in an aligned lattice. Different states correspond to different conformations of a motor. In a special case where many motors are coupled to an elastic element, it was shown that the motor ensemble is able to experience spontaneous oscillatory displacements relative to the filament [23]. Hopping models for ensembles of motors presuppose motor advancement on filaments. The microscopic origin is out of the scope of these descriptions. It is

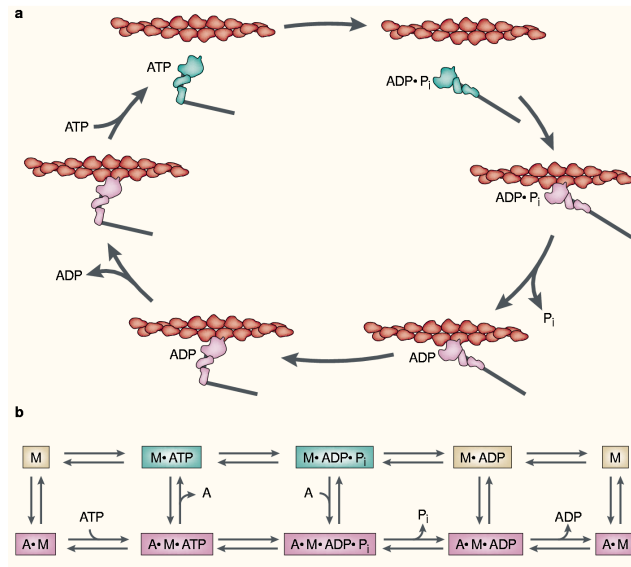


Figure 3.2 Myosin-II cycle. (a) Arrows indicate the likely cycle due to the rate constants of the reactions [19, 20]. Starting upper left, unbound myosin’s conformation changes through ATP hydrolysis. The complex binds to actin and loses the P_i group, which induces a conformational change while being bound to actin. This step is referred to as the power stroke. The conformational change enables removal of ADP. When an ATP molecule arrives at the bound myosin, the motor is able to unbind from actin. (b) Chemical bonds of the cycle in a). Notation: A—actin and M—myosin. Edited from [19].

rather the impact of the motor’s motion that is under consideration [24, 25]. In a further step even more of the microscopic action of molecular motors is released. Since molecular motors operate out of thermal equilibrium, phenomenological descriptions treat motor action only as non-equilibrium processes [26].

3.1.4 Self-organized cytoskeletal structures *in vitro*

Biomimetic assays contain purified proteins in solution. An assay containing bundles of kinesin motor proteins and microtubules has been shown to spontaneously form patterns in the presence of ATP, see figure 3.3. At low motor concentration the distribution of filaments is isotropic. Higher concentrations induce spontaneous formation of vortices. Asters form out of vortices for even higher concentrations. For very high concentrations, filaments bundle.

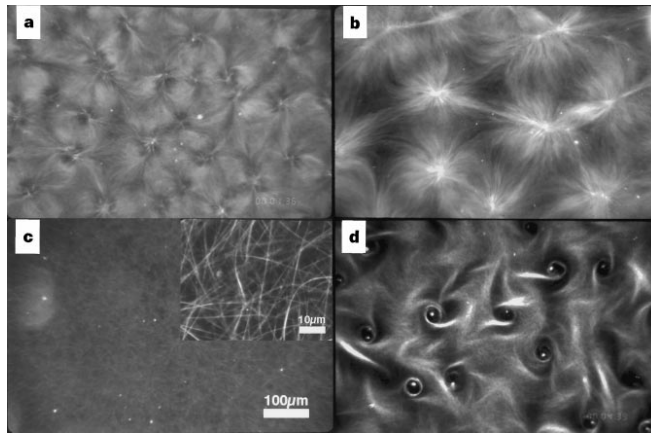


Figure 3.3 Large scale pattern formation in a filament–motor assay for increasing kinesin concentrations. The lowest concentration is in d) and increases from a) over b) to c). (a) Asters and vortices. (b) Irregular lattice of asters. (c) Filaments bundle. (d) Lattice of vortices. Taken from [27].

In the skin of fish keratocyte cells are important for wound healing. Fragments of keratocytes presumably self-organize into crawling motion [28]. Actin filaments in the front and myosin aggregations in the back can account for crawling. Waves of actin can lead to cell migration in *Dictyostelium discoideum* [29] and Neutrophils [30]. Actin interacts with the cells' plasma membranes. The actin front can become unstable and forms spirals. On theoretical grounds about cytoskeletal pattern formation, see [31].

Living cells are self-organized objects. Subsets of cell constituents presumably self-organize into dynamical patterns with distinct associated functions. It is likely that distinct subsets and patterns interact with each other yielding complex dynamical structures. In systems biology a similar situation is under consideration: Subsets of complex networks, network motifs, have distinct functions and the motifs possibly interact and form highly complex networks [32]. Despite the strong evidence for self-organized subsystems, there is no scientific satisfying proof of this sort of organization in cells. More experiments have to be carried out to answer this challenging question. Here I provide evidence for another class of pattern formation in a self-organized filament–motor system: Spontaneous muscle activity. The following sections first introduce muscles and then summarize the experimental evidence.

3.2 Muscle — *Machina carnis*

Many life-forms actively move. For thousands of years animal motion was virtually tied to muscles. For thousands of years humans have been exploring [33] the *machina carnis*². Nature's concept of a specialized force generating tissue is highly conserved among the animal kingdom. Practically every macroscopic motion of animals and humans is based upon muscle contraction. This section is dedicated to introduce muscle tissue. For review see [34].

Muscles generate traction based on the interaction of myosin-II and actin. Muscle types can be divided roughly into two classes: Smooth and cross-striated muscles. Smooth muscles are responsible for involuntary motion during digestion and blood flow regulation. Within this work smooth muscles will be of no concern any further. Striated muscles sub-divide into cardiac and skeletal muscles. Both form more or less distinct fibres with a typical striated structure, see figure 3.4.

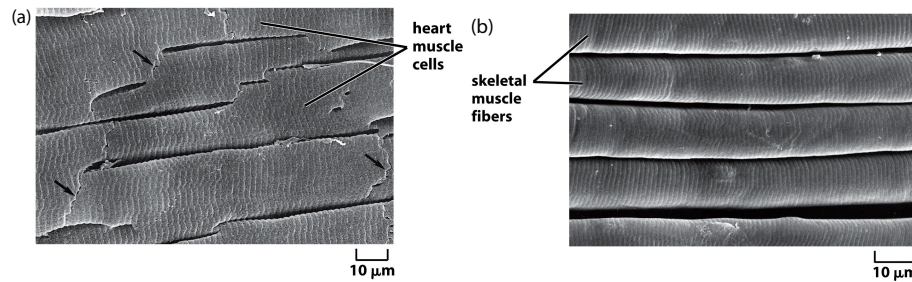


Figure 3.4 Striated muscles. Electron micrographs adapted from [15], originally a courtesy of R. CRAIG. (a) Heart muscle cells. Arrows indicate typical misalignments. (b) Skeletal muscle fibres are very regular.

Muscle fibres consist of bundles of myofibrils. Myofibrils are composed of a regular almost crystalline arrangement of interdigitating actin and myosin filaments. A cross section of insect fibrils in figure 3.5a reveals a hexagonal arrangement of thin (actin) and thick (myosin) filaments. Both types of filaments are aligned in parallel, see side view in figure 3.5b. Two dark discs composed of many distinct proteins, the Z-discs, confine sarcomeres and account for the cross-striation of these muscle types. Sarcomeres are the elementary structural and force generating units of muscles. Within sarcomeres another protein disc, the M-line, connects the thick filaments.

²*Machina carnis* (latin): Carnal machine.

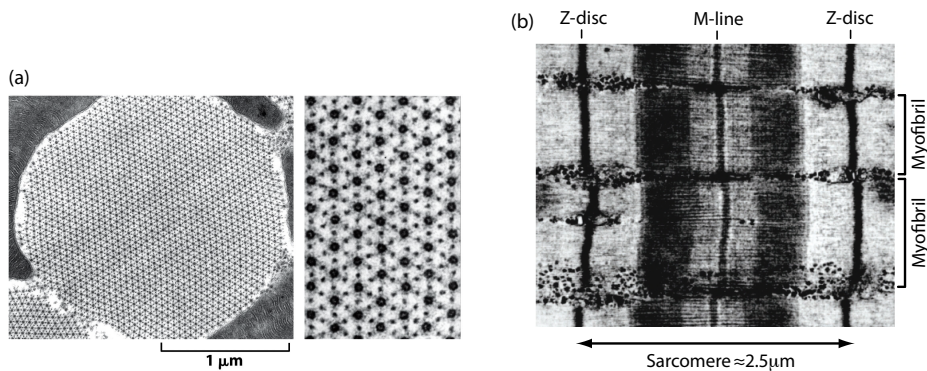


Figure 3.5 Myofibrillar composition. (a) Cross section of an insect myofibril. Thin (actin) and thick (myosin) filaments are arranged in a hexagonal lattice. Adapted from [15, 35]. (b) Side view of a muscle fibre, which is composed of several myofibrils. Z-discs correspond to the striation in figure 3.4 and confine a sarcomere. Bright regions are composed of thin (actin) filaments, dark regions are composed of thick (myosin) filaments and in very dark regions both filament types overlap. The M-line connects the centres of mass of the thick filaments. Micrograph adapted from [36], originally a courtesy of R. CRAIG.

A side view on a striated muscle myofibril is schematically depicted in figure 3.6. Actin filaments' plus ends are joint to the Z-discs. Myosin motors form bipolar filaments with the motors on both ends heading outwards. The motor filaments are linked together by the M-line in their bare, i.e. motor free, middle zone. Z-discs are connected via the giant protein titin, which goes through the myosin filament. During muscle contraction motors bind to actin filaments advancing towards actins' plus ends. Sarcomeres are shortened since both filament types are relatively stiff. Filaments slide along each other giving rise to the sliding-filament mechanism [37–40] of muscle contraction. Shortening is restricted by the filaments' lengths, since the protein discs are impenetrable.

What is titin's role in muscle contraction? The titin proteins assure the structural integrity of sarcomeres upon external forces. These can overstretch sarcomeres so that actin and myosin filaments lose overlap, leaving the sarcomeres disabled. Titin provides elastic restoring forces against stretch, see figure 3.7, which increase nonlinearly with the amount of stretch. Other proteins contribute to the sarcomere's elasticity: Myosin motors that are bound to actin and waiting for an ATP molecule in order to detach from the filament are strongly bound and the myosin's elastic tail contributes. A major source of the Z-disc's elasticity is provided by the protein desmin. Although actin filaments are regarded as stiff

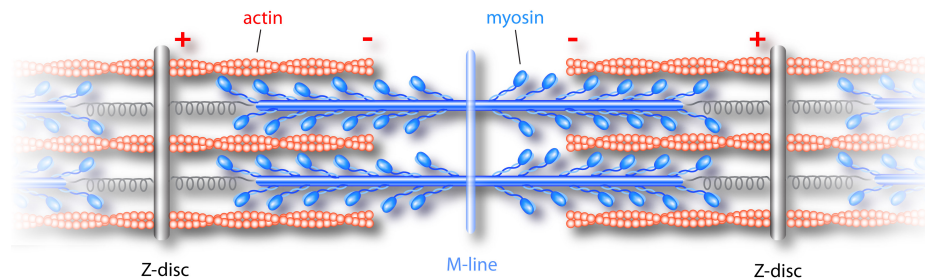


Figure 3.6 Sarcomere scheme. Actin filaments' (red) plus ends are connected to the Z-discs. Myosin motors form bipolar filaments (blue), which are connected by the M-line. Titin (gray) belts the structure connecting both Z-discs.

in this context, the bonding to the Z-disc provides a source of elasticity for the sarcomeres. Bending of actin during contraction is also elastic. All these elastic components contribute to muscle's well known elasticity [41].

Striated muscles' structure is highly preserved among vertebrates and invertebrates. Empirically, such generic structures show up in different implementations. The average sarcomere length varies roughly from 2...3 μm . Resting lengths vary. Insect flight muscles, for example, have a huge overlap area of actin and myosin filaments in the inactive state. Strengths of elasticities as well as contraction speeds also vary. Nature preserves the structure but it takes the liberty to adopt muscle properties to specific situations.

How is muscle action regulated under physiological conditions? At least one way of regulation is well established [42, 43]: Relaxation and contraction is triggered by free Ca^{2+} . Either through an electrical stimulus of the muscle's enclosing sarcoplasmic reticulum or by mechanical stretch, muscle fibres are flooded with Ca^{2+} . Incoming Ca^{2+} binds to troponin proteins that are attached to actin. A conformational change in troponin affects tropomyosin proteins, which wrap actin filaments and block the myosin binding sites. Subsequently, tropomyosin proteins free the myosin binding sites. Myosin motors can bind to actin and the muscle starts to contract. Besides Ca^{2+} , ADP , P_i and the pH value can, at least partially, activate muscles.

In 1949 PRINGLE found that neural excitation and activity of insect flight muscles are asynchronous. This response is related to muscles' unexpected response to stretch. Under physiological conditions a stretch can partially activate contraction, which is temporally limited and Ca^{2+} independent. This effect is barely understood. Recent works, however, suggest tension sensing

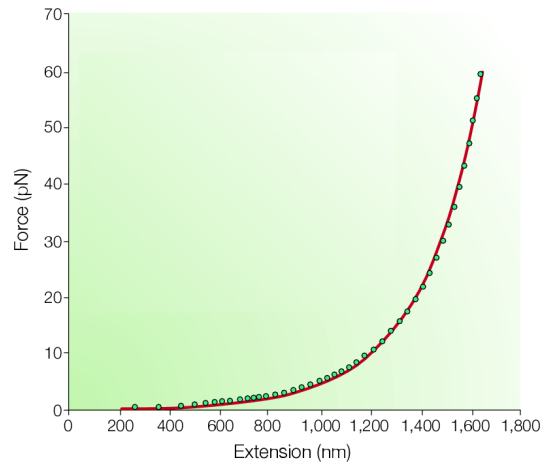


Figure 3.7 The force–extension curve of titin is highly nonlinear according to [36].

capacities of proteins, highlighting titin [44], which allows sarcomeres to actively regulate their contraction. A missing link between mechanical stimulation and chemical signaling is disclosed.

Experiments on muscles are carried out at three standard conditions. Having isolated muscles, fibres and myofibrils yields the question of how to measure forces or how to observe the structures under a microscope. Usually fibrils are winded up on micro-needles and are held under either isometric, isotonic or auxotonic conditions. Isometrically fixed fibrils are kept at a constant length, which is not necessarily the fibril’s resting length. Applying a constant external load to a fibril corresponds to isotonic conditions, increasing its load as a function of the fibril’s length to auxotonic conditions. The latter condition has the functional dependence and the initial load at the fibril’s resting length as degrees of freedom.

Throughout this work the terminology concerning active muscles follows the suggestions of FAULKNER in [45]. *Contraction* will be used exclusively for the process of force generation of muscles. These forces act on external loads. Possibly, contraction is accompanied by length changes of muscles, depending on the boundary conditions. The interaction between the generated force and the external load can either *shorten* or *lengthen* muscles or end up with no length change (*isometric*). Contractile forces are always directed so that muscle shortens when external loads vanish.

Muscles behave surprisingly different under partial activation. In the following section a set of experiments will be presented, showing that striated muscle fibres show spontaneous cyclic motion.

3.3 Spontaneous muscle oscillations

In 2004, the appearance of two ground-breaking works on muscle contraction was celebrated: Half a century before, the sliding-filament mechanism of muscle contraction [46, 47] had been established. Filaments composed of myosin and actin that slide along each other were found to be responsible for muscular force generation. Usually, muscle activity is either deliberately or unconsciously controlled. At microscopic scales such controlled activity is regulated by external stimuli of cells. In any case, muscles are found to contract without external stimuli. In the following section such activity shall be illuminated, highlighting spontaneous oscillatory activity. The section will close with previous attempts to explain this behaviour.

3.3.1 Cyclic contractions and waves

Striated muscle cells show spontaneous activity *in vitro*. Cells contract and relax macroscopically in a regular and repeating fashion [48–55]. The source of energy for the activity is the hydrolysis of ATP. Muscle oscillations continue on time scales that are large compared to the cycle's period. These periodic contractions are a manifestation of intrinsic oscillations of the Ca^{2+} concentration. When the Ca^{2+} concentration suddenly rises towards physiological levels, cells are completely activated and contract. Full activity follows a decreasing Ca^{2+} concentration, which relaxes muscles due to its elastic elements. Intracellular oscillations of Ca^{2+} concentrations are well known, for review see [56]. Stochastic behaviour of channels, which depend on the Ca^{2+} concentration, in combination with Ca^{2+} buffers can lead to calcium oscillations [57]. Channels open at low and close at high concentrations. Cooperative behaviour of channels rapidly increases the concentration. Channels start to close, while the buffer absorbs Ca^{2+} on larger time scales via actively pumping channels. In the experiments mentioned above, the sarcoplasmic reticulum, which acts as a Ca^{2+} reservoir [58] and shows Ca^{2+} dependent release of Ca^{2+} , has not been removed. Thus periodic contractions are attributed to self-organized oscillations of calcium through the sarcoplasmic reticulum and therefore shall not be subject to this work any further.

3.3 Spontaneous muscle oscillations

Mechanically or chemically skinned muscle fibres, which certainly have lost their sarcoplasmic reticulum, still exhibit cyclic contractions. The fibres are disassembled except for the essential structural elements of the contractile apparatus that is illustrated in figure 3.6. Experiments starting in the 1970's on isolated fibres find spontaneous muscle oscillations [59–75] using sub-micromolar concentrations of Ca^{2+} . The amount of Ca^{2+} that is externally added is below physiological levels of full activation. Importantly, during activity the membrane potential and the ionic strength are constant. There is no change of free Ca^{2+} concentration at all during the oscillations. Precisely the same results are obtained under comparable calcium conditions but adding ADP above physiological levels [76–78]. Recently, such oscillations have been observed as well after sudden Ca^{2+} removal [79–82] from myofibrils without other additives. These experiments seem to be closely related to those experiments that use sub-micromolar Ca^{2+} concentrations. Similar results are found under conditions where no Ca^{2+} is present at all. Instead, non-physiological pH-values [83–85] are used. Spontaneous oscillations are found likewise without Ca^{2+} but with ADP and P_i concentrations above known physiological levels [68–71, 74, 86–92]. Remarkably, oscillatory activity exists even in reconstituted myofibrils [91]. Actin filaments in skinned myofibrils are dissolved including actin regulatory proteins. Later on, actin filaments reassemble from actin monomers in bulk solution. These reconstituted myofibrils without actin regulatory proteins show spontaneous oscillations.

Besides the different chemical conditions used, in all experiments the chemical environment is held constant. For the duration of the experiments no change and least of all oscillations of Ca^{2+} or pH can be detected. The ATP, ADP and P_i ratio is held constant by means of a continuous flow of a prepared solution in a flow chamber. It is now generally accepted that all applied chemical environments lead to an intermediate level of muscle activation [68, 74]. Oscillations are also observed in intact myofibrils, which are partially active between the state of contraction (full activation) and relaxation.

A temporal asymmetry between the contraction and relaxation duration is a general feature of the cyclic activity. The sarcomere length oscillates with a typical saw-tooth like shape, see figure 3.8. Slow shortening is followed by a rapid lengthening phase. The distinct time scales of contraction and relaxation share similarities with the behaviour of typical relaxation oscillators. Characteristic oscillation periods are of the order 1...10 s. Amplitudes reach values up to 30% of the resting length under relaxing conditions, which corresponds to amplitudes up to 0.5 μm . Insect flight muscles show significantly lower oscillation amplitudes but much higher frequencies. Oscillations in good experimental setups can be maintained for up to an hour.

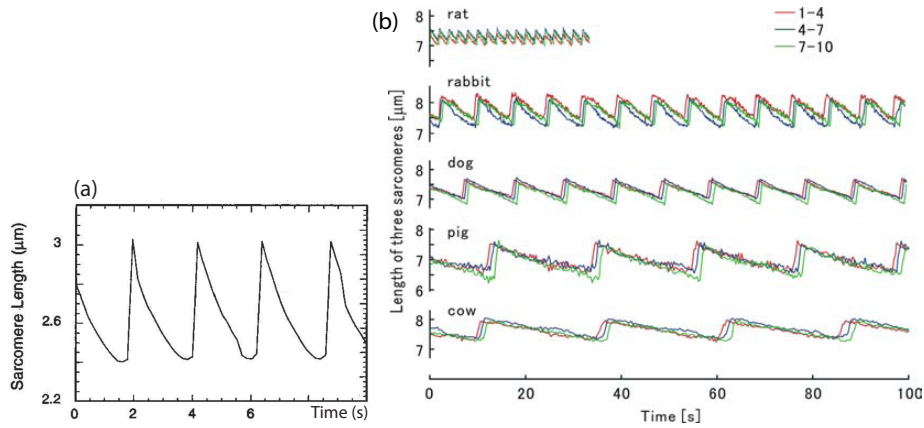


Figure 3.8 (a) Showcase recording of typical spontaneous muscle oscillations. Sarcomere length is plotted versus time. The length is an average from several sarcomeres. Adapted from [90]. (b) Oscillations of heart muscles of different mammals with distinct frequencies and equal amplitudes [72]. Each curve is an average of three adjacent sarcomere lengths. A set of three curves is shown in different colors.

Spontaneous muscle oscillations are a general phenomenon observed in striated muscles. Cardiac and skeletal muscles of mammals are used for experiments as well as skeletal muscles of amphibians and insect flight muscles. All muscle types have in common that they are composed of chains of sarcomeres. Indeed, oscillations are measured by analyzing *in vitro* the dynamics of short myofibrils, while individual sarcomeres are periodically contracting and relaxing. More precisely, half-sarcomeres are the elementary oscillators [82, 86–88]. Although the elementary *structural* units of muscles are sarcomeres, half-sarcomeres are the elementary *functional* units, which show spontaneous oscillations.

Can oscillating half-sarcomeres that are arranged in a chain in series, see figure 3.6, interact or synchronize so that new global phenomena emerge? On the one hand sarcomeres are found to oscillate asynchronously [70, 86] within myofibrils. On the other hand, spontaneous oscillations in synchrony [89, 90] are observed. There is evidence that the different states can be triggered by external chemical conditions and/or externally applied forces. However, the vast majority of works that identified oscillations, also find relaxation waves: Shortening and lengthening phases of adjacent sarcomeres are slightly shifted. The lengthening, i.e. relaxation phase, clearly propagates along myofibrils, see figure 3.9.

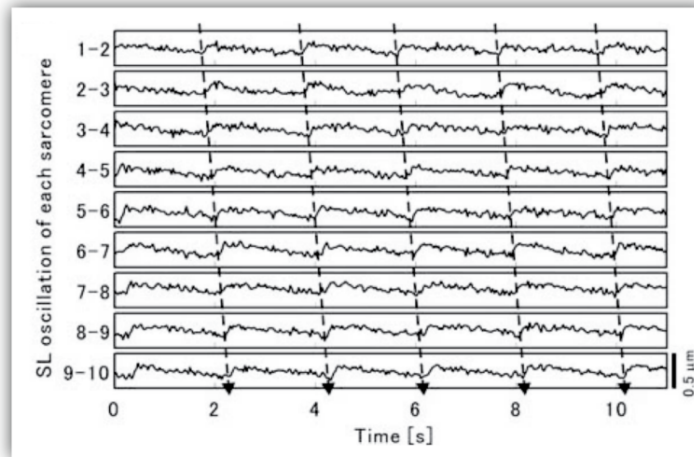


Figure 3.9 Spontaneous relaxation wave in an isolated myofibril. In each box the length of a sarcomere is plotted versus time, while the sarcomeres in series are labelled from 1 to 10. Adjacent sarcomeres oscillate similarly in length but are slightly phase shifted. A wave propagates towards adjacent sarcomeres [72].

In cells where the sarcoplasmic reticulum is still present and active, waves are found [55, 93–95] and are understood by means of propagation of Ca^{2+} oscillations via sarcoplasmic reticula [96]. Calcium waves induce contraction waves. In the experiment shown in figure 3.9 the sarcoplasmic reticulum had been removed and the myofibril spontaneously shows wave patterns.

Spontaneous waves of contraction and relaxation are observed using sub-micromolar concentrations of Ca^{2+} [61, 62, 65, 66] and with sudden removal of Ca^{2+} [79–82]. The most prominent protagonist for spontaneous waves is certainly the ISHIWATA laboratory, which named the spontaneous oscillatory contraction SPOC. They find waves with sub-micromolar Ca^{2+} concentrations [68–75] (Ca-SPOC), as well as under high concentrations of ADP and P_i [68, 69, 71, 74, 86–89, 91, 92] (ADP-SPOC). Waves usually propagate over several adjacent sarcomeres along myofibrils. These waves nucleate spontaneously within fibrils at random, propagate some distance and disappear. Sometimes waves travelling in opposite directions collide and disappear at the collision point. Waves start in nucleation points and propagate in both directions along the fibril. Occasionally, waves emerge at the left or right end of the myofibril and propagate through the whole fibril. Neither the nucleation site nor a waves' propagation direction

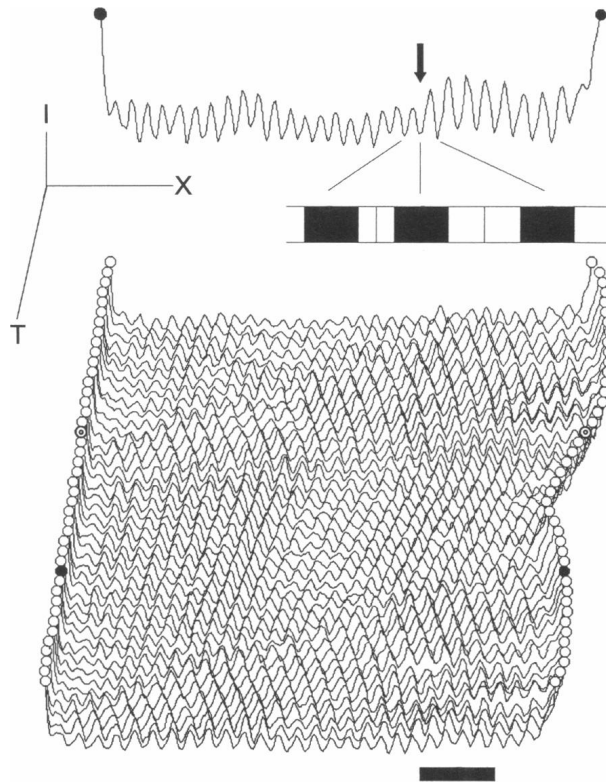


Figure 3.10 Muscle relaxation waves observed in isolated myofibrils. Intensity (I) of a phase contrast microscopy recording versus space (X) and time (T) is shown. Waves emerge at random within the fibril and propagate in different directions. The scale bar is 10 μm . Taken from [88].

is determined or controllable. The emergence of waves seems to be spatially and temporally at random, while a sort of coupling allows for temporary wave trains. A snapshot of such activity can be found in figure 3.10.

Admittedly, these waves are poorly characterized, despite the huge effort gone to in order to observe them. Numbers about wavelengths are rare, statistics about wave trains are not available to the best of my knowledge. Neither a quantification of the location of the emergence of waves has been made. However, wavelengths are of the order of 100 μm , which corresponds to approximately 40 sarcomere lengths [72].

Finally, I will make a remark concerning the mechanical boundary conditions of myofibrils in the experiments that observe oscillatory behaviour. In all experimental setups myofibrils are held between micro-needles. One of the micro-needles is stiff while the other one is chosen according to one of the three standard experimental conditions for muscle fibre research, which were introduced in section 3.2: Either the fibril is held at a constant overall length (isometric) or the fibril bears a constant external load (isotonic) or the external load depends on the fibril length (auxotonic), usually obeying Hooke's law of elasticity. Although details of the results differ under distinct mechanical boundary conditions, the major results of spontaneous oscillations and wave propagation remain unaltered. Interestingly, intact fibrils, which are not held in place by micro-needles, contract only once. When a relaxing solution³ is exchanged by any partially activating solution fibrils shorten towards their minimum length, see [86]. In this case no length oscillations are observed.

In the following section I will give a short sketch on available theoretical attempts that try to identify mechanisms, which account for the experimental results.

3.3.2 Available models for muscle oscillations

Self-organized oscillations in cell biology are quite common [97, 98]. Examples are circadian clocks, which are of genetic origin, or spatiotemporal protein concentration oscillations in bacteria like the Min system. Vertebrate hair cells' cytoskeleton can oscillate and are presumably important for hearing. In general, ensembles of cyclically working molecular force generators, connected to elastic elements, are capable of generating spontaneous oscillations [23]. A stationary state's symmetry is broken spontaneously through a HOPF-bifurcation. Such mechanical oscillations have been proposed to account for wave generation in flagellar and ciliary beats [99–101]. These mechanisms might play a role in mitotic spindle oscillations during asymmetric cell divisions [25].

Based on different implementations of the cross-bridge cycle of muscle myosin, reviewed in [19], various attempts to explain spontaneous muscle oscillations have been made. Three-state models of the myosin cycle account for a lot of muscles physiology, including oscillatory behaviour on the level of isolated half-sarcomeres, see [102, and references therein]. Usually, the results, which rely on the cross-bridge cycle, are very sensitive to the cycle's rate constants, which are not very well known. One study that explicitly implements

³In relaxing solution muscles are relaxed, i.e. motors are unbound. In the opposed rigor solution, muscles are stiff. Motors are bound like in rigor mortis due to ATP depletion.

the myosin cycle in terms of ordinary differential equations finds periodic states [103]. The states neither account for saw-tooth like oscillations nor for wave generation in chains of oscillatory elements.

Theoretical work on the wave phenomena focuses on synchronization effects of chains of coupled HOPF-oscillators [104]. Only a global coupling of oscillatory elements through a mass allows for synchronization effects. Rich phase diagrams of synchronous and asynchronous states are found. Any motivation for a resonant inertial load in the experiments sketched in section 3.3.1 is missing. Flexible micro-needles transmit forces only and are not in resonance with oscillating elements, which has been counterchecked in several experimental setups.

In a further study a spatial gradient of sarcomere tension capacity is necessary for wave phenomena [105]. The gradient accounts for force creep and delayed length activation of adjacent sarcomeres causing synchronization, which ultimately yields coherent contraction waves. The existence of such a gradient is currently not supported by any experiment.

Sarcomeres are able to oscillate spontaneously in length. Cyclic shortening and lengthening of adjacent elements is phase-shifted and yields the impression of propagating waves. This behaviour is independent of species and the type of striated muscle. Wave phenomena are a generic capacity of striated muscles. The chemical environment is held constant at non-physiological as well as physiological conditions. Cyclic patterns rely on active processes driven by the hydrolysis of ATP. In summary, these experiments provide strong evidence for self-organized behaviour, which leads to the emergence of new dynamical structures. To date there is no consistent theory available that accounts for the wave patterns. In order to understand the phenomenon, the following chapters will not cover individual experiments. It will be rather general mechanisms identified, which lead to the observed behaviour. The descriptions will pay less attention to the microscopic differences of distinct striated muscle types, but respect the structural similarities of all striated muscles. In a first attempt, the following chapter provides a phenomenological description, which is based on symmetry considerations and on conservation laws.

Chapter 4 Phenomenological description of muscle fibres

Generic theories, which rely on phenomenological parameters only, are enormously tempting. This class of theories describe empirical observations of natural phenomena. Very often in physics such theories form the starting point of a deeper understanding of their origin. Examples are the RUTHERFORD model before quantum mechanics was thought of or the second law of thermodynamics before BOLTZMANN and others started thinking about statistical mechanics. The theories' catch is that the microscopic origin of the phenomena remains concealed. Occasionally, connections between the microscopic behaviour and the phenomenological manifestation is found as in the GINZBURG-LANDAU theory of superconductivity, which can be derived from the microscopic BCS theory.

Muscles are a complex system of many interacting molecules and proteins. Which of all possible interactions are important for muscle action is not well understood. Whether all major molecular players are already identified is likewise unclear. For muscle oscillations the microscopic details are less important, since this behaviour is generic for striated muscle types. Obviously, a good start to approach muscle oscillations is a phenomenological description, which ignores microscopic causes to a large extent.

Life tries to escape the second law of thermodynamics by active processes. From a thermodynamic perspective, myofibrils in the experimental setups form an *open system* at constant temperature. Exchange of energy for active processes occurs in form of a reservoir of ATP, whereas no further particles are exchanged. Consequently, the search for a phenomenological description implicates an exploration out of thermal equilibrium.

In the following section a generic phenomenological description of active polar gels will be sketched, following [26, 106, 107]. Explicitly for muscle fibrils such a description will be deduced in section 4.2 yielding an equation of motion for striated muscles as a continuous material.

4.1 Generic description of active polar gels

Understanding the cytoskeleton of cells is a major challenge. For much simpler, yet still complicated compositions of locally cross-linked polymers, several advances have been made [108, 109]. Phenomenologically both systems exhibit visco-elastic properties and therefore are denoted as *gels*. The cytoskeleton is a spatially extended system consisting of protein filaments, which are transiently cross-linked by proteins. Proteins can be active, i.e. they are out of thermal equilibrium and *dissipate* energy. Most prominently, motor proteins convert chemical energy into mechanical work. Cytoskeletal filaments are commonly polar and alignment towards similar polarity on large length scales is possible. Thus, gels can be polar and active. Conceivably, such gels exhibit complex and unusual mechanical responses to stress and strain.

On large length scales and long time scales such complex materials can be treated as a continuous medium [26, 110, 111], which is described by generic hydrodynamic theories. These kinds of theories have been successfully applied to complex fluids, crystals, liquid crystals and polymers and it is coherent to expand these ideas to active polar gels. Correspondingly, the generic description is derived following standard procedures.

In isothermal equilibrium systems the free energy F has a minimum. Without external influences, the rate of change of the total entropy S vanishes in this case. Non-equilibrium processes drive the system away from this state, thus $dS/dt \neq 0$. In order to quantify the rate of change of the total entropy it is necessary to define a free energy for non-equilibrium systems. The rate of change of this free energy is often expressed through generalized fluxes j^g and forces f^g . Fluxes are generated by the forces,

$$-T \frac{d}{dt} S \equiv -T \dot{S} = \dot{F}(\varphi_1, \dots, \varphi_n) = \sum_{i=1}^n \frac{\delta F}{\delta \varphi_i} \cdot \dot{\varphi}_i \equiv \sum_{i=1}^n f_i^g \cdot j_i^g \quad , \quad (4.1)$$

with functions φ_i defining the free energy and T as the system's temperature. Purely dissipative fluxes and forces do not change the sign of the product $f^g \cdot j^g$ upon time reversal $t \rightarrow -t$, while reversible processes implicate the opposite sign. Restricting the description of the gel's behavior to the linear response regime, each flux and force can be written as a simple sum of a dissipative and a reactive (reversible) component. Linear responses can be expected close to thermal equilibrium. Along the line of linear response, both types of fluxes are expanded in terms of the forces according to the ONSAGER theory, $j_i^g = \sum_k L_{ik} f_k^g$. The behaviour of the product of fluxes and forces upon time reversal demands that some of the coefficients L_{ik} vanish.

Besides the active response, the passive response of the gel is taken into account. Further use of general conservation laws for each fluid component [112] results in a purely phenomenological description. Finally, the system's response to perturbation of the equilibrium state can be analysed.

How can a free energy in a non-equilibrium system be defined? Non-equilibrium thermodynamics distinguishes between slow and fast variables. The latter are taken to be equilibrated here, but can be incorporated as noise terms [113]. A quasistatic change allows for the assumption of local equilibrium: The system is subdivided into small volume elements. Each element is small compared to the whole system, but large enough to allow for a thermodynamic description. The single small volume elements are supposed to be in thermal equilibrium. A free energy F of the whole out of equilibrium system is given by the sum of the free energies of the elements. Each local equilibrium free energy can be written as a sum of internal energy and local entropy. The rate of change of the system's whole entropy is given by the rate of change of the system's whole free energy F , since the internal energy vanishes. The assumption of local thermal equilibrium is appropriate only in the limit of large length and long time scales. More specifically, in the case of hydrodynamic modes [114] with the wave number q , which relax with a characteristic time $s \propto q^{-2}$, the approximation above is applicable. Conservation laws are associated with hydrodynamic modes. In addition, every transition yielding a broken continuous symmetry is related to the emergence of hydrodynamic modes [115].

Active processes are of special importance in the description. Life's use of ATP as an energy source for active processes is remarkably conserved. The free energy, which is transduced into mechanical work by the hydrolysis of ATP into ADP and P_i , can be interpreted as a chemical driving force, which powers protein activity. Such an *activity* force is characterized via the difference in chemical potential $\Delta\mu = \mu_{\text{ATP}} - \mu_{\text{ADP}} - \mu_{P_i}$. Note that $\Delta\mu$ is only a measure for the gel's activity if none of the reactants are chemically active with other constituents of the gel. Myofibrillar oscillations have been observed being altered by P_i , alongside the energy transduction process, see section 3.3.1.

In its present form, the generic theory of active polar gels [26, 107] takes temperature as a constant parameter. On a cellular level this may apply, but there are exceptions on the level of tissues. Bundles of muscle fibres heat up during contraction. Extensions to non-constant temperatures need to be performed.

The general framework of the generic theory for active polar gels will be used to approach muscle oscillations. Since muscles have certain special properties some adaptations to the framework will be carried out. Myofibrils are chains that are composed of recurring half-sarcomeres with alternating alignment. The

filament orientation is fixed within half-sarcomeres. Consequently, on large length scales myofibrils form a non-polar gel. The objective of the following section is to phenomenologically describe myofibrils as an active gel, which extends effectively in one dimension. The gel is described as a one component¹ complex fluid.

4.2 Hydrodynamic theory of muscle fibrils

First and foremost, a hydrodynamic theory has to identify its hydrodynamic modes. Either conserved quantities or a broken continuous symmetry yield hydrodynamic modes. Muscle fibrils are substantially one-dimensional. Within a fibril the alignment of all filaments is fixed with respect to each other. Unlike dynamically remodeling actin–myosin networks, in muscles there are no rearrangements of filaments during contraction. Filaments only actively slide along each other. Thus, myofibrils do not exhibit any broken continuous symmetry. Three quantities are conserved: Fibril mass, momentum and energy. Denoting a fibril's density of protein discs by ρ and their local velocity with v , the continuity equation yields

$$\partial_t \rho + \partial_z \rho v = 0 \quad , \quad (4.2)$$

while z is the spatial coordinate along the myofibril. The length scale z is large in comparison to the average half-sarcomere length. Momentum conservation with an externally applied force density f_{ext} implies

$$\partial_t \rho v - \partial_z \sigma = f_{\text{ext}} \quad , \quad (4.3)$$

in which σ denotes the inner fibril stress. Since the motion of myofibrils is highly dampened, inertia cannot play a significant role. Consequently, in equation (4.3) the term $\partial_t \rho v$ vanishes so that internal stresses are balanced by external forces. Experiments on myofibrils are carried out in flow chambers. The continuous flow of a prepared solution with known chemical ingredients thermodynamically acts as a heat bath. Consequently, the fibril's temperature T is constant and energy conservation is not an issue.

In order to specify the gel's equation of motion the different contributions to the stress σ have to be identified with the help of a free energy. Non-equilibrium states allow for a non-vanishing rate of change of the gel's total entropy and its free energy. Above all, active processes unbalance thermodynamic systems.

¹Two or more component fluids are definitely conceivable. Here, the gel's surrounding water is incorporated as an external source of friction.

4.2 Hydrodynamic theory of muscle fibrils

Assuming local thermodynamic equilibrium, the rate of change of the free energy can be written as a sum of generalized fluxes, each multiplied with its conjugate generalized force,

$$T\dot{S} = -\dot{F} = \int (\sigma \partial_z v + r \Delta\mu) dz > 0 \quad . \quad (4.4)$$

The stress σ is chosen as one generalized flux, which is conjugate to the force $\partial_z v$, the rate of strain. The second flux, the ATP hydrolysis rate r per unit volume and time, is conjugate to the difference in chemical potentials $\Delta\mu$. Expression (4.4) takes the translational and rotational invariance of the gel into account. According to the muscles' normal regime of operation, fibrils contract due to the relative sliding of actin and motor filaments. Free sliding is restricted by the impenetrability of the half-sarcomeres' delimiting protein discs. By restricting myself to the regime of free sliding, the gel is assumed to be compressible and its pressure vanishes.

In the linear response regime it is possible to split up \dot{F} into a reversible part and an irreversible component. Reversible means that the free energy changes sign upon time reversal $t \rightarrow -t$. Consequently, the fluxes can be decomposed into a reactive and a dissipative part, since equation (4.4) holds. Respectively, $\sigma = \sigma^r + \sigma^d$ and $r = r^r + r^d$, the superscripts r and d denote the reactive and the dissipative component.

In order to proceed further I will expand the respective components of the fluxes in terms of the generalized forces up to linear order. The forces' behaviour under time reversal is $\partial_z v \rightarrow -\partial_z v$ and $\Delta\mu \rightarrow \Delta\mu$. Dissipative components of the fluxes have the same sign as their conjugated forces under time reversal, while reactive components have the opposite sign. That is, the dissipative products of fluxes and forces in expression (4.4) are invariant, while the reactive products have the opposite sign through time reversal, yielding

$$\sigma^r = -L_{\sigma\mu} \cdot \Delta\mu \quad (4.5)$$

$$\sigma^d = L_{\sigma v} \cdot \partial_z v \quad (4.6)$$

$$r^r = -L_{rv} \cdot \partial_z v \quad (4.7)$$

$$r^d = L_{r\mu} \cdot \Delta\mu \quad . \quad (4.8)$$

This expansion introduces phenomenological coefficients whose microscopic origins remain concealed. Active processes through the action of molecular motors contribute to the gel's stress for which $L_{\sigma\mu}$ defines a measure. Internal friction accounting for dissipative stress is elucidated by $L_{\sigma v}$. The ATP-hydrolysis rate for a given difference of the reactants' chemical potential is quantified by $L_{r\mu}$. By symmetry, $L_{rv} = -L_{\sigma\mu}$, according to the ONSAGER relations.

By means of striated muscle's structure the overlap of actin filaments and motor filaments depends on the tissue density. For constant $\Delta\mu$, the active stress increases with increasing density. Consequently, $L_{\sigma\mu}$ is expanded up to linear order in ρ , yielding

$$L_{\sigma\mu} = L_{\sigma\mu}^{(0)} + L_{\sigma\mu}^{(1)} \cdot \rho \quad . \quad (4.9)$$

So far, the contributions of active elements to the stress are specified so that the equations (4.5)–(4.8) provide the constitutive equations for an active myofibrillar gel. The passive response of the gel for $\Delta\mu = 0$ accounts only for dissipative contributions. Muscles contain elastic elements, which maintain the structural integrity of the sarcomeres. Elastic contribution to the overall stress in the active fibril must not be neglected. On long time scales muscles response predominantly elastic. On short time scales motor molecules detach and rebind subsequently. Proteins acting in such a manner give rise for a viscous response [116, 117] of the fibril. This internal friction is taken into account by the expression for σ^d in equation (4.6).

How is the elastic contribution taken into account? Different responses on distinct time scales can be modelled with standard rheological elements. The KELVIN-VOIGT element exhibits an elastic response on long and a predominantly viscous behaviour on short time scales, see figure 4.1. In a KELVIN-VOIGT element a linear spring acts in parallel with a dashpot so that both stress contributions can simply be added. Correspondingly, with an elastic stress σ^e , which is related to the gel's density by an elastic modulus E and the equilibrium density ρ^* , so that $\sigma^e = E\rho/\rho^* - 1$, the reactive stress is finally given by $\sigma^f = -L_{\sigma\mu} \cdot \Delta\mu + \sigma^e$.

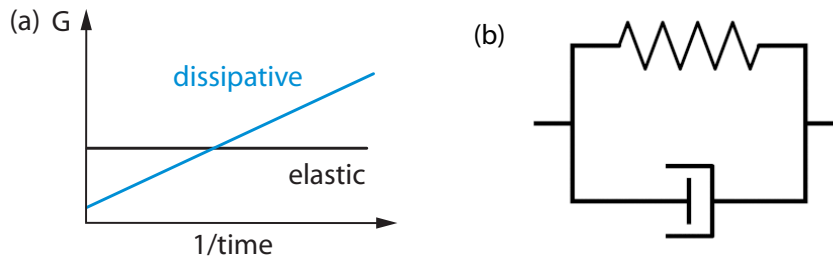


Figure 4.1 Muscle response to external stress. (a) Linear response G of muscle fibrils on different time scales, schematically. On long time scales an elastic (black) response dominates, while on short time scales the system's response is mainly viscous (blue). (b) Kelvin-Voigt element. A linear elastic element and a dashpot act in parallel. The element's linear response complies with the response sketched in a).

All contributions to the overall stress σ are specified. In order to obtain the gel's equation of motion from the momentum conservation in equation (4.3), the fluid that surrounds the gel has to be taken into account. In a one-component description, the surrounding fluid is treated as an external source of friction. Without further external contribution and denoting the friction coefficient with η_e , the fluid friction implies that $\partial_z f_{\text{ext}} = -\eta_e \partial_t \rho / \rho^*$. With the help of the relation $\partial_z v = \partial_t \rho / \rho^*$ the time evolution of deviations from the equilibrium distribution ρ^* finally reads

$$\eta_e \partial_t \rho = \left(E - \rho^* \Delta\mu L_{\sigma\mu}^{(1)} \right) \cdot \partial_z^2 \rho + L_{\sigma v} \cdot \partial_t \partial_z^2 \rho \quad . \quad (4.10)$$

Analysis of the gel's stability with the ansatz $\rho(z,t) = \rho^* \exp(iqz + st)$, which contains the wavenumber q and the complex time scale s , results in the dispersion relation

$$s = -q^2 \frac{E - \rho^* \Delta\mu L_{\sigma\mu}^{(1)}}{\eta_e + q^2 L_{\sigma v}} \quad . \quad (4.11)$$

Any perturbation of the equilibrium state will grow iff $E - \rho^* \Delta\mu L_{\sigma\mu}^{(1)} < 0$, leading to a high density state. For this to happen, stress generated by active processes has to overcome the elastic stress. This holds for large² length scales ($q \rightarrow 0$). Density oscillations, however, are impossible, since s is always real³.

Why does the visco-elastic gel not oscillate? For one thing, there is no reason to assume that the observed muscle oscillations operate in the linear response regime, e.g. close to the thermodynamic equilibrium. The description of the gel given above is an expansion around equilibrium states up to linear order. Muscle oscillations can be far out of the range of validity of this approximations. One might argue for higher order terms in other linear expansions. Any higher order term in the expansion of the density dependence of the activity dependent stress $L_{\sigma\mu}$ in equation (4.9) leads to a nonlinear partial differential equation of motion. This would introduce nonlinearities in an inconsistent way since the whole theory is restricted to the linear response regime.

All hydrodynamic modes have been identified. There are no further conserved quantities. Thus it is reasonable to associate the emergence of spontaneous waves with the existence of essentially non-hydrodynamic modes. However, for the

²Small length scales are out of scope of this continuous description. On such scales the system becomes independent of friction, which is unphysical.

³The continuity equation in expression (4.2) simply determines the velocity v and cannot induce oscillations in overdamped media.

Chapter 4 Phenomenological description of muscle fibres

time being one may only speculate about the nature of the non-hydrodynamic modes. Still, answering this question serves as a motivation for the following chapter. The chapter will devise a microscopic description of muscle myofibrils. Anticipating its success in spontaneous wave generation, it may provide clues to answering the remaining open question in section 5.4.

Chapter 5 Microscopic description

Myofibrils are chains of half-sarcomeres, which are the force generating units. Each unit's contractile forces are generated collectively by ensembles of molecular motors. Collective actions can lead to the emergence of self-organized dynamical structures. The objective of this chapter is to explain spontaneous muscle oscillations and myofibrillar wave phenomena as a consequence of the action of many myosin-II motors. Correspondingly, microscopic details of each motor will be less important. The model will not and cannot account for all of the muscle's features, since the validity is restricted to isolated myofibrils and the corresponding conditions in the experiments.

What about a simple, inertia based description? The vanishing importance of masses and inertia for the muscle oscillations have already been mentioned in chapter 4. The relevance of inertia for motion that occurs within a fluid with a certain *density* and *viscosity* is captured by the REYNOLDS number. Any moving object within a fluid is associated with a certain *speed* and a characteristic *length* (size). The fraction of relative importance of inertia forces and friction forces defines the REYNOLDS number,

$$\text{Re} \equiv \text{length} \cdot \text{speed} \cdot \frac{\text{density}}{\text{viscosity}} . \quad (5.1)$$

At low REYNOLDS number friction forces dominate over inertia forces and vice versa. The amplitudes of sarcomere oscillations reach the order of μm with length changes up to $10 \mu\text{m}/\text{s}$. Assuming an inner myofibrillar fluid density comparable to water and a viscosity that is ten times higher than in water, the REYNOLDS number yields $\text{Re} \sim 10^{-6}$. Advancement is dominated by friction, any motion is highly overdamped. Thus, oscillations are not simply generated by resonant inertia.

This chapter exposes a distinct mechanism for cyclic activity. First and foremost, symmetry based considerations on muscular force generation shall be given. Thereafter, a microscopic model for a half-sarcomere will be introduced. Its

dynamics reveal spontaneous cyclic shortening and lengthening. A chain of half-sarcomeres self-organizes into propagating waves. Finally, a non-hydrodynamic mode will be identified, which allows for waves on macroscopic length scales. No attempt will be made to quantitatively match the model to a specific experiment. Rather general mechanisms shall be identified. Therefore parameter values are chosen according to typical values for partial activation, see appendix A.1.

5.1 Simple homogeneous chain of force generators

Early muscle research provided two break-through insights. Firstly, muscular forces are produced by myofibrils, which are composed repeatedly of contractile subunits in a regular manner. Secondly, these subunits have a length dependent overlap of thin (actin) filaments and thick (myosin) filaments. Current knowledge about the microscopic composition of myofibrils and recent experiments suggest that half-sarcomeres are the elementary contractile units [82, 86–88].

In a first simplistic model, myofibrils shall be represented by one-dimensional chains, which are composed of identical force generating units. Coupling between the elements is rigid, see figure 5.1. Each element i has a certain length x_i . The contractile forces generated within each element shall only depend on the element's length, so that its force can be written as $f(x_i)$. Contractile forces are balanced by friction forces f_f . In the simplest case friction hampers length changes and is expressed as $f_f = -\zeta \dot{x}_i$ with a friction coefficient ζ . Without external forces acting on a chain of n elements, the equations of motion read,

$$\zeta \frac{dx_i}{dt} \equiv \zeta \dot{x}_i = \begin{cases} -2f(x_1) + f(x_2) & \text{for } i = 1 \\ -2f(x_i) + f(x_{i-1}) + f(x_{i+1}) & \text{for } 1 < i < n \\ -2f(x_n) + f(x_{n-1}) & \text{for } i = n \end{cases} \quad (5.2)$$

Inertia forces can be neglected. Consequently, momentum conservation reduces to force balance and there are no second order time derivatives in the length. A linear stability analysis reveals at least one surprising result: Such a chain will never contract homogeneously so that $x_i(t) = x_j(t)$ for all i, j , see appendix C.1. Any small heterogeneous perturbation of the stationary state will grow. Perturbations of an element's stationary length alter this element's contractile force $f(x)$. The force of an adjacent element and therefore the rate of change of the element's length is different due to the length dependence of the contractile forces. Such an initial imbalance of forces grows further.

The same can be expected to happen in relaxed muscles that undergo activation. Activating all elements of a chain of perfectly identical half-sarcomeres at once, contraction between neighbouring elements, at least, will be asymmetric.

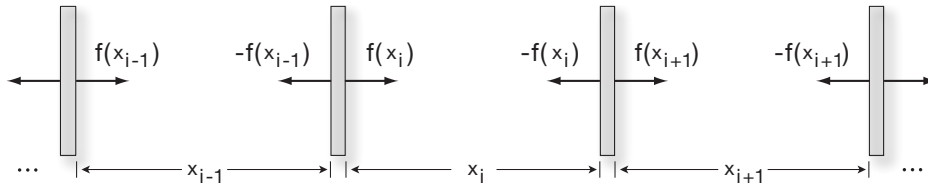


Figure 5.1 Chain of identical subunits. Each subunit i exerts a length dependent force $f(x_i)$ to its neighbour element.

Owing to their structure, muscles are unstable. Furthermore, the simplistic model above with a simple length dependent contractile force cannot oscillate. Length oscillations in muscles may rely on microscopic grounds, which are intrinsic to half-sarcomeres. Consequently, the following section will set up a model for half-sarcomeres, which includes the major microscopic constituents that are responsible for muscle function and force generation.

5.2 Half-sarcomere element

Muscle contraction is a collective process of many molecular motors. Details of a single motor's state are only important to the extent of its contribution to the contraction process. In this spirit, molecular motors will be treated as force generators, neglecting the motors' internal states according to the myosin cycle. Consequently, motors can be in two states, either a motor is bound to an actin filament or it is not.

The model incorporates the two major constituent filament types: A motor filament and a polar filament interdigitate, see figure 5.2. In the overlap region of both filaments contractile forces can be generated, which act against elastic elements. Motors are attached to a backbone with equal spacing d between adjacent motors. Each motor is elastically linked by a spring of stiffness K and extension y . In the region of overlap of the motor backbone and the polar filament, motors stochastically bind to and unbind from the polar filament with rates ω_b and ω_u , respectively. Specific binding sites of the actin filaments are neglected so that the motors can bind everywhere on the polar filament. Bound motors unidirectionally advance with velocity v . Eventually, moving motors pull the motor-backbone along the polar filament and act against a linear elastic element of stiffness k . The latter elasticity accounts for the passive elasticity of muscle tissue. Shares of this generalized elastic term come from the proteins

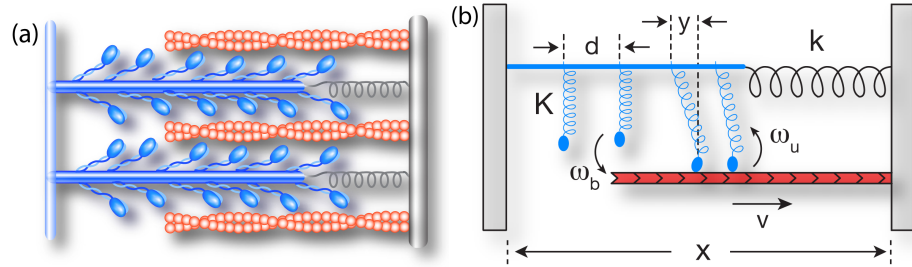


Figure 5.2 (a) Composition of a half-sarcomere. (b) Schematic representation of the half-sarcomere model. A filamentous backbone to which motors are linked to and a polar filament, which motors can interact with, constitute the element. Motors are attached elastically to the backbone with stiffness K and with equal spacing d between adjacent motors. In regions where both filaments overlap, motors can bind and unbind with the rates ω_b and ω_u , respectively. Bound motors move with the velocity v on the polar filament. Eventually, the element's length x changes by moving motors, which elongate their spring extension y and thereby act against an elastic element of stiffness k .

titin and desmin, see section 3.2. Myosin-II proteins that are bound to actin filaments but do not move also account for muscle elasticity. For simplicity I assume a linear elastic response of the element. Denoting the rest length of the element's elasticity by ℓ_0 , the elastic force then reads $f_e = -k(x - \ell_0)$, where x is the element's length.

While the element is submerged in a fluid and operates in the low REYNOLDS number regime it is reasonable to assume that friction plays a central role in the element's movements. Friction in muscle tissue results from hydrodynamic friction with the surrounding fluid and from protein-protein friction. In particular, motors can contribute to friction by means of temporal non-advancing binding to actin filaments [116, 117]. Passive bound motors, which do not actively produce forces, hamper length changes of the element. Nonetheless, such motors can detach and rebind. Such processes reflect currently discussed ideas for the understanding of friction in general on a molecular level [118]. Thus, length changes of the structure shall be accompanied by a friction force $f_f = -\zeta \dot{x}$, where ζ is an effective friction coefficient. Here again, I use an expression, which takes all sources of friction into account by one effective friction term. In general ζ depends on the fluid's viscosity η . Hydrodynamic interactions are excluded at this point and will be discussed in chapter 7.

5.2.1 Collective motor force

Forces produced by motors are of intrinsic stochastic nature. By describing muscle action as a collective process of many motors acting together, it is a reasonable approach to approximate the dynamics via continuous expressions, which neglect fluctuations due to stochastic effects. In order to derive such expressions for the motor force, I follow some ideas introduced in [25] for the description of mitotic spindle oscillations.

A motor in the overlap region of the motor backbone and the polar filament can bind to the polar filament with rate ω_b and unbind with rate ω_u . In general these rates depend on the forces acting on the motors. KRAMERS rate theory gives a first approximation for the fraction of both rates subject to external forces [119]. Motivated by experiments on single myosin motors [20, 120, 121] I restrict the force dependence to the unbinding rate so that $\omega_u \propto \omega_u^0 \exp(-|f_{me}|a/k_B T)$. Here, the force f_{me} is mediated by the spring, to which the motor is attached to, so that $f_{me}(y) = Ky$. On a microscopic length scale a , the force f_{me} gives rise for the performed work, which is normalized by the thermal energy $k_B T$ at room temperature.

In order to find an expression for the motor force I first consider a single motor i , which is bound to the polar filament. Its spring extension y_i changes due to its own velocity v on the polar filament and due to changes in the length of the whole element \dot{x} so that

$$\dot{y}_i = v(y_i) + \dot{x} \quad . \quad (5.3)$$

The velocity of each motor is likewise force dependent. For simplicity, but in agreement with experiments on myosin motors [20, 122, 123], I use a linear force–velocity relationship: $v(y_i) = v_0 \cdot (1 - f_{me}(y_i)/f_0)$. Unloaded motors have velocity v_0 and heavily loaded motors have a stall force f_0 . The expression for the velocity $v(y_i)$ is only well defined for processive motors, which walk for a certain time on a filament. Given the highly non-processive nature of muscle myosin-II, expression 5.3 can only be used for bundles of myosin-II proteins. Bundles of non-processive motors mimic processivity of the bundle through subsequent action of different non-processive motors, which are attached to the bundle. Indeed, experiments measuring force–velocity curves are carried out using bundles of myosin-II motors instead of single myosin-II proteins. Thus from now on a motor in the model corresponds to a bundle of myosin-II motors.

Formally, the collective motor force f_m is expressed as a sum over all contributions from motors, which are able to interact with the polar filament. Interaction is possible for the N motors, which are in the overlap region of motor and polar

filament. The motor force is given by

$$f_m = - \sum_{i=1}^N \sigma_i \cdot f_{me}(y_i) = -K \sum_{i=1}^N \sigma_i \cdot y_i \quad (5.4)$$

with $\sigma_i = \begin{cases} 1 & \text{motor } i \text{ is bound} \\ 0 & \text{motor } i \text{ is not bound} \end{cases}$.

In the spirit of collective processes, which should not depend on fluctuations of single motors, a first approximation is to neglect fluctuations of the spring extension of single motors. Therefore, I replace y_i by its expected value, so that $y_i \rightarrow \langle y_i \rangle$. Further, I assume that all bound motors have the same expected spring extension $\langle y_i \rangle \equiv y$ for all i .

Consequently, in this mean-field description the remaining sum in the expression of the motor force, $\sum_i \sigma_i$, equals the number of bound motors. The fraction of bound motors Q is given by $Q \equiv \sum_i \sigma_i / N$ and the corresponding probability density of bound motors $P_b(y, t)$ then reads $P_b = Q(t) \cdot \delta(y - y_i)$, see appendix B.1. The expectation value is given by $\langle \circ \rangle \equiv \int \circ P_b(y_i, t) dy_i$. For a consistent use of the approximations above it is necessary to reconsider equation (5.3) in the light of averaging the y_i ,

$$\left\langle \frac{dy_i}{dt} \right\rangle = \langle v(y_i) \rangle + \langle \dot{x} \rangle \quad (5.5)$$

$$\int \dot{y}_i P_b(y_i, t) dy_i = Q \cdot (v(y) + \dot{x}) \quad (5.6)$$

The time derivative term \dot{y}_i on the left hand side cannot be evaluated by deducing an expression for the rate of change of the averaged y . Instead, I use yet another substitution. The differential rate of change \dot{y}_i is substituted by the elongation y_i divided by the average time that motors stay attached to the polar filament, which is given by the unbinding rate ω_u^{-1} , so that

$$y \cdot \omega_u(y) = v(y) + \dot{x} \quad (5.7)$$

The time evolution of the binding probability Q is derived from the element's associated FOKKER-PLANCK equations, see appendix B.1. Fast relaxation of unbound motors in comparison to rebinding times is taken into account. Experimentally measured rebinding times exceed relaxation times of myosin elasticity by up to five orders of magnitude [20]. Eventually, the fraction of bound motors evolves according to

$$\dot{Q} = (1 - Q) \cdot \omega_b - Q \cdot \omega_u \quad (5.8)$$

The fraction of bound motors Q increases with rate ω_b by binding of unbound motors and decreases with rate ω_u via unbinding of bound motors. Consequently, the collective motor force reads

$$f_m = -N(x)QKy \quad , \quad (5.9)$$

where N depends on the length x of the element. By restricting the dynamics to states with an overlap between motor and polar filaments, $x \leq \ell_p + \ell_m$ with the length of the polar and motor filament denoted by ℓ_p and ℓ_m , respectively, and to element lengths that are longer than any of the concerned filaments, $x \geq \max(\ell_p, \ell_m)$, implies¹

$$N(x) = (\ell_p + \ell_m - x)/d. \quad (5.10)$$

After all, the active motor force f_m and the elastic force f_e balance with the friction force f_f and possibly by a constant external force f_{ext} ,

$$f_m + f_e + f_f + f_{\text{ext}} = 0 \quad . \quad (5.11)$$

Inertia forces are negligible due to the strong damping of any movement. Motion is completely specified by the equations (5.7), (5.8) and (5.11). Yet introduction of an average spring extension y is redundant in determining the length of the element x from the elongation y . Only one of the two length variables is needed to describe the element's dynamics. Eventually, the equations of motion read, see appendix B.2,

$$\dot{Q} = (1 - Q) \cdot \omega_b - Q \cdot \omega_u \quad (5.12)$$

$$\dot{y} = \frac{g(y)(QKy - dk)^2/d - \dot{Q}Ky [f_{\text{ext}} - k(\ell_p + \ell_m - \ell_0) - \xi g(y)]}{\xi(QKy - dk)g'(y) + KQ [f_{\text{ext}} - k(\ell_p + \ell_m - \ell_0) - \xi g(y)]} \quad , \quad (5.13)$$

with $g(y) = v_0 [Ky/f_0 - 1] + y \cdot \omega_u(y)$, while the element's length reads

$$x(Q, y) = \ell_0 - \frac{(\ell_p + \ell_m - \ell_0) QKy - df_{\text{ext}} + d\xi g(y)}{dk - QKy} \quad . \quad (5.14)$$

The latter algebraic expression for $x = x(Q, y)$ is only valid for $QKy \neq dk$. In the case $QKy = dk$, the element's dynamics is independent of its length. For

¹An expression for $N(x)$, which implicitly restricts x to $\max(\ell_p, \ell_m) \leq x \leq \ell_p + \ell_m$ would demand a sort of hard core potential at the minimum length and a non-continuous drop to $N = 0$ for the maximum length. Alternatively, the constraints on x can be modeled as hybrid dynamical systems, which describe the system via switching realizations [124]. Both approaches are hard to analyse according to general principles of the dynamics.

arbitrary lengths x within the possible regime, motor forces are exactly balanced by the elastic restoring force, so that

$$x(t) = x(t_0) + \zeta^{-1} (f_{\text{ext}} - (\ell_p + \ell_m - \ell_0)k) \cdot t \quad . \quad (5.15)$$

Sufficiently large external forces lengthen the element otherwise it is shortening. Both expressions in the equations (5.14) and (5.15) are limited to $\max(\ell_p, \ell_m) \leq x \leq \ell_p + \ell_m$.

Ensembles of motors that act together can be described by the formalism introduced above. Myosin's attachment rates to actin and detachment rates from actin are known from single molecule experiments. Whole ensembles of myosin motors, however, have different binding and unbinding rates than the single motors that form an ensemble.

5.2.2 Ensemble average

Bundles of non-processive motors form an effectively processive motor. In sarcomeres, approximately 1000 myosin filaments act in parallel, each allocating in average three actin filaments. Myosin motors can only bind to special binding sites on actin filaments. The sites are evenly spread on the actin filaments. Consider a sarcomere, which is cut into slices of thickness d . Assuming an even distribution of myosin motors on the myosin filament, each slice contains a limited number of motors. Each motor can bind to an actin binding site only within a certain limited range around the motor's equilibrium position. The number of motors that can interact with actin in each slice reduces to M motors, which form an bundle. A bundle of motors has different average binding times on filaments than the single motors of the ensemble. With single motor attachment and detachment rates ω_{on} and ω_{off} respectively, the whole bundle binds to and unbinds from a filament with rates ω_b and ω_u respectively, according to [125, 126]

$$\omega_b = M \cdot \omega_{\text{on}} \quad (5.16)$$

$$\omega_u(y) = \omega_b \cdot \left[\left(\frac{\omega_{\text{on}}}{\omega_{\text{off}}(y)} + 1 \right)^M - 1 \right]^{-1} \quad . \quad (5.17)$$

Single motors are force dependent so that the detachment rate of a single motor depends on y ,

$$\omega_{\text{off}}(y) = \omega_{\text{off}}^0 \cdot \exp(|Ky|a/k_B T) \quad . \quad (5.18)$$

Detachment rates of single motor molecules ω_{off}^0 in the absence of external forces are measured experimentally via the average time motors stay attached to actin filaments. Attachment rates ω_{on} are deduced from the time these motors stay detached from actin filaments. The fraction of time a single motor molecule is bound to an actin filament defines the *duty ratio*. It is a classification measure of a motor protein's processivity. A bundle's unbinding rate is approximately an exponentially decreasing function of the force on the bundle $\omega_{\text{u}} \propto \omega_{\text{u}}^0 \exp(-|f_{\text{me}}|a/k_{\text{B}} T)$. Correction terms vanish for large forces.

The half-sarcomere element's equations of motion are completely specified. The following sections reveal the dynamics of the element including a comparison to the experimental results.

5.2.3 Spontaneous oscillations of half-sarcomeres

What is the dynamics of the half-sarcomeric element capable of? In order to understand the dynamics, first and foremost the static behaviour has to be probed². In the proximity of steady states tools like linear stability analysis can be used. In combination with numerical solutions of the equations of motion a picture of the possible dynamics assembles. Standard analysis tools of non-linear dynamics can be reviewed in [127–129] and will not be introduced here.

First and foremost, the half-sarcomere element has steady states, which will be denoted with a star (*) attached to the corresponding variables. The binding probability is stationary for

$$Q^* = \frac{\omega_{\text{b}}}{\omega_{\text{b}} + \omega_{\text{u}}(y^*)} \quad , \quad (5.19)$$

while the motor's average spring elongation is stationary for either $Q^*Ky^* = dk$ or $g(y^*) = 0$. The former possibility will be discussed in chapter 6. In the latter case the steady y^* is implicitly given by

$$0 = g(y^*) = [Ky^*/f_0 - 1] \cdot v_0 + y^* \cdot \omega_{\text{u}}(y^*) \quad . \quad (5.20)$$

The steady length of the element $x^*(Q^*, y^*)$ is obtained using the equations (5.14) and (5.15). For certain parameter values, this length can be unphysical, so that $\max(\ell_{\text{p}}, \ell_{\text{m}}) \leq x^* \leq \ell_{\text{p}} + \ell_{\text{m}}$ is violated. These parameter values are rejected.

Astonishingly the stationary state (Q^*, y^*) is determined by the subset of physical parameters, which are related to single effective motors: The state

²Finding an analytic solution for the equations of motion is challenging up to impossible due to the inherent nonlinearities This is a general problem in theories about biological systems.

depends on the binding and unbinding rate ω_b and ω_u , the motor's elasticity constant K , its velocity v_0 and stall force f_0 , the fraction $a/k_B T$, which scales the force dependence of the unbinding rate, and the number M of motors forming an ensemble. All remaining parameters, such as the lengths defining the element (d, ℓ_p, ℓ_m and ℓ_0) as well as the element's elasticity constant k and the external force f_{ext} determine the element's stationary length x^* .

What about the stability of the stationary states? The states are stable against external perturbations but can become unstable for certain parameter values: The element's length can oscillate spontaneously. An oscillatory instability occurs when two conditions are fulfilled, see appendix B.3: $Q^*Ky^* < dk$ and $\omega_b + \omega_u(y^*) < y^* \omega'_u(y^*)$. On the left hand side of the former condition is the force that one single motor exerts. On the right hand side is the change of elastic restoring force f_e when the element's length changes by d so that $x^* \rightarrow x^* \pm d$. Thus, shortening of the element by a length d gains one more motor in the overlap region of motor and polar filament. This motor helps shortening the element counteracting the increased restoring force. The condition demands that the restoring force exceeds the additional motor force. Motors must be *weaker* than the elastic force. The second condition highlights the importance of the force dependence of the rates. Both conditions are necessary but not sufficient for oscillations.

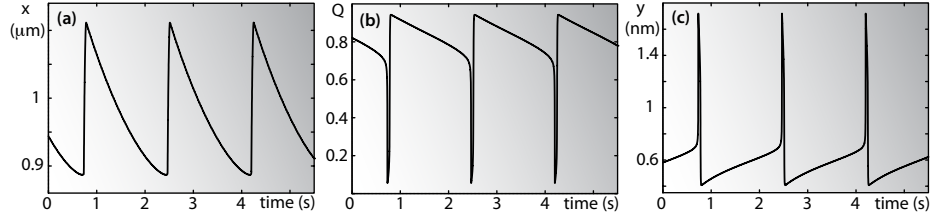


Figure 5.3 Typical spontaneous oscillations. (a) Saw tooth like shape of slow shortening and rapid lengthening. (b) Fraction of bound motors. (c) Elongation of the motor spring extension.

I will try to give an intuitive picture of the process that drives the periodic contractions. In figure 5.3a the typical saw tooth like shape of the length oscillations is shown. A rapid lengthening phase follows a slow phase of shortening. In an element's state that is close to the elasticity's resting length ℓ_0 motors are barely subject to pulling forces. Motors bind to the polar filament, contract and eventually shorten the element. Subsequently, the element's internal tension rises. In a high tension state, eventually a few motors detach, while the remaining ones bear the same overall load. Due to the exponential increase of the

unbinding rate of the remaining motors, inevitably an avalanche of unbinding events occurs, see figure 5.3b,c. The element rapidly relaxes due to the elasticity. Motors start to rebind without immediate unbinding and the cycle restarts. Now, the condition above is more clear: Would the motors be stronger than the elastic restoring force, the element would simply contract to its minimum length.

Repetitively a fast lengthening phase follows a slow shortening phase, which points to a separation of time scales. Such oscillations are generally known as relaxation oscillations and ubiquitous in models of biological phenomena [98, 130–132].

Figures 5.4 and 5.5 provide insight to the parameter dependence of the element's states. Asymptotic states as a function of the element's elasticity constant k and an external force f_{ext} are shown in figure 5.4a: Muscles have a nonlinear elastic response [36, 133]. Stretched muscles are stiffer than relaxed muscles. Under experimental conditions (isometric, isotonic or auxotonic, see section 3.2) myofibrils are stretched by an external force. The element has stable *stationary* states, see figure 5.4c, where motor forces, elastic forces and external forces balance. Beyond a critical value $k = k_c$ with $k_c = k_c(f_{\text{ext}})$, the state becomes *oscillatory*, see figure 5.4b. Weak elasticities can lead to a state, where the element is *maximally shortened*, see figure 5.4e. Further shortening is prevented by the impenetrability of the element's restricting discs against the filaments. For large external forces the motor and polar filament can also lose overlap, so that the element is *overstretched*, see figure 5.4c. The coexistence of the latter two states is possible in the *bistable* regime. By approaching the border line between the oscillatory and the maximally shortened state, oscillation become confined by the restricted minimum elongation of the element. The constraint destroys the periodic contractions. The singular point, where all state separation lines meet each other, is a consequence of the simplification of a linear change of the number of motors in the overlap region and a linear change of the element's elastic restoring force. Within this point all forces balances for any arbitrary length x of the element³. Non-linear motor and elastic forces would spirit away this singularity.

Why does bistability occur? Below the singular point the motors are stronger than the elasticities, $Q^*Ky^* > dk$. In the bistable region it is possible that shortening towards the minimum length occurs because the increase of the number of motors cannot be balanced by the elasticity. External forces, however, can contribute to counteract an initially small number of motors in the overlap region and finally overstretch the element. Note that the equations of motion

³Within the singular point I encounter an *anholonomy* effect, which is an example for a BERRY phase in the theory of differential equations. For review, see [134].

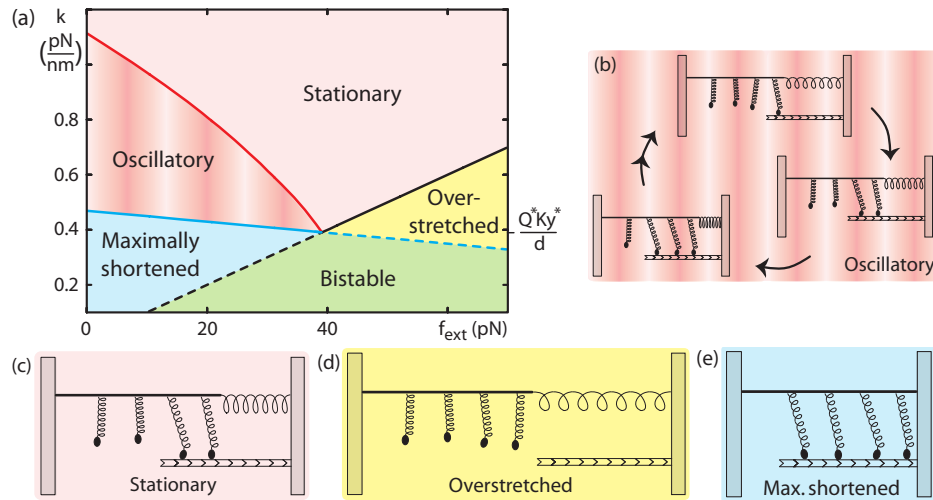


Figure 5.4 Half-sarcomere states. (a) Phase diagram indicating stationary, oscillatory, maximally shortened, overstretched and bistable regimes as functions of an external force f_{ext} and the element's elasticity k . (b) Oscillatory state, schematically. (c) Stationary state, schematically. (d) Overstretched state, schematically. (e) Maximally shortened state, schematically.

presented here are only applicable in the red (stationary and oscillatory) region of the diagram where $\max(\ell_p, \ell_m) \leq x \leq \ell_p + \ell_m$.

Another parameter space cut is shown in figure 5.5. Variations of the rate ω_{on} and the friction coefficient ζ can induce oscillations: The binding rate of myosin-II depends on the p_i concentration, the pH value and is most affected by the Ca^{2+} concentration, see section 3.2. Friction can indirectly also be controlled in experiments. In the flow chambers highly viscous media can be used. Besides, the ATP concentration alters the element's friction. Myosin needs ATP to detach from actin. Low ATP concentrations increase the number and the average time myosin motors stay bound waiting for detachment. Inactive, i.e. post powerstroke, bound motors hinder the ongoing motion of the whole motor filament. This is nothing else than friction against length changes of the element and is an example of general ideas about protein-protein friction [116–118]. In the state diagram in figure 5.5, strong friction does not allow for periodic contractions. Inevitably, high binding rates lead to maximal shortening, where low rates allow for cyclic contractions. Experiments that vary the p_i concentration find stationary states for low binding rates and oscillatory states with increasing binding rates, see section 3.3.1.

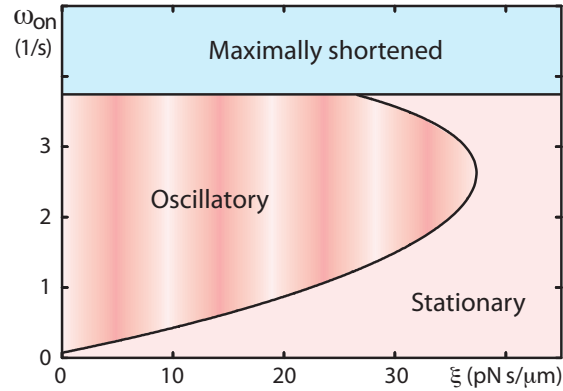


Figure 5.5 Phase diagram of the element's asymptotic states as a function of the friction coefficient ζ and the single motor attachment rate ω_{on} .

Experiments are nicely reconstructed through the state diagrams in the figures 5.4 and 5.5. Stationary and overstretched states are observed for high external stretching forces. Force free myofibrils are reported to simply shorten to their minimum length. Subsequent stretching induces macroscopic, saw-tooth like oscillations of sarcomeres. In theory the state diagram suggests that oscillations in this case set in by crossing the border line between the maximally shortened state and the oscillatory region. Borderline crossing can happen far from the oscillatory instability and therefore can be saw-tooth like. Periodic contractions are impeded when maximally shortened. External forces increase the length and macroscopic oscillations set in. Bistability, however, has not been reported so far in the experiments. On the one hand the initial conditions are hard to control and it is possible that bistability has been overseen. On the other hand it is not clear how much the bistable region in figure 5.4 is affected by non-linearities that are certainly present in myofibrils.

Spontaneous muscle oscillations have been established experimentally as an intermediate state between full activation and relaxation of muscles [68, 74]. Both theoretical state diagrams show oscillatory states sandwiched between stationary states and maximally shortened states.

To what extend do parameter values influence the oscillations? Close to the oscillatory instability the numerically obtained oscillations are sinusoidal with a small amplitude and the frequency matches the critical frequency, see appendix B.4. Experimentally observed amplitudes are macroscopic and saw-tooth like, indicating that the muscle's state is not close to an oscillatory instability.

Therefore, I numerically analyse the influence of parameter values, which can be experimentally controlled, on the element's state apart from the oscillatory instability. In addition to the parameters discussed in the figures 5.4 and 5.5 the motors' elasticity K is varied. This elasticity has been found to be susceptible to the pH value and the Ca^{2+} concentration of the surrounding medium. The rate ω_{off}^0 depends on the ATP concentration, see the motor cycle in section 3.1.2. Ultimately, different striated muscle types have different resting lengths ℓ_0 . Amplitude and frequencies vary with the parameters as shown in table 5.6.

Parameter \uparrow	k	f_{ext}	ω_{on}	ξ	K	ω_{off}^0	ℓ_0
Amplitude	\uparrow	\downarrow	\uparrow	\downarrow	\uparrow	\downarrow	\downarrow
Frequency	\uparrow	\uparrow	\downarrow	\uparrow	\uparrow	\uparrow	\uparrow

Table 5.6 Change of the element's oscillation frequency and amplitude with varying parameter values. Upward pointing arrow corresponds to an increase while downward pointing means a decrease in value. Single-lined arrows is up to a moderate change while double-lined arrows indicates a very sensitive response. All parameter values are increased, while the frequency and amplitudes behave as indicated. The respective reverse holds for decreasing parameter values.

Noteworthy, the element's oscillatory state is quite robust against variations of parameter values. In the following section the robustness of the oscillatory state in the presence of noise will be shown.

5.2.4 Stochastic simulations

Binding and unbinding events of motors are of intrinsic stochastic nature. Here, I reject the mean-field approximation that neglects distributions of the motor's spring elongations. Consequently the binding probability Q is subject to fluctuations. In appendix B.5 the procedure is described in detail. Here, the main results in comparison with the mean-field theory will be discussed [135]. All parameter values are identical in the simulation and in the mean-field description.

In figure 5.7 a typical simulation in the oscillatory regime is compared with the corresponding mean-field solution. In both cases the elements' lengths oscillate with a saw-tooth like shape. The fraction of bound motors shows the typical fast drop and its recovery. Figure 5.8 shows a histogram of the length distribution of the spring extension of bound motors. Only a small fraction of all available motors participate in contraction, which is general a property

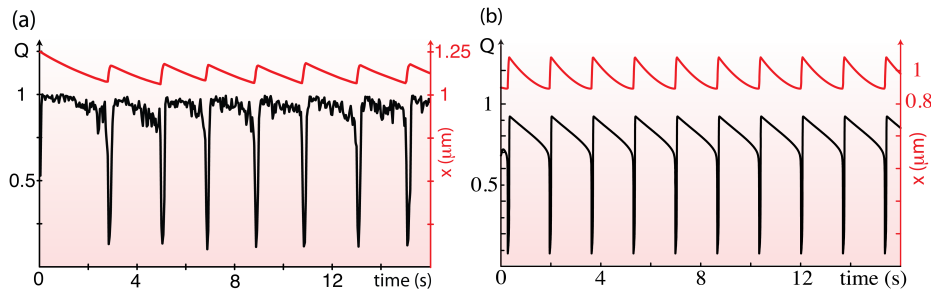


Figure 5.7 (a) Stochastic simulation of an oscillating half-sarcomere element. The binding probability Q is shown in black, the element's length x is shown in red. (b) The same situation like in (a) in the mean-field limit.

of ensembles of low duty ratio motors. The asymmetry of the the bell-shaped distribution results from the active motion of the motors.

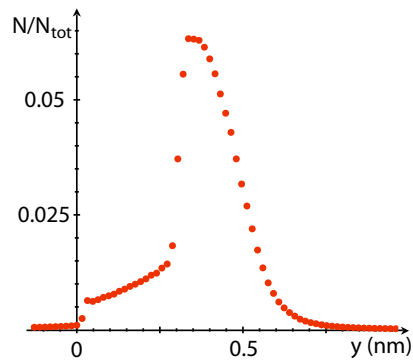


Figure 5.8 Distribution of the spring extension y of motors. N/N_{tot} is the fraction of motors participating in contraction. Asymmetry in the bell-shaped distribution is presumably due to the motors' active motion on the polar filament.

Oscillations are robust in the presence of noise. The ability of cyclic contractions is intrinsic to the element due to its composition. In order to back up the relevance of the model for muscle contraction two physiological effects of muscles will be discussed: Stretch activation and shortening deactivation, see [34].

5.2.5 Stretch activation

Stretch activation⁴ of muscles [78, 136] is observed in all types of striated muscles. In heart muscle research, stretch activation accounts for the FRANK-STARLING law: A sudden stretch and release of myofibrils show a typical response curve in the myofibrils' tension as depicted in figure 5.9. On a short time scale the response is elastic due to the elements' and the motors' elasticities. Instead of a decreasing tension due to motor unbinding events and the subsequent loss of elements bearing elastic energy, a delayed rise in tension is observed, which drops as expected after some time. The molecular mechanisms for stretch activation have not been identified yet. However, it is known that motor activity increases with fast stretching.

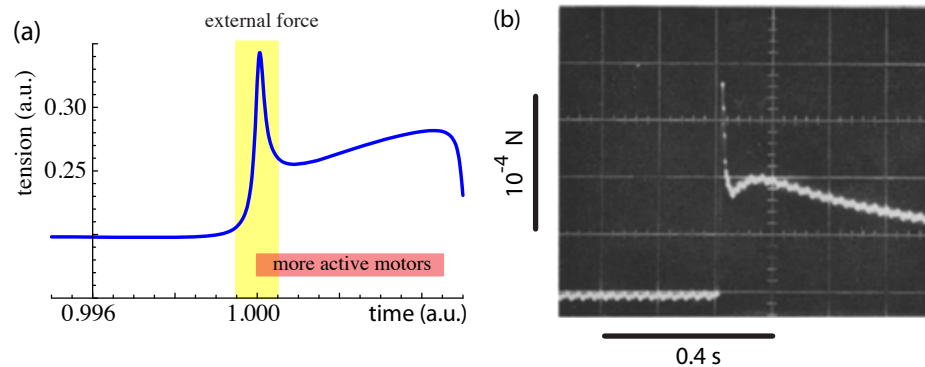


Figure 5.9 (a) Stretch activation response of the half-sarcomeric element. A bell-shaped external force during the duration indicated in yellow stretches the element. A subsequent increase of the number of available motors by 5% for the time indicated in red results in a typical two maxima response curve. (b) Experimental recording of stretch activation shows the typical two maxima in the response curve. Taken from [137].

The half-sarcomere model, in its native version, shows no (and cannot show any) stretch activation. Stretch does not activate more motors. However, increasing the number of available motors by hand by 5% at the time a stretch sets in, yields a typical response curve, see figure 5.9.

⁴Motor activation via stretching can be induced by tension sensitive Ca^{2+} channels. Here, Ca^{2+} independent activation of the contractile apparatus is considered.

5.2.6 Shortening deactivation

Intuitively reasoning muscular force should increase with shortening sarcomeres. The shorter, the more motors can participate in contraction. This is observed for fully activated muscles. Partially activated muscles are found to reach maximal forces for longer sarcomere lengths [75, 92, 138]. Figure 5.10a shows data of active forces plotted against sarcomere length for different levels of muscle activation. Barely activated muscles have low active forces and are bell-shaped. With increasing activity, the left edge of the bell becomes steeper and eventually vanishes. The half-sarcomere element shows a comparable response for partial activation, see figure 5.10b. Externally probing the overall force reveals a maximum, which is not close to the element's shortest length. The active force of shorter elements is balanced by passive restoring forces.

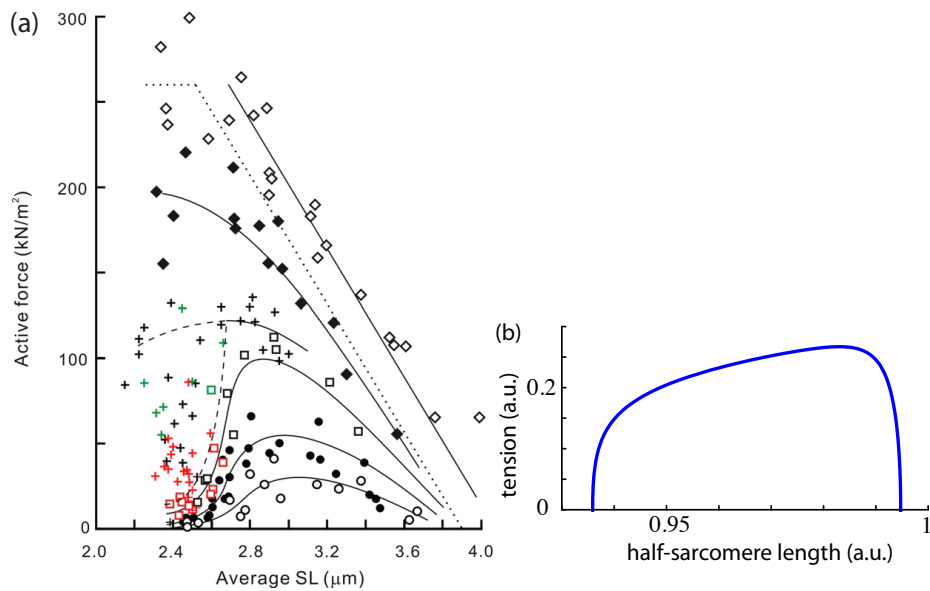


Figure 5.10 Shortening deactivation. (a) Experimental data of various concentrations of Ca^{2+} , i.e. distinct levels of activation. The curves represent the average course of the data points. Blanc circles correspond to the lowest level of activation. Higher levels of activation have higher maximal active forces. The active force is obtained by subtracting the resting states elasticity from the active states overall force. Edited from [75]. (b) Showcase curve from the model. Elastic forces at rest are lower than in the active case, where motors shorten the element. Correspondingly, the tension decreases.

In the following section several half-sarcomere elements will be coupled to a chain. This composition puts the model in a position for direct comparison with the experiments that find spontaneous waves.

5.3 Chains of half-sarcomeres

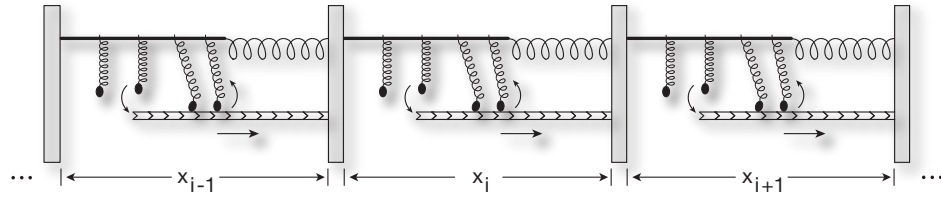


Figure 5.11 Chain of half-sarcomere elements. Each element is rigidly coupled to its neighbour to mimic a myofibrillar chain of half-sarcomeres.

Myofibrils are chains that are composed of half-sarcomeres. Leftward heading motors alternate with elements with motors heading in the opposite direction. Macroscopic contractions are possible since adjacent half-sarcomeres are rigidly coupled together. Chains of rigidly coupled half-sarcomeric elements reflect such a composition, see figure 5.11. Correspondingly, the force balance equations for n elements reads

$$0 = (1 + b_d)(f_1^m + f_1^e) - (f_2^m + f_2^e) + f_1^f \quad (5.21)$$

$$0 = 2(f_j^m + f_j^e) - (f_{j-1}^m + f_{j-1}^e) - (f_{j+1}^m + f_{j+1}^e) + f_j^f \quad (5.22)$$

$$0 = 2(f_n^m + f_n^e) - (f_{n-1}^m + f_{n-1}^e) + f_n^f + (1 - b_d) \cdot f_{\text{ext}} \quad (5.23)$$

where subscripts indicate the element number with $2 \leq j \leq n - 1$. For an unfortified chain $b_d = 1$ and for a chain with a fixed left end $b_d = 0$. The full set of equations of motion for the chain's variables Q_i, y_i with $1 \leq i \leq n$ and the corresponding lengths x_i can be found in appendix C.2.

5.3.1 Single sarcomere element

A chain of two elements, $n = 2$, corresponds to a single sarcomere. The chain is able to oscillate spontaneously. Saw tooth like cyclic contractions for the same parameter values as in the half-sarcomere element are found. Both halves of

the two element chain are always in the same stationary state or oscillate with identical frequency, amplitude and shape. Either both halves oscillate with a phase shift of half of the oscillation period or a small, but non-vanishing phase shift, see figure 5.12a. Since a sarcomere element is symmetric with respect to exchange of the left and right half, $(Q_1, y_1) \leftrightarrow (Q_2, y_2)$, swapping initial conditions, exchanges the dynamics states of the halves. Both oscillatory modes in the model do not coexist. Instead, variations of parameter values induces a transition between both modes, which will be discussed in section 6.2. The low phase shift mode is strikingly similar to the experimentally accessible⁵ recording of sarcomere lengths, compare therefor figure 5.12b and 5.12c. The shortening phase in the slightly phase shifted mode also remembers to the experimental observation that sarcomere shortening is always asymmetric [82, 86–88], so that there is always a slight phase shift between adjacent shortening half-sarcomeres.

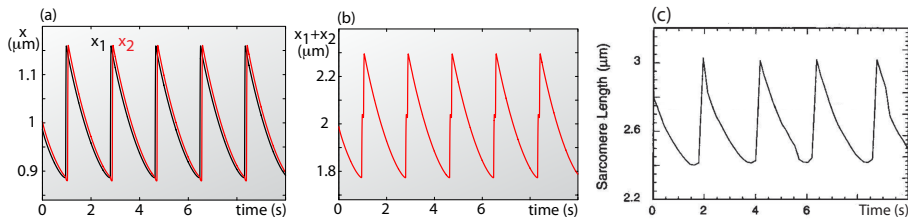


Figure 5.12 Sarcomere oscillatory mode. (a) Saw tooth like oscillations of both halves' lengths with a small phase shift. For parameter values see appendix A.1. (b) Same mode as in a) but the whole sarcomere length $x_1 + x_2$ is measured. (c) Experimental showcase recording of averaged sarcomere length oscillations from [90], see section 3.3.1.

Within a chain of elements each element's steady state decouples from its neighbour, see appendix C.3. The stationary state of each element is identical to a single half-sarcomeric element's state for the same boundary conditions. All conditions for spontaneous oscillations in a half-sarcomeric element hold for spontaneous oscillations of a chain of two elements, see appendix B.3 with $\zeta \rightarrow \zeta/2$. Close to the oscillatory instability, the sarcomere element is always in the mode with a phase shift of half a period, see section 6.2.

⁵Tracking half-sarcomere lengths is experimentally challenging and to date only reliable by fluorescent markers, see [82]. In general however, the influence of the markers on the experiment remains unclear.

5.3.2 Short chains

Chains of half-sarcomere elements exhibit spontaneous relaxation waves. The small phase shift mode between adjacent elements is also present in chains. Elements within a short chain oscillate spontaneously with equal period and almost equal amplitude. Only boundary elements notably differ. Figure 5.13 exemplifies a spontaneous relaxation wave of adjacent sarcomeres in comparison to an experimental recording from [72]. In both cases a relaxation wave emerges at one end of the chain and propagates towards the other end. Oscillations have the same period but slightly differ in amplitude. The relative phase shift differs by less than 10% in experiment and theory. The speed of the wave is determined by the amount of the phase shift, whose values in theory will be discussed in section 6.3.

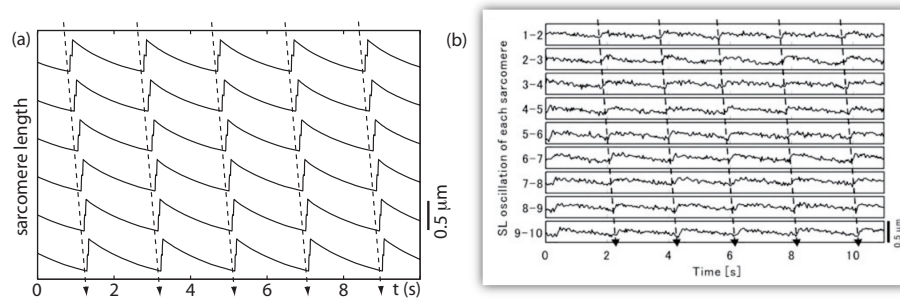


Figure 5.13 Relaxation waves in chains of sarcomeres. Adjacent sarcomere lengths are shifted against each other for a better visualization of the wave. The wave propagates from the upper (left end of the chain) to the lower elements (right end). (a) Numerical solution of a chain [139]. Parameter values are like in figure 5.12. (b) Experimentally recorded wave [72].

Where within a chain do waves nucleate and in which direction do they propagate? The chains have no preferred direction so that the nucleation site and the wave's propagation direction is set by inhomogeneities of the initial conditions. The experimental boundary conditions imply inhomogeneities at the myofibril's ends. Thus ends can be preferred nucleation points. Figure 5.14 exemplifies the random nucleation comparing theory and experiment via kymograph representations. In kymographs of movies a one to several pixel thick curve (e.g. a straight line) of each movie frame is plotted versus time, here using the free program ImageJ. The curve is fixed with respect to the movie frame. Figure 5.14a shows a numerical solution of a wave nucleating within a chain of the model. Adjacent half-sarcomere elements are plotted side by side

while each element's length is color coded. A wave nucleates between element seven and eight, while waves are propagating towards both ends of the chain. The corresponding kymograph for this situation is shown in figure 5.14c. The experimental kymograph in figure 5.14d is obtained from a showcase recording of spontaneous muscle oscillations from [140], see snapshot in figure 5.14b.

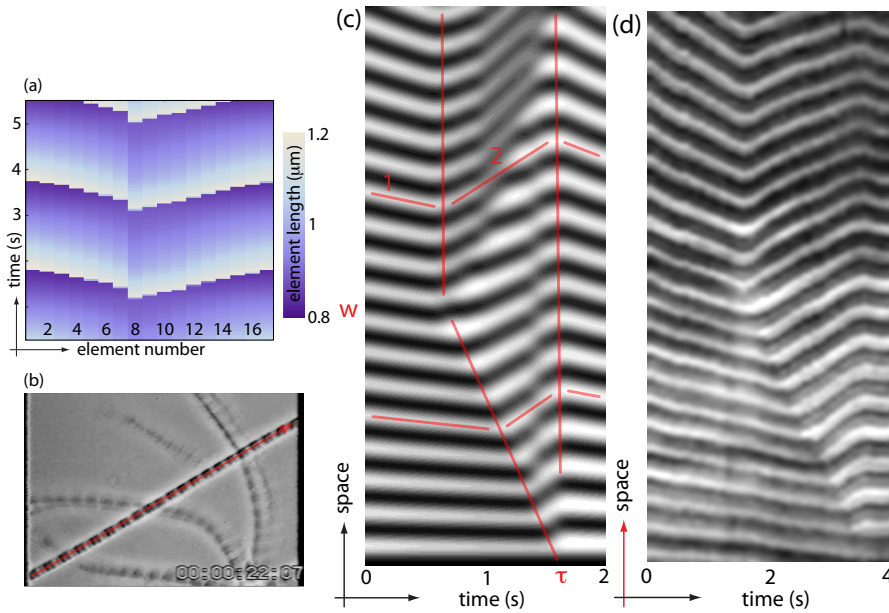


Figure 5.14 Spontaneous wave nucleation within a chain. (a) Numerical solution of a chain. Adjacent elements are plotted versus time, while each element's length is color coded. Waves nucleate spontaneously within the chain between element seven and eight. (b) Snapshot of a showcase movie of spontaneous muscle oscillations [140]. A myofibril under non-isometric conditions in a phase-contrast microscope. The fibril is fixed with a stiff needle at the bottom and attached to flexible needle at the top. Dark regions within the myofibril correspond to myosin filaments, which have a constant length. Bright regions correspond to the changeable inner sarcomeric space. A red arrow indicates the recording direction for the kymograph in d). (c) Kymograph representation of the numerical solution in a). Blur and artificial noise in the picture is used to inveigle the readers eye and mind to regard the numerical solution as an experimental video recording. Follow the eye guidelines for comparison with the experiment in d). At location *W* a rupture wave emerges within the chain. (d) Kymograph of the movie from b). A duration of four seconds from the whole recording is shown. The picture has been modified with a gaussian blur to smoothen the grainy low resolution video snapshot.

In the kymograph in figure 5.14c, first there is a drift of the whole chain due to the contraction of each of the chain's elements, see guideline 1. A relaxation wave spontaneously initiates at location W within the chain. Due to the boundary conditions, successive relaxation of elements leads to a drift of the non ruptured parts of the chain towards the flexible needle at the top, see guideline 2. At a certain time point one part of the chain drifts to the top, while the other part still drifts towards the bottom through shortening of the elements. After time τ , waves have reached the chains ends and the whole process restarts.

In a noisy homogeneous chain wave nucleation points should appear at random. A stochastic simulation of a chain of 20 half-sarcomere elements is shown in figure 5.15. Clearly, waves nucleate here and there and propagate over a distance of some elements and then they disappear. Sometimes wave trains simply collide or pass through each other. This behaviour matches quite well the written description about the wave trains' behaviour found in experiments, see section 3.3.1. In the simulation in figure 5.15 the relative phase shift between adjacent oscillatory elements is large in comparison to the element's oscillation period. Therefore wave trains are slower than in the mean-field description and in the experiments.

Within the mean-field description, i.e. without noise, I also find irregular dynamics. Periodic contractions of the elements of the chain do not form coherent relaxation waves. Some experiments [86, 90] report such behaviour but it remains unclear to what extent the experimental results are attributed to the damage of the myofibrils during the isolation process.

What about the boundary conditions? Experimental papers on spontaneous muscle oscillations collectively report on the importance of non force-free boundary conditions on the myofibrils: Isometric, isotonic or auxotonic conditions are used. Each condition exerts a prestress on fibrils. Reports agree that fibrils have to be prestressed for spontaneous oscillations. Unfortified myofibrils simply contract once. Beyond, the impact of different boundary conditions on the experimental results is not clearly characterized.

So far, I have shown that spontaneous muscle oscillations can have their origin in the coupling of elastic elements with microscopic force generators. Homogeneous chains self-organize into dynamic states that exhibit spontaneous wave patterns. At this point it is appropriate to reconsider the phenomenological approach in chapter 4. Why does the microscopic theory reveals wave patterns but the phenomenological description does not? By putting the results from the microscopic description in a broader context this question will be answered in the following section.

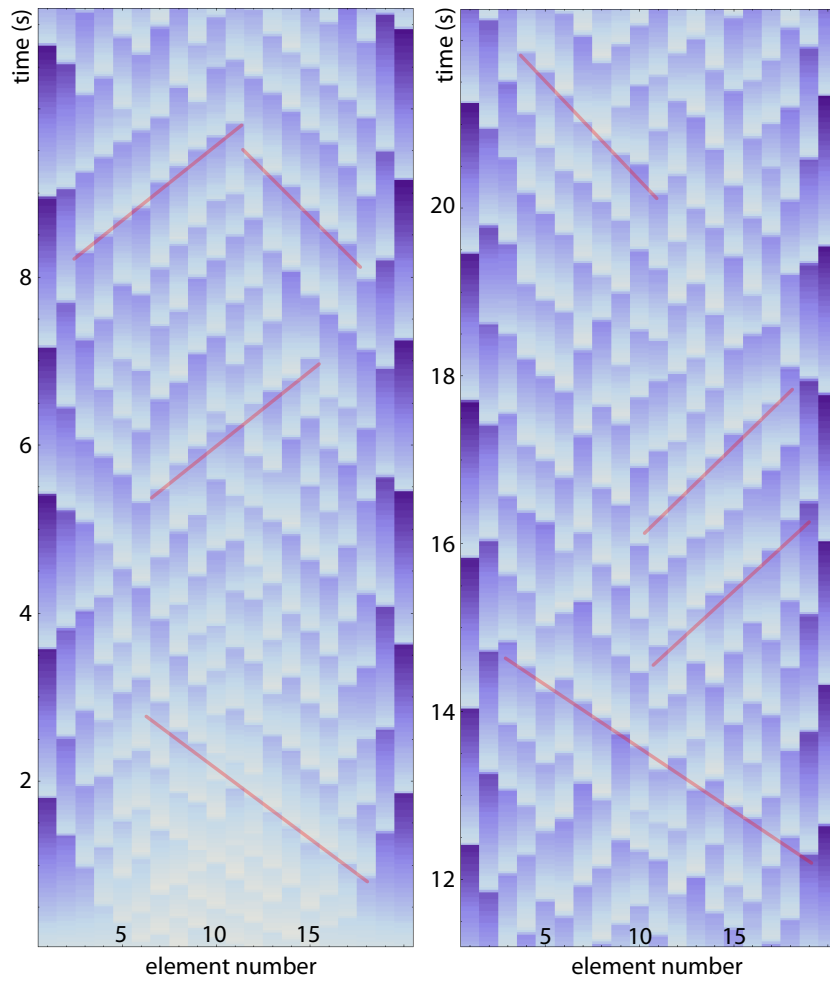


Figure 5.15 Random wave phenomena within a chain. (a,b) Adjacent element's length is color coded and plotted against time. In an unfortified chain waves spontaneously emerge within the chain and propagate some distance. Red lines indicates examples for wave trains. Details about the stochastic simulations can be found in appendix C.5. For parameter values see appendix A.1.

5.4 Continuum limit

In order to bridge the gap between the microscopic and the phenomenological description I will pass to the continuum limit of an infinite long chain of half-sarcomere elements. In a first step the microscopic equations of motion are linearized around their steady state. Introducing z as the spatial coordinate along the chain with $z \gg x^*$ and the density of half-sarcomere elements ρ , the time evolution of perturbations of the stationary state evolves according to the continuous equations, see appendix C.4,

$$\xi \partial_t \rho = c_1 \partial_z^2 \rho + c_2 \partial_t \partial_z^2 \rho - c_3 \partial_z^2 Q \quad (5.24)$$

$$\partial_t Q = c_4 \partial_t \rho - c_5 Q \quad (5.25)$$

where the coefficients are related to the microscopic parameters via

$$c_1 = [Q^* K y^* / d - k] (x^*)^2 \quad (5.26)$$

$$c_2 = -(x^*)^2 \cdot N(x^*) Q^* K / [\omega'_u(y^*) y^* + \omega_u(y^*) + K v_0 / f_0] \quad (5.27)$$

$$c_3 = -\rho^* x^* \cdot N(x^*) K y^* \quad (5.28)$$

$$c_4 = x^* \cdot Q^* \omega'_u(y^*) / \{\rho^* [\omega'_u(y^*) y^* + \omega_u(y^*) + K v_0 / f_0]\} \quad (5.29)$$

$$c_5 = \omega_b + \omega_u(y^*) \quad (5.30)$$

The steady density ρ^* is spatially homogeneous and corresponds to a state where active and passive forces balance. Hence, the tissue is stationary but not in thermal equilibrium. Do the continuum equations (5.24) and (5.25) allow for oscillatory instabilities? A linear stability analysis of the homogeneous stationary state with the ansatz $\rho(z,t) = \rho^* \exp(iqz + st)$ and $Q(z,t) = Q^* \exp(iqz + st)$ denoting the wavenumber with q and the complex time scale with s , results in the dispersion relation

$$2s = -a_1 \pm \sqrt{a_1^2 - 4a_2} \quad (5.31)$$

$$\text{with } a_1 = \frac{\xi c_5 + q^2 (c_1 + c_2 c_5 - c_3 c_4)}{\xi + q^2 c_2} \quad , \quad a_2 = \frac{q^2 c_1 c_5}{\xi + q^2 c_2} \quad .$$

In the continuum limit, a chain of half-sarcomeres can have three states: The chain has a stable stationary state, is unstable or oscillatory. In the stable regime $\Re(s) \leq 0$. For $\Re(s) \geq 0$ and $\Im(s) = 0$, i.e. for $a_1^2 > 4a_2$, small perturbations of the stationary state will lead to a fully contracted state. For $\Re(s) \geq 0$ and $\Im(s) \neq 0$, the equations allow for waves with certain wavenumbers q , see figure 5.16. The conditions recover the same necessary conditions $Q^* K y^* < dk$ and $\omega_b + \omega_u(y^*) < y^* \omega'_u(y^*)$, which appeared before in the microscopic description.

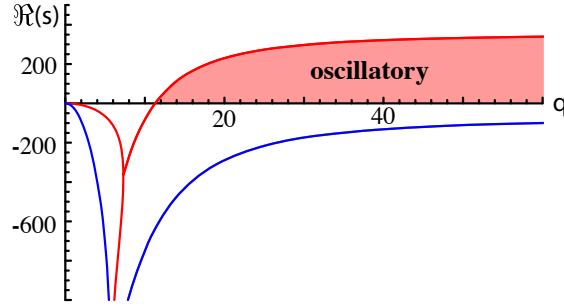


Figure 5.16 Dispersion relation of the continuum equations for varying d . The continuous chain is stable (blue curve) for $d = 0.001$ and oscillatory (red shaded region) for $d = 0.0003$.

In the limiting case $q \rightarrow 0$, i.e. on large length scales, the continuous chain is always stable, since $s < 0$. Spontaneous waves emerge from cooperative microscopic effects. Consequently, waves are not found on arbitrary large length scales. On small length scales, $q \rightarrow \infty$, oscillations are still possible reflecting the oscillatory nature of the medium's constituents, the half-sarcomeres. However, on length scales that are smaller than the size of the constituents of a continuous material phenomenological theories fail in general.

The continuum limit, see equations (5.24) and (5.25), can be compared with the phenomenological result from chapter 4. In the limit of a stationary probability density, $\partial_t Q = 0$, the continuous equations reduce to

$$\zeta \partial_t \rho = c_1 \cdot \partial_z^2 \rho + \left(c_2 - c_3 \frac{c_4}{c_5} \right) \cdot \partial_t \partial_z^2 \rho \quad , \quad (5.32)$$

while the phenomenological equation (4.10) reads

$$\eta_e \partial_t \rho = \left(E - \rho^* \Delta \mu L_{\sigma\mu}^{(1)} \right) \cdot \partial_z^2 \rho + L_{\sigma v} \cdot \partial_t \partial_z^2 \rho \quad . \quad (5.33)$$

Both equations have the same form. Macroscopic coefficients from the phenomenological approach can directly be related to the microscopic parameters through a comparison of the coefficients. The microscopic origin of the phenomenological description is revealed. Moreover, an essentially non-hydrodynamic mode, namely Q , is necessary for oscillatory behaviour and wave patterns. A chain of half-sarcomere elements in the continuum limit can contract for $\partial_t Q = 0$ but cannot show cyclic contractions.

Chapter 5 Microscopic description

Within this chapter it was shown that a homogeneous chain of length dependent force generating units neither contracts homogeneously nor allows for oscillations. A microscopic mechanism for spontaneous periodic contractions of half-sarcomere elements was suggested: Motors collectively act against elastic elements. Wave patterns emerge in chains of such elements. The cyclically contracting elements self-organize into states that reveal relaxation waves. In the presence of noise waves nucleate at random within chains with undetermined propagation direction. A continuous description of deterministic chains uncovers a non-hydrodynamic mode, which allows for wave patterns on macroscopic length scales. In the process the microscopic origin of the phenomenological description of myofibrils is revealed. In the following chapter the microscopic element's dynamics that goes beyond the emergence of spontaneous oscillations will be analyzed.

Chapter 6 Advanced nonlinear dynamics

Half-sarcomeric elements show spontaneous oscillations that ultimately yields wave patterns. In this chapter advanced nonlinear dynamics concepts will be used to reveal the possible dynamics of half-sarcomere elements, which will go beyond spontaneous oscillations. Comprehension of this chapter requires basic knowledge on nonlinear dynamics. Wonderful introductions can be found in the books of STROGATZ [127], WIGGINS [128] and KUZNETSOV [129]. On the numerical side I use self-made standard techniques and the available software packages XPPAUT [141], Auto07p [142] and Mathematica [143].

6.1 Half-sarcomeres reloaded

For an analysis of the possible dynamics of the half-sarcomeric element I write the equations of motion in a dimensionless form. Time is rescaled by ω_b yielding the equations of motion

$$\frac{dQ}{dt} \equiv \dot{Q} = (1 - Q) - Q \cdot \omega(y) \quad (6.1)$$

$$\dot{y} = \frac{\tilde{g}(y)(Qy - \kappa)^2 / \kappa - \dot{Q}y(\tilde{f}_{\text{ext}} - L - \zeta\tilde{g}(y))}{\zeta\tilde{g}'(y)(Qy - \kappa) + Q(\tilde{f}_{\text{ext}} - L - \zeta\tilde{g}(y))} \quad (6.2)$$

with $\omega(y) = \omega_u(y)/\omega_b$ and $\tilde{g}(y) = y(\gamma\omega(y) + 1) - 1$. The elongation y is rescaled by the stall length f_0/K , given by the stall force and the motor's spring constant. The element's length x is rescaled by the resting length ℓ_0 and is given by

$$x = \begin{cases} 1 - \frac{LQy + \kappa(-\tilde{f}_{\text{ext}} + \zeta\tilde{g}(y))}{L_0(\kappa - Qy)} & \text{for } Qy \neq \kappa \\ x(t_0) + (\zeta L_0)^{-1}(\tilde{f}_{\text{ext}} - L) \cdot t & \text{for } Qy = \kappa \end{cases} \quad (6.3)$$

The dimensionless parameters are given by $\kappa = dk/f_0$, $\tilde{f}_{\text{ext}} = \omega_b f_{\text{ext}}/(kv_0)$, $L = \omega_b(\ell_m + \ell_p - \ell_0)/v_0$, $\zeta = \zeta\omega_b/k$, $\gamma = f_0\omega_b/(Kv_0)$ and $L_0 = \omega_b\ell_0/v_0$.

Note that L_0 is unimportant for the motor dynamics since it is not part of the equations of motions (6.1) and (6.2). However, L_0 influences the corresponding length of the element.

In the following analysis I concentrate on changes of the parameter κ in the absence of external forces ($\tilde{f}_{\text{ext}} = 0$). Lengths related variables such as L and L_0 , as well as ζ are experimentally not easily accessible in the sense of well defined control parameters and are therefore kept unaltered. As the variation of γ shows the same but not all possible solutions, which occur via changes in κ , analysis of dynamical states is performed in κ . First of all there will be a canard chasing.

6.1.1 Canard phenomenon

At least one stationary state is always found in the equations of motion (6.1) and (6.2). This state corresponds to $\tilde{g}(y^*) = 0$, which can be fulfilled for any set of parameter values. The fraction of rates $\omega(y^*)$ is approximately exponential in y^* , so that there is always a y^* obeying $y^* \exp(y^*) + y^* = 1$. The stationary state can be unphysical in the case where the stationary length of the element is shorter than the longest filament within the element $\ell_0 \cdot x^* < \max(\ell_p, \ell_m)$. Those states are rejected as the validity of the equations of motion is restricted to regimes with $\max(\ell_p, \ell_m) \leq \ell_0 \cdot x \leq \ell_p + \ell_m$.

For large κ the stationary state (Q^*, y^*) is always stable. Decreasing κ below a critical value κ_h destabilizes the stationary state and the dynamics ends up with stable oscillations on a limit cycle. Linear stability analysis confirms the existence of a HOPF-bifurcation for $\kappa = \kappa_h$. The oscillatory instability turns out to be supercritical. The necessary but insufficient conditions for spontaneous oscillations read in dimensionless form $\kappa > Q^* y^*$ and $y^* \omega'(y^*) > \omega(y^*) + 1$. The oscillations close to the instability are sinusoidal and the frequency matches the critical frequency, which is obtained from linear stability analysis.

What happens when κ is decreased further? Linearizations of the equations around the stationary state will not be sufficient anymore to account for the system's behaviour. Nonlinear terms become more and more important. Amplitude equations take these nonlinearities into account and give a good approximation for the amplitude and frequency behaviour close to supercritical oscillatory instabilities. In the half-sarcomere case the corresponding amplitude equations predict a smooth increase of amplitude and oscillation period. Surprisingly, this is not what happens when κ is decreased. Instead a massive deformation of the limit cycle for tiny changes of the control parameter close to a critical value κ_c is observed, see figure 6.1a. Changing the distance¹ from the

¹Distance in parameter space from a critical value can be defined as $|\kappa/\kappa_c - 1|$.

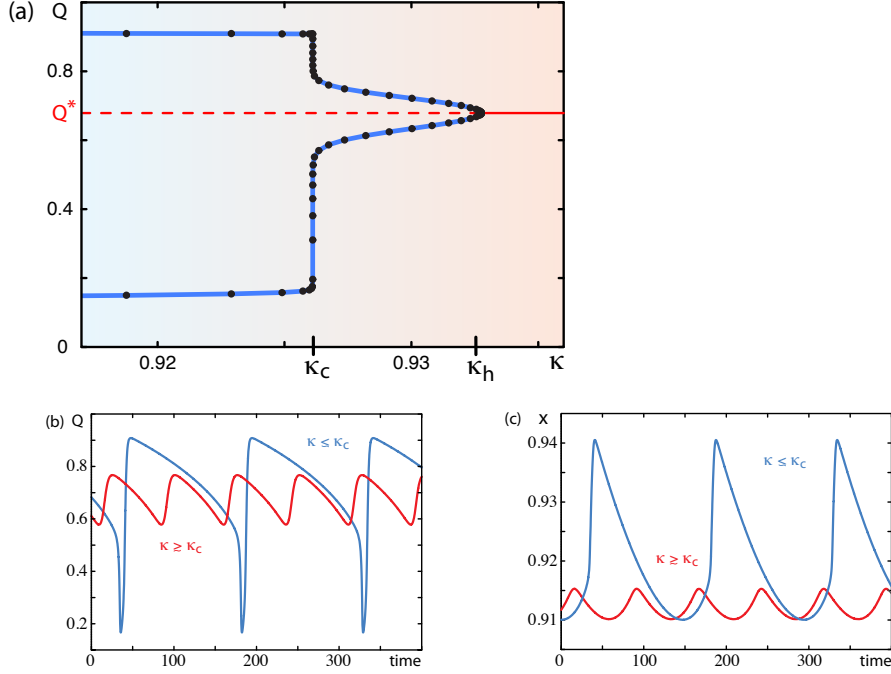


Figure 6.1 Canard explosion in a half-sarcomere element. (a) Bifurcation diagram for the binding probability's amplitude upon the variation of the control parameter κ . For decreasing κ the stationary state Q^* (red) becomes unstable at $\kappa = \kappa_h$ yielding small amplitude limit cycle oscillations. At $\kappa = \kappa_c$ the amplitude literally explodes and the system suddenly follows a relaxation cycle. (b,c) $Q(t)$ and $x(t)$ close to the canard explosion. The red curve is for $\kappa = 0.926 \lesssim \kappa_c$ and the blue curve is for $\kappa = 0.9265 \gtrsim \kappa_c$. For parameters, see appendix A.1.

oscillatory instability of the order $\mathcal{O}(10^{-5})$ induces a change of the amplitude of the binding probability Q by 300%. The period and the shape of the oscillation also changes drastically. For $\kappa \gtrsim \kappa_c$ the element's length oscillates with a deformed sinusoidal shape, while for $\kappa \lesssim \kappa_c$ the shape is saw-tooth like with a much bigger amplitude as before, see figure 6.1b,c. There is a sudden transition towards relaxation oscillations, which are observed far away from the oscillatory instability, a *canard explosion* has occurred.

The relaxation cycle is excitable. In the oscillatory regime close to the Hopf-instability, perturbations of the oscillatory state can lead to a huge excursion on a relaxation cycle before returning to the limit cycle, see figure 6.2a,b. Only perturbations through an increase of y in the upper part of the limit cycle in

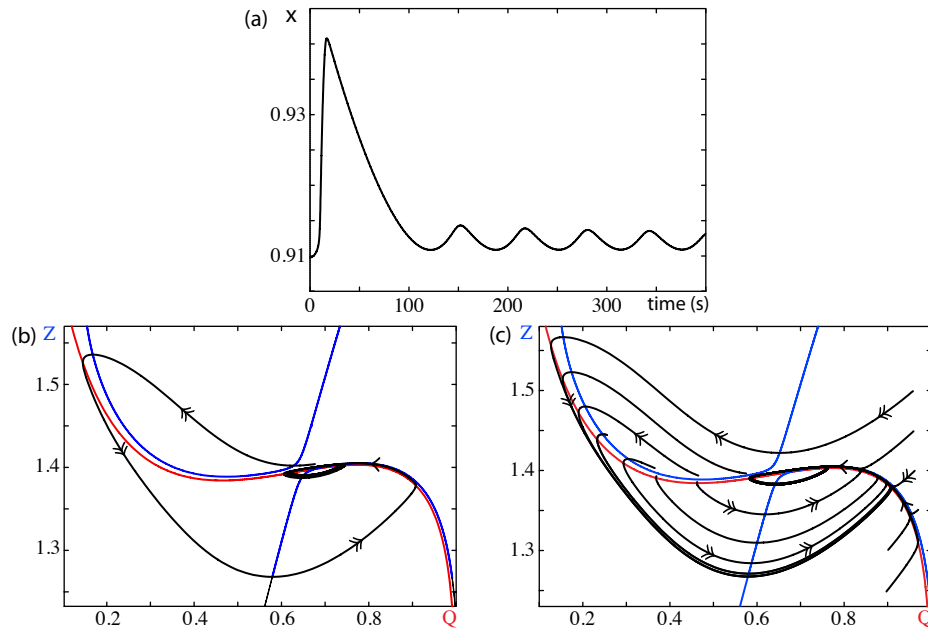


Figure 6.2 Excitability of half-sarcomere elements. (a) Excitability of a relaxation cycle in the regime of limit cycle oscillations with $\kappa = 0.93$ in terms of the element's length x . (b) (Q, z) phase plane for the situation in a). For better visibility the variable $z = Q + y$ is introduced. Nullclines for Q (red) and z (blue) are highlighted. Single arrows corresponds to slow, doubled arrow to fast dynamics. (c) Trajectories for distinct initial conditions in the phase plane for the situation in a). Parameters like in figure 6.1.

the phase plane in figure 6.2c leads to an excursion of the trajectory. The same kind of excitability is observed in the non-oscillatory regime, see figure 6.3a,b. Perturbations of the stationary state with increasing y leads to an excursion on a relaxation cycle before returning to the stable stationary state. Note that in both cases perturbations that are too small will not lead to an excursion. Local stability is not violated.

6.1.2 Generic canard phenomenon

In 1981 the french mathematician F. BENOIT and co-workers discovered a new set of solutions, which can occur in relaxation oscillators [144]. Close to an oscillatory instability of the HOPF type, an explosion of the oscillation amplitude

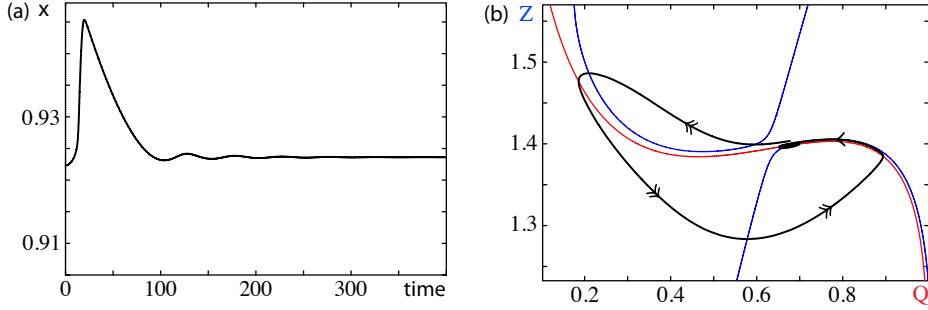


Figure 6.3 Excitability of half-sarcomere elements in the stable regime far away from the oscillatory instability with $\kappa = 1$. (a) A perturbation of the state leads to a huge excursion of $x(t)$ before returning to the stable stationary state. (b) Phase plane (Q, z) with $z = Q + y$ for the situation in a). Parameters are the same like in figure 6.1.

can occur. Limit cycle oscillations with small amplitudes undergo a transition towards relaxation oscillations with large amplitudes via canard cycles. The transition is continuous but occurs for very small variations of the control parameter.

I will introduce the phenomenon with a textbook example [145, 146] of a relaxation oscillator: The VAN DER POL oscillator. In a simple form the oscillator reads

$$\epsilon \dot{x} = y - \frac{x^3}{3} + x \equiv f(x, y; a, \epsilon) \quad (6.4)$$

$$\dot{y} = a - x \equiv g(x, y; a, \epsilon) \quad , \quad (6.5)$$

while ϵ is a small parameter with $0 < \epsilon \ll 1$ and a is a control parameter. The dynamics of the system with decreasing a for $\epsilon = 0.01$ is illustrated in figure 6.4. The only stationary state $(x^*, y^*) = (a, a^3/3 - a)$ is stable for $a > 1$, see figure 6.5a, and the state becomes unstable via a HOPF-bifurcation at $a = 1$. While decreasing a further the limit cycle oscillations evolve towards increasing amplitudes, see figure 6.5c. Suddenly, the cycle's amplitude literally explodes during an exponentially small decrease of a . The transition from limit cycle oscillations to relaxation oscillations is mediated continuously through stable canard cycles. A canard explosion has occurred. Finding canard cycles is numerically challenging due to the high sensitivity of the system on the value of a . Correspondingly, the observation of these cycles is very hard in the presence of noise and especially in experimental setups. Note, the transition is not a bifurcation since no new solutions appear by a canard explosion.

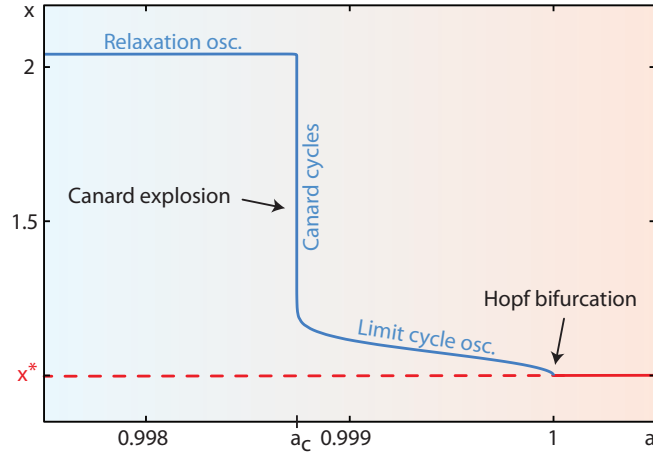


Figure 6.4 Canard explosion in the VAN DER POL oscillator. Bifurcation diagram with the amplitude x under variation of the control parameter a . The stationary state x^* (red) loses stability via a HOPF-bifurcation whose limit cycle oscillations explode via canard cycles towards relaxation cycles.

What is the reason for the transition? Relaxation oscillators have a typical separation of time scales of the dynamic. Approaching the canard phenomenon a first step is the separation of the inherent time scales. In the system

$$\epsilon \dot{x} = f(x,y;a,\epsilon) \tag{6.6}$$

$$\dot{y} = g(x,y;a,\epsilon) \quad , \tag{6.7}$$

with $\epsilon \ll 1$ the variable x evolves faster than the variable y . They are referred to as the fast and the slow variable, respectively. Singular perturbation theory separates the time scales into a fast and a slow subsystem for the limiting case of infinitely fast and slow dynamics. While the slow subsystem (the reduced problem) is given for $\epsilon \rightarrow 0$,

$$0 = f(x,y;a,0) \tag{6.8}$$

$$\dot{y} = g(x,y;a,0) \quad , \tag{6.9}$$

the fast subsystem (the layer problem) is revealed by switching the time scale with $\tau = t/\epsilon$ in the limit $\epsilon \rightarrow 0$,

$$\frac{dx}{d\tau} \equiv x' = f(x,y;a,0) \tag{6.10}$$

$$y' = 0 \tag{6.11}$$

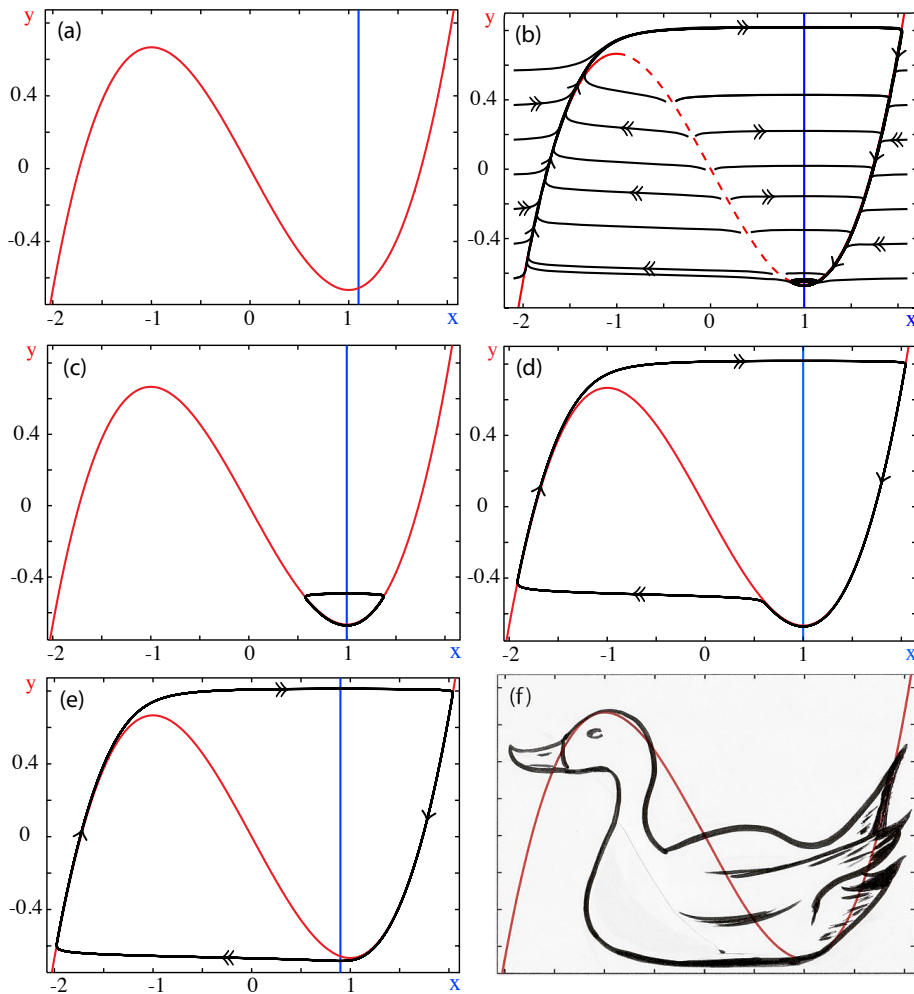


Figure 6.5 (a) Phase diagram with nullclines for x (blue) and y (red) within the stable regime for $a = 1.1$. (b) Trajectories for distinct initial conditions in the oscillatory regime with $a = 0.999$. The y nullcline is cubic shaped with an attractive branch (solid) and a repulse branch (dashed). (c) HOPF-oscillations on a limit cycle with $a = 0.998740451246 \gtrsim a_c$. The limit cycle partially follows the repulsive branch. (d) Relaxation cycle oscillations with $a = 0.998740451245 \lesssim a_c$. The repulsive branch distracts the trajectory towards an attractive branch. (e) Relaxation cycle with $a = 0.9$. (f) Here is the canard. Courtesy of J. MÜLLER.

Relation 6.8 defines the critical manifold $S \equiv \{(x,y) : f(x,y;a,0) = 0\}$. In the slow subsystem the fast variable $x = x(y)$ is given by the critical manifold S , while the slow variable y evolves as before. In turn, in the fast subsystem the slow variable y is constant as x evolves. Suitable recombination of the dynamics in both subsystems reveals the dynamics of the initial problem in equation (6.6) and (6.7). In the VAN DER POL case, a critical parameter value a_c for the occurrence of canard cycles close to a HOPF-bifurcation exists under the following constraints [146]:

- The critical manifold S is cubic, i.e. S-shaped, with exactly two folds, see figure 6.5b.
- Between the two folds, the branch is repulsive, while the other two branches are attracting the dynamics towards the folds in the layer problem, see figure 6.5b.
- The two folds of S are generic, see [146].

Under these circumstances the system moves quickly towards one of the attracting branches heading towards the folds, compare with figure 6.5b. Approaching the fold, which forms a maximum, the dynamics quickly switches to the second attractive branch. In the oscillatory regime, the dynamics close to the fold, which forms a minimum, is locally attracted by a small amplitude limit cycle instead of switching to the second attracting branch. Obeying the conditions above, the limit cycle may follow partially the repulsive branch, which connects the two folds. As the control parameter a decreases the oscillation amplitude grows, thus follows a longer piece of the repulsive branch, see figure 6.5c. When the critical value a_c is approached, the repulsive nature of the non-attractive branch takes over and pushes the dynamics towards the second attractive branch onto a relaxation cycle, compare figure 6.5d,e.

Consequently, by the attractive and repulsive nature of the branches, relaxation cycles in this case can be excited. In any case, for $a < a_c$ the system follows the relaxation cycles. For $a > a_c$, there are initial conditions, which lead to a huge excursion via the left attracting branch before settling down close or at the minimum fold, compare with figure 6.5b. In particular, the system is highly sensitive to strong perturbations below the fold, close to the minimum. In this case, before returning to the attractor the dynamics follows at least one relaxation cycle. The oscillatory limit cycle solution (for $a_c < a < 1$) as well as the stationary solution (for $a > 1$) are locally stable against perturbations. However, both solutions are only locally stable within a very small region of the phase space.

A classical VAN DER POL oscillator of biological relevance in nerve fibre dynamics is the FITZHUGH-NAGUMO model [147–149]. It is a two-dimensional simplification of the famous HODGKIN-HUXLEY model [150], which tries to explain spike generation of action potentials and neuronal excitability. Quite recently canard phenomena have been found in different flavours of the HODGKIN-HUXLEY model [151–154] and finally lead to an understanding of the reason of firing and excitability. Before the discovery of the canard phenomenon in the model, at least, the firing events were not well understood since there is no clearly defined firing threshold within the HODGKIN-HUXLEY model. Furthermore, canard phenomena are also observed within the pattern forming BELOUSOV-ZHABOTINSKY reaction [155].

Where is the canard in the phenomenon? There are two explanations, which I am currently aware of [156]: For the occurrence of a canard transition the critical manifold necessarily must be cubic-shaped. As depicted in 6.5f a canard can be associated to a cubic shape. Alternatively, since canard cycles are hard to find, the phenomenon is related to newspaper canards.

Canards in half-sarcomeres

Apparently, the half-sarcomere model has all the properties of systems exhibiting the canard phenomenon: Explosions of the oscillator's amplitude with a jump in frequency are observed as well as excitable dynamics. However, the equations of motion for the half-sarcomere model allow not directly for a rigorous mathematical treatment of the canard phenomenon. The problem has to be unfolded before. To meet the conditions for a mathematical treatment, such as a standard form of a singular perturbed system, see equations (6.6) and (6.7), and a cubic shaped critical manifold, a nonlinear transformation from the physical variables Q and y to two new variables needs to be performed. Unfortunately this transformation is not obvious and I have not succeeded in finding one.

Experiments on muscle oscillations never reported a HOPF-like transition from the non-oscillatory to the oscillatory regime. This may be due to the fact that the experiments are inherently noisy and the HOPF-bifurcation can be blurred [157]. In addition, the excitability of relaxation cycles has interesting consequences in noisy environments: Noise induced relaxation excitations are not strictly periodic but are not easily distinguishable from noisy relaxation oscillations.

The following section describes the dynamics when κ is decreased below the critical value where the canard explosion occurred for $\kappa < \kappa_c$ where global bifurcations affect the dynamics.

6.1.3 Global bifurcations

Global bifurcations involve and affect large regions of the phase space in contrast to local bifurcations, such as HOPF-bifurcations, for example. By decreasing κ one naively would expect the relaxation cycles to continue or to vanish via a reversed HOPF-bifurcation. This is not what happens. Close to a critical value κ_{hom} a strong increase of the oscillation period is observed, while the amplitude remains unaltered, see figure 6.6a. The period scales logarithmically, see figure 6.6b. For even smaller values of κ , the dynamics becomes unbound. Since there is no stable dynamical state anymore the limit cycle must have been destroyed.

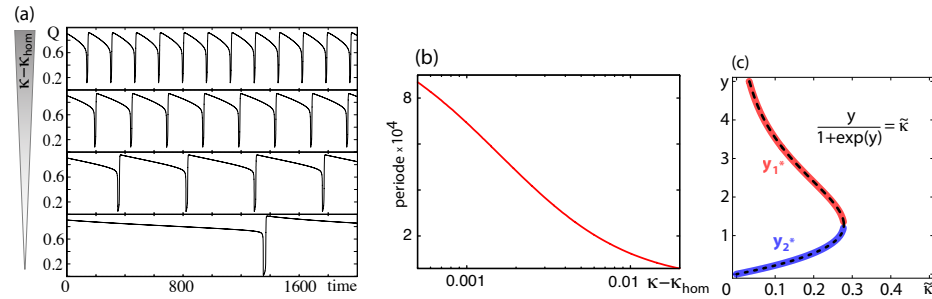


Figure 6.6 (a) Oscillation period strongly increases with decreasing κ . (b) The period scales logarithmically approaching the critical value κ_{hom} . (c) Emergence of two new fixed points y_1^* (red, dashed) and y_2^* (blue, dash-dotted), schematically. The black curve obeys $y / (1 + \exp(y)) = \bar{\kappa}$.

The strong alterations of the period correlates with the emergence of two new fixed points from nowhere, see figure 6.6c and bifurcation diagram in figure 6.7a. Remarkably, the equations of motion, see equations (6.1) and (6.2), allow for more than one stationary state. Besides the state that corresponds to $\bar{g}(y^*) = 0$ exists another state for $Q^* y^* - \kappa = 0$ with $Q^* = 1 / (1 + \omega(y^*))$. This state corresponds to an exact balance of elastic and motor forces for arbitrary element lengths and consequently is not present for $N = \text{const}$. Since $\omega(y)$ is approximately exponential the emergence of the two new fixed points can be schematically traced in figure 6.6c. There is a threshold value for κ at which $Q^* y^* - \kappa$ can be zero. Beyond the threshold there are always two values y_1^* and y_2^* , which fulfill $Q^* y^* = \kappa$.

A linear stability analysis around the two fixed points reveals one zero eigenvalue $\lambda_1 = 0$ and $\lambda_2 = y^* \omega'(y^*) - \omega(y^*) - 1$. Treating the curve in figure 6.6c as a function $\kappa(y)$, the maximum corresponds to the point of emergence of the

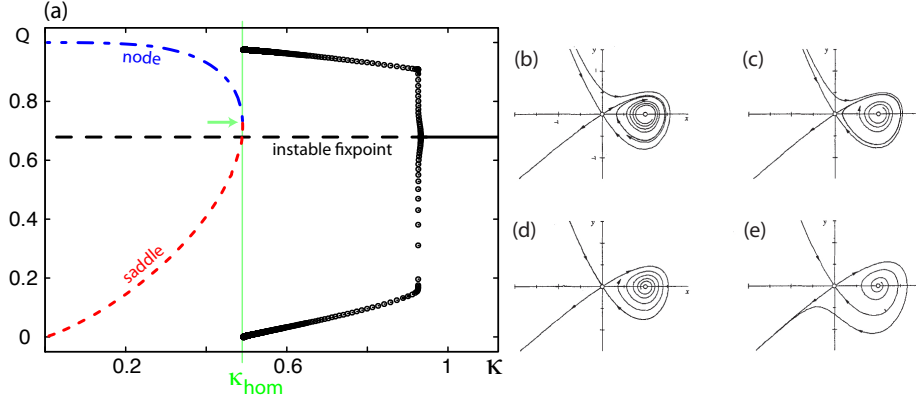


Figure 6.7 (a) Bifurcation diagram for a half-sarcomere element in κ . Decreasing κ destabilizes the only fixed point yielding limit cycle oscillations and a subsequent canard explosion. For $\kappa = \kappa_{\text{hom}}$ two new fixed points emerge via a saddle (red, dashed) - node (blue, dashed-dotted) bifurcation. The cyclic orbit is destroyed through a homoclinic bifurcation. (b-e) Generic homoclinic bifurcation taken from [127]. (b) A limit cycle in proximity to a saddle point (c) expands towards the saddle (d) and eventually collides with the saddle (e) yielding homoclinic orbits.

new fixed points. At this point $\kappa'(y) = 0$ while in the y_1^* regime $\kappa'(y_1^*) > 0$ and in the y_2^* regime $\kappa'(y_2^*) < 0$. Since $\kappa'(y) = \lambda_2(y) / (1 + \omega(y))$ and $\omega(y) > 0$, the second eigenvalue must have a different sign in the different y regimes: $\text{sgn}(\lambda_2(y_1)) \neq \text{sgn}(\lambda_2(y_2))$. This confirms that the emergence of the two fixed points above is a saddle-node bifurcation of fixed points. The flow in one direction (λ_2) changes sign between the fixed points while the flow in the other direction is determined by nonlinear terms only as $\lambda_1 = 0$. In order to obey the index theorem [127], one node must be a saddle point while the other node is either a stable or an unstable fixed point. Numerically I find that the second node is unstable.

The alterations of the oscillation period of the half-sarcomere element and the subsequent destruction of the limit cycle for small κ happens via a homoclinic bifurcation. This bifurcation type is linked to saddle points.

Homoclinic bifurcations

A homoclinic bifurcation occurs when parts of a limit cycle approach a saddle point [127, 128]. As shown in figure 6.7b-e, first a saddle node and a limit cycle coexists in phase space. By variation of a control parameter value the limit cycle

may approach the saddle point. Close to the saddle any trajectory on the limit cycle stays much longer close to the saddle than apart from the saddle point. Eventually, the limit cycle touches the saddle point and leaves a homoclinic orbit, while the loop is destroyed. By means of a dimensionless measure μ , which is zero at the bifurcation, the generic scaling law in this case are for the amplitude $\mathcal{O}(1)$ and the period of the cycle scales with $\mathcal{O}(-\ln \mu)$.

In the half-sarcomere case the global fixed points emerge for $\kappa = \kappa_{\text{hom}}$ very close to the limit cycle, see figure 6.8a. Due to the proximity, the dynamics is influenced by the preceding deformation of the phase space in anticipation of the emergence of the global fixed points. For that reason the period scales similar like for a homoclinic bifurcation at $\kappa = \kappa_{\text{hom}}$. However, the limit cycle does not collide at this point with the emerging saddle point. Therefore, the scaling of the period in figure 6.6b slabs from $\mathcal{O}(-\ln(\kappa - \kappa_{\text{hom}}))$. Decreasing κ does not so much alter the limit cycle, rather the new fixed points move along the Q nullcline, see figure 6.8b,c. The collision of the saddle and the limit cycle may occur for $\kappa \ll \kappa_{\text{hom}}$. In any case, non of the three fixed points could *escape* from the limit cycle without violating the index theorem. The theorem states that any closed orbit must enclose fixed points whose indices sum up to $+1$, while a node's index is $+1$ and a saddle point's index is -1 . Should one fixed point escape, the sum would change.

How does the system behave, when the limit cycle is destroyed? The dynamics follows a homoclinic orbit and becomes unbound. This corresponds to the case where the element shortens towards its minimal length. Since the description does not include a hard potential at the minimum length, the dynamics does not find an attractor at finite y . An introduction of a hard potential would barely alter the dynamics. The equations of motion would be unchanged for $\max(\ell_p, \ell_m) \leq \ell_0 \cdot x \leq \ell_p + \ell_m$. The previous unstable fixed point from the saddle-node bifurcation, would provide an attractor. In this case the emergence of the fixed points would involve a different scaling law for the oscillation period. A saddle node bifurcation with a saddle and stable fixed point on a limit cycle gives rise to a *sniper*² bifurcation, which scales with $\mathcal{O}(\mu^{-1/2})$.

Can the homoclinic behaviour be experimentally relevant? Muscle cells would have to fine tune parameter values to actively use the bifurcation as a oscillation period control. However, the influence of noise on the bifurcation is not clear. Very likely, nonlinearities play a role in half-sarcomeres, too. The saddle-node bifurcation in the model relies on the exact balance of elastic and motor forces for arbitrary element lengths. It is unlikely that this balance is fulfilled in the presence of nonlinearities.

²Saddle node infinte periode

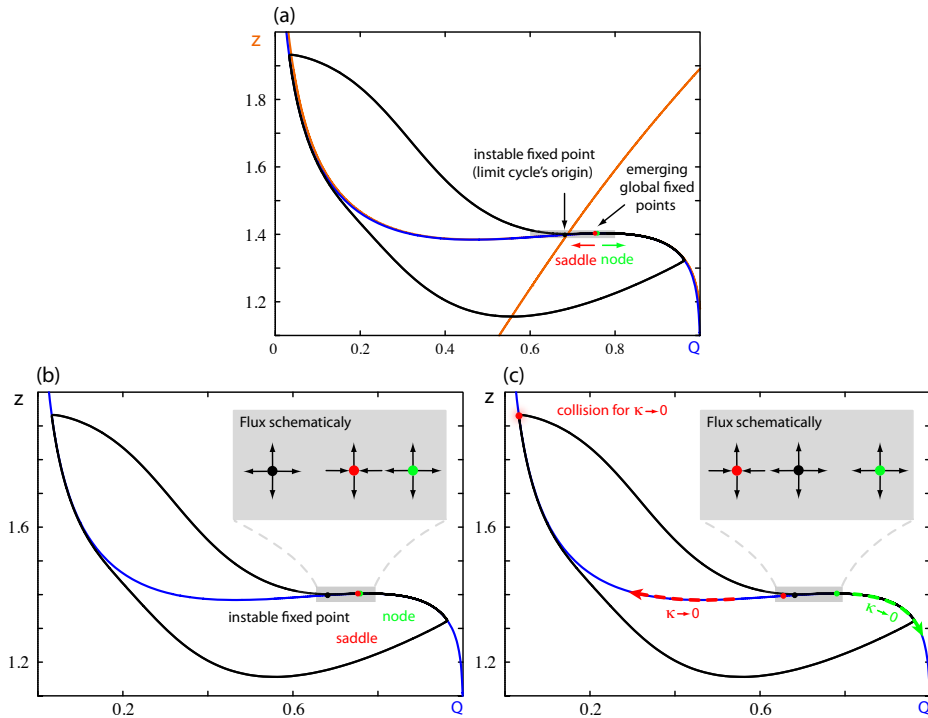


Figure 6.8 (a) Position of fixed points in the phase plane for $\kappa = 0.6$ with $z = Q + y$. Nullclines for Q (blue) and z (orange) and the corresponding relaxation cycle (black) are shown. (b) The flux in the phase plane of the fixed points with $\kappa = \kappa_{\text{hom}}$, schematically. (c) The flux for $\kappa \rightarrow 0$, schematically. Global fixed points move along the Q nullcline, eventually colliding with the relaxation cycle for $\kappa \rightarrow 0$.

6.2 Sarcomeres reloaded

The coupling of two half-sarcomeric elements to a sarcomere revealed in chapter 5 different oscillatory modes with distinct relative phase shifts of the two elements. This section's objective is to investigate these modes on a more profound level. By reflection symmetry the equations of motion for a sarcomere are \mathcal{Z}_2 symmetric, see the dimensionless equations of motion for a two element chain in appendix C.2: Exchange of left and right $(Q_1, y_1) \leftrightarrow (Q_2, y_2)$ does not alter the equations of motion. Any dynamical state of the left half swaps with the state of the right half by exchange of left and right.

The steady states of the two halves decouple from each other, see appendix C.3. Consequently, the linear stability conditions for spontaneous oscillations of half-sarcomeres remain valid for each element within a chain of elements. Sarcomere elements are able to oscillate spontaneously. All conclusions from the analysis of the half-sarcomere dynamics are valid for sarcomeres as well. It turns out that there are two oscillatory modes induced by HOPF-instabilities. One mode, denoted by \mathbf{O}_1 , obeys $x_1(t) = x_2(t + T/2)$ with the oscillation period T . In the second mode \mathbf{O}_2 the two extensions x_1 and x_2 are in phase, thus $x_1(t) = x_2(t)$.

\mathbf{O}_1 emerges at $\zeta_1 = 2\zeta$ while \mathbf{O}_2 emerges at $\zeta_2 = \zeta$ for the ζ in the sufficient stability condition in appendix B.3. By means of this condition, the \mathbf{O}_2 oscillations are always in the oscillatory regime of \mathbf{O}_1 , see [126]. The in-phase mode \mathbf{O}_2 is always unstable. Perturbations of the state with $x_1(t) = x_2(t)$ unbalance the forces in both halves of a sarcomere element. Due to the same mechanism that does not allow for homogenous contractions of chains the perturbations grow, see section 5.1.

Figure 6.9 summarizes the bifurcation scenario for the variation of ζ . For decreasing ζ the out-of-phase mode \mathbf{O}_1 becomes unstable at a critical parameter value $\zeta = \zeta_c$ [158]. While the frequency and the amplitude do not change the relative phase shift starts to deviate from half a period: $x_1(t) = x_2(t \pm \varphi)$ with $\varphi \neq T/2$. This state is denoted by \mathbf{Sw} . The \mathcal{Z}_2 symmetry ensures the emergence of two of these new solutions in accordance with the index theorem. The phase shift φ decreases but does not vanish for small ζ , since states with $\varphi = 0$ cannot be stable, see section 5.1. In figure 6.9 parameter values are chosen, where the canard phenomenon is not present. The canard case will be discussed below. Any parameter inducing spontaneous oscillations in half-sarcomeres leads to the emergence of oscillations for two coupled half-sarcomeres. Within the oscillatory regime, γ and κ can induce the phase deviation from $T/2$. Only ζ is observed to induce oscillations and destabilize the out-of-phase mode.

It is tempting but wrong to regard a sarcomere as two oscillators whose relative phase synchronizes. Classical physical synchronization is the adaptation of the cadence of weakly interacting self-sustained oscillators [159]. Due to the strong coupling between the half-sarcomere elements a sarcomere forms one self-sustained oscillator. In-phase, out-of-phase and dephased oscillations are different oscillatory modes [160] and are not a synchronization effect.

Is there a intuitive picture why the phase bifurcates? The following sections tries to get on in explaining the bifurcation scenario in figure 6.9 in terms of mode interactions and by a comparison to models for pulse coupled oscillators.

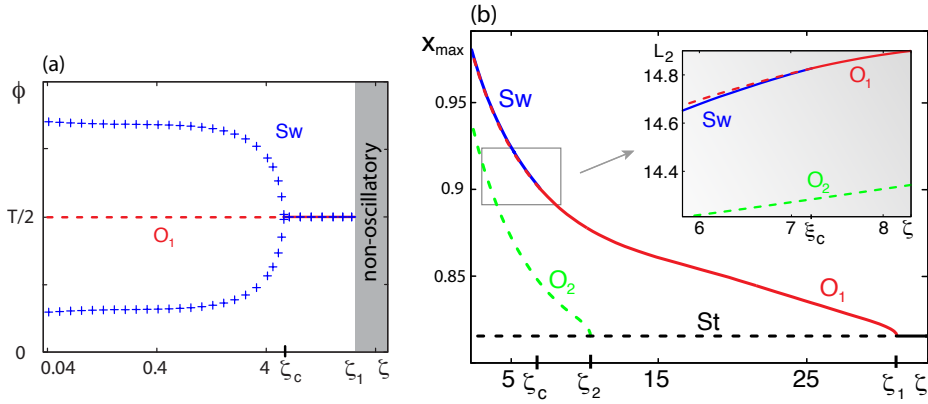


Figure 6.9 Oscillatory modes of sarcomere elements. (a) Pitchfork bifurcation of the relative phase $\phi(\zeta)$. For $\zeta = \zeta_1$ the stationary state becomes unstable yielding stable oscillatory states O_1 , which are phase shifted by $\phi = T/2$. For $\zeta = \zeta_c$, O_1 becomes unstable and the phase starts to deviate from $T/2$. (b) Bifurcation scenario of the amplitude of the half-sarcomere length x_{\max} for variation of ζ . Unstable states are dashed, stable states are continuous. For $\zeta > \zeta_1$ the system has a stable stationary state St , which destabilizes at $\zeta = \zeta_1$ yielding the oscillatory state O_1 . For $\zeta = \zeta_2$ a mode with $\phi = 0$ emerges, denoted by O_2 . For $\zeta = \zeta_c$, O_1 loses stability and another stable state Sw emerges. Inset: The destabilization of O_1 and the emergence of Sw in terms of the L_2 norm, which is defined by $L_2 = T^{-1} \int_0^T (Q_1^2 + Q_2^2 + y_1^2 + y_2^2) dt$ and better visualizes the cusp-like bifurcation of cycles. Parameter values in both figures corresponds to parameter values found in appendix A.2. For these parameters the system does not show an canard explosion. Hydrodynamic interactions between elements are included here, see chapter 7. The qualitative behaviour is unaltered by the interactions.

6.2.1 Mode interactions

Interaction³ of modes can lead to the occurrence of new solutions [161]. Here, the possibility of interactions between the two oscillatory modes O_1 and O_2 is revealed by the isotropy lattice corresponding to the dynamics equations [162, 163]. Such a lattice describes the symmetry hierarchy of possible solutions. Let \mathcal{Z}_2 denote the symmetry operation of exchanging left and right, $x_1(t) \leftrightarrow x_2(t)$, while \mathcal{T}_τ corresponds to a shift in time by τ , so that $x_1(t) = x_2(t + \tau)$. Oscillatory modes generally obey \mathcal{T}_T . In addition, the out-of-phase mode O_1 is symmetric with respect to the combination of the symmetry operations $\mathcal{Z}_2\mathcal{T}_{T/2}$, while

³Mode interaction may not be mixed up with usual *mode coupling* from classical mechanics.

the in-phase mode \mathbf{O}_2 is symmetric with respect to \mathcal{Z}_2 . Correspondingly, the isotropy lattice for increasing ζ from left to right reads

$$\begin{array}{ccc}
 \mathbf{Sw} : \mathcal{T}_T & \begin{array}{l} \swarrow \\ \searrow \end{array} & \begin{array}{l} \mathbf{O}_1 : \mathcal{Z}_2 \mathcal{T}_{T/2} \times \mathcal{T}_T \\ \mathbf{O}_2 : \mathcal{Z}_2 \times \mathcal{T}_T \end{array} & \begin{array}{l} \swarrow \\ \searrow \end{array} & \mathbf{St} : \mathcal{Z}_2 \times \mathcal{T}_\tau \\
 & \longrightarrow \zeta & & &
 \end{array} \quad (6.12)$$

For large ζ the system is in stationary state \mathbf{St} with $x_1 = x_2 = x^*$ and the state is symmetric with respect to \mathcal{Z}_2 and arbitrary shifts in time τ . This solution is the most symmetric and displays the same symmetry as the dynamic equations. HOPF-bifurcations spontaneously break this symmetry and generate the solutions \mathbf{O}_1 and \mathbf{O}_2 on the next hierarchy level for decreasing ζ . If mode interaction would generate the dephased solution \mathbf{Sw} at the next hierarchy level, then the nonlinear coupling of the modes \mathbf{O}_1 and \mathbf{O}_2 demanded for a shared symmetry of the two modes. The only shared symmetry is the periodicity \mathcal{T}_T . However, mode interaction demands that the frequencies of the interacting oscillatory modes \mathbf{O}_1 and \mathbf{O}_2 at the critical value $\zeta = \zeta_c$ are equal. Numerically I find that they are not equal in general. Thus, mode interaction does not create the dephased mode \mathbf{Sw} .

6.2.2 Pulse-coupled oscillators

Intuitively sketched, oscillations of a half-sarcomere element results from cyclic shortening and motor detachment avalanches, see section 5.2.3. From a different perspective the elements' tensions cyclically vary. In an element in the relaxed state, tension is low since weak motor forces are sufficient to balance the element's elasticities, which are almost at rest. Tension slowly increases due to the ongoing action of motors against elastic elements. The increase in tension is approximately linear since the shortening velocity is nearly constant. Reaching a critical tension the motors have to let go and the element lengthens. The element's tension is released fast in comparison to the duration of the tension build up. Consider two half-sarcomeric elements, which are coupled together to a sarcomere. A sudden lengthening of one element is felt by the neighbour as a mechanical pulse⁴, a kick. The shorter the lengthening phase, the sharper the kick. With decreasing ζ a half-sarcomere element stretches faster and eventually submits a shorter kick⁵.

⁴In an overdamped environment (at low REYNOLDS number) the mechanical pulse is less a momentum transfer than a temporal limited strong external force.

⁵Setting $Q = 0$ in the force balance equation gives an explicit expression for the element's response time scale in dependence of ζ .

The relaxation of half-sarcomeric elements is comparable to pulse-coupled oscillators in models for integrate-and-fire neurons [164]. The membrane potential of neurons increases with a constant rate and is instantaneously reset when a certain threshold potential is reached. Cyclic repetitions of the rising and falling potential are a built-in feature of the models. Consider now two of such neurons that are coupled so that upon resetting a neuron transmits an electric pulse to the adjacent neuron. The pulse influences the neighbour's membrane potential. In the case described by VAN VREESWIJK in [164] it is an inhibitory coupling, which decreases the neighbour's membrane potential. Broad pulses lead to a state of periodically firing neurons with a relative phase shift of half of the oscillation period. This state becomes unstable for short pulses [164, 165]. The relative phase shift starts to deviate from half a period. Here, a phase equation gives the critical value of the parameter, which determines the half-life of the transmitted pulse.

What the electrical pulse for the neuron is the mechanical pulse for the half-sarcomeres. Membrane potential on the one hand and mechanical tension on the other hand, both reach a threshold. Shorter pulses lead to dephased solutions in both cases.

Muscle oscillations emerge via spontaneously broken symmetries, while membrane potential oscillations are enforced. I did not find a way to map the sarcomere's equations of motion directly to the simple neuronal model. Although I currently lack a thorough understanding of the reason for the emergence of the dephased solution, the similarities to pulse-coupled oscillators have been exposed [166].

The following section expands the homoclinic behaviour of half-sarcomere elements from section 6.1.3 to sarcomere elements.

6.2.3 Gluing-like bifurcations

Homoclinic behaviour persists in a chain of two half-sarcomeres. This not so much a surprise since its origin from a global saddle-node bifurcation is unaltered in a chain of elements. However, here, homoclinic behaviour comes in a different raiment and has a very descriptive name: A gluing bifurcation. I will now give a short introduction on gluing bifurcations.

In 1984 a group of french mathematicians discovered a new sort of bifurcation: The gluing of cycles [167]. Homoclinic bifurcations occur through the collision of limit cycles with saddle points, eventually destroying the cycle. A gluing bifurcation is quite similar. In essence, two limit cycles that both approach a saddle point, would be destroyed as in the homoclinic case. Here,

the two partially destroyed cycles pool together, they *glue* together, keeping up oscillatory behaviour. Figure 6.10 sketches the sequence. Since a gluing bifurcation is composed of a homoclinic bifurcation (two cycles approach the saddle node) followed by a reversed homoclinic bifurcation (one glued cycle departs from the saddle node), the period's scale behaviour is the same as for homoclinic bifurcations. Gluing bifurcations have been observed experimentally, although a loss of a perfect \mathcal{Z}_2 symmetry is unavoidable [168]. Further insight into gluing bifurcations is reviewed in [169].

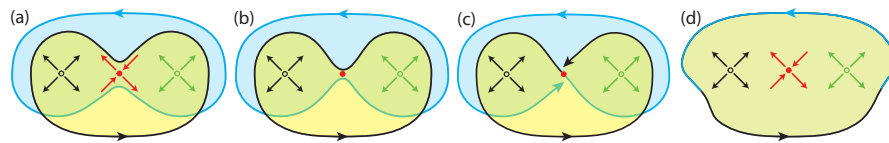


Figure 6.10 Gluing bifurcation in a projection of a four-dimensional phase-space, schematically. (a) Two distinct limit cycles each enclosing an unstable node (black and green) approach a saddle point (red). (b) Collision of the cycles with the saddle. (c) Limit cycles are destroyed through the collision. (d) Phase space is unchanged, thus gluing of both cycle's remaining parts can keep up oscillatory behaviour.

In sarcomere elements I find gluing-like dynamics [170]. Figure 6.11 summarizes a gluing of two cycles at $\kappa = \kappa_g$ in terms of the element's length. For $\kappa \lesssim \kappa_g$, reflection symmetry is spontaneously broken: Exchange of $x_1 \leftrightarrow x_2$ does not leave the same solution as before, see figure 6.11a. Upon an increase in κ so that $\kappa \gtrsim \kappa_g$ the \mathcal{Z}_2 symmetry is spontaneously restored, see figure 6.11c. Restoring happens via a gluing of the system's limit cycles. A projection of phase space in figure 6.11b shows two distinct limit cycles, which glue together to one single cycle⁶, see figure 6.11d. The scale behaviour of the periods at the bifurcation is as expected, see figure 6.12. The dynamics is reminiscent of a gluing bifurcation but it is not such a bifurcation. Generically, gluing bifurcations are of codimension-2, at least two parameters have to be varied for the dynamics to bifurcate. What is observed here is gluing-like ghost dynamics. In nonlinear dynamics one tries to understand the dynamics of a system starting with its stationary, fixed, points. Such points can emerge by parameter variation. Approaching the critical parameter value also means that the dynamics possibly behaves as if the fixed point would already have appeared. Such a situation is sketched in figure 6.13. Although the saddle node is not present at first, the dynamics is well aware of its *approach*.

⁶The index theorem is not violated in a gluing bifurcation. Both limit cycles share one degenerate unstable node.

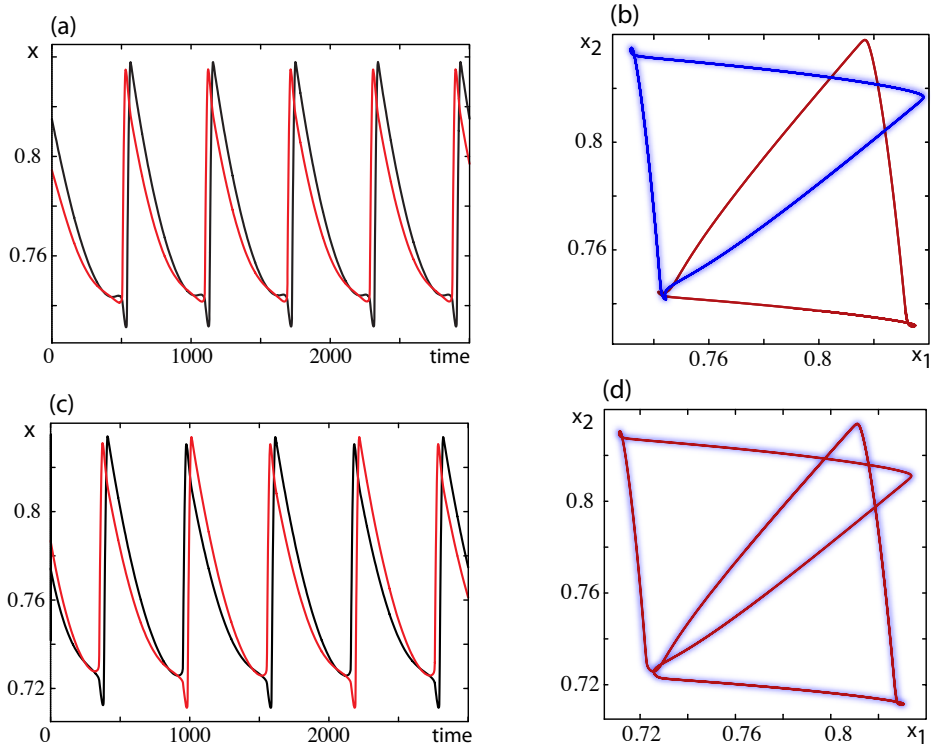


Figure 6.11 Gluing bifurcation in sarcomere elements with $\zeta = 33$. (a) One possible solution of the system for $\kappa = 0.63$. (b) Phase space of the cycle in a) in red and the corresponding second cycle for exchange of $x_1 \leftrightarrow x_2$. (c) Both cycles glue together for $\kappa = 0.64$. (d) Phase space of the cycle in c). Only one degenerate cycle remains.

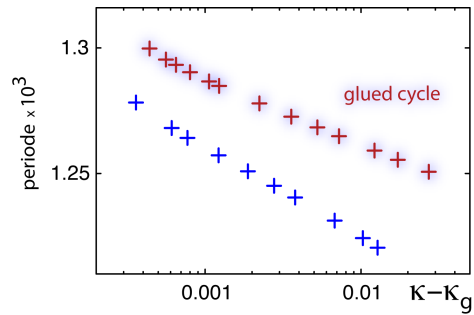


Figure 6.12 Scale behaviour of periods of the gluing of cycles in figure 6.11. Periods of the unglued cycles (blue) and the glued cycles (red) scale similarly like in the homoclinic case.

Gluing-like dynamics is observed although for the parameters in figure 6.11 no saddle point is present. Since the emergence of the saddle node is independent of ζ but $\kappa > \kappa_{\text{hom}}$, compare section 6.1.3, the saddle cannot be present. The dynamics, however, behave like there is a saddle point.

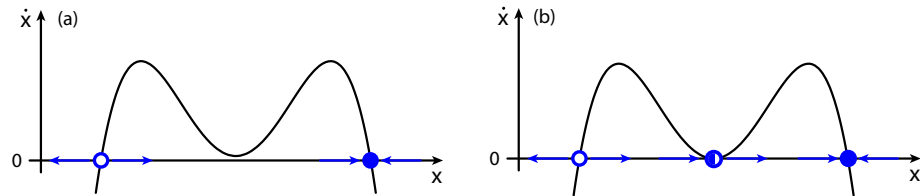


Figure 6.13 Ghost dynamics, schematically. Arrows indicate the system’s dynamics. Filled circles are stable, blank circles are unstable nodes. The semi-filled circle is a saddle. (a) Situation without a saddle point. (b) Parameter variation makes the saddle appear. In both cases a) and b), the dynamics is similarly.

Experimental detection of a gluing transition in sarcomeres would not be possible by specifying the sarcomere’s length through tracking of Z-discs. Before and after the gluing-like transition the lengths of the sarcomere element $x_1 + x_2$ are indistinguishable. Detection demands half-sarcomere length recordings via fluorescent markers of the M-line like it was demonstrated in [82]. The spontaneous restoring of the \mathcal{Z}_2 symmetry through the gluing-like behaviour has a dramatic effect when hydrodynamic interactions are taken into account and will be discussed in chapter 7.

6.2.4 Period doubling and chaotic behaviour

Sarcomere elements are capable of undergoing pitchfork bifurcations of cycles [126]. In terms of the half-sarcomeric element lengths, a dephased solution of equal amplitude oscillations bifurcates into solutions with different amplitudes of neighbouring elements. Hence, another symmetry is spontaneously broken. Since a previously dephased solution has already spontaneously broken \mathcal{Z}_2 symmetry a destabilization of equal amplitude oscillations gives rise to two new solutions since the equations are \mathcal{Z}_2 symmetric. Period doubling bifurcations are also observed. Cascades of period doubling bifurcations occur and intermittent chaotic behaviour is found, compare with [171]. In the chaotic regime, the sarcomere element oscillates with a fixed frequency. The amplitude of one half of the sarcomere element behaves chaotic while the other half oscillates regularly.

6.2.5 Generalized canard phenomenon

An equivalent to the canard phenomenon in half-sarcomere elements exists in systems with two coupled elements: *Mixed-mode* oscillations. Cyclic dynamics switch between small amplitude oscillations and large relaxation cycles. Figure 6.14 shows a phase space projection of the process. Small amplitude oscillations dynamically switch towards relaxation cycles. On the relaxation cycle, the system undergoes a huge excursion. The relaxation cycles, drive the system back to the basins of attraction of the small amplitude oscillations and the whole cycle restarts.

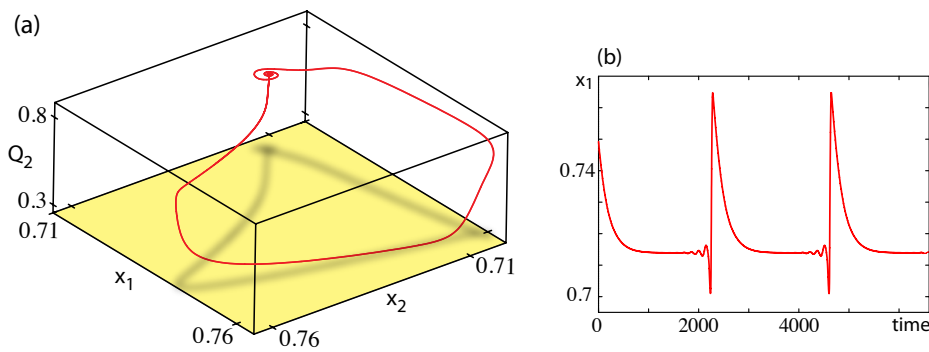


Figure 6.14 Mixed-mode oscillations with $\zeta = 63$. (a) For a better visibility of mixed mode cycles the phases space is extended by the element's length x_1 and x_2 . Small amplitude oscillations alternate with relaxation cycles. (b) Element length x_1 versus time for the situation in a).

Mixed-mode oscillations are intimately linked to the canard phenomenon [153, 172] and can be interpreted as a generalization of the canard phenomenon [173]. On the experimental side mixed-mode oscillations are observed in the BELOUSOV-ZHABOTINSKY reaction.

6.3 Chain of half-sarcomeres

In chains of half-sarcomeric elements no conceptually new dynamical effects are found. A chain's steady state decomposes into the identical steady states of its constitutive half-sarcomere elements. Spontaneous oscillations emerge close to an HOPF-instability so that adjacent elements oscillate with equal amplitude and frequency but phase shifted by $T/3$ [126]. The mode can destabilize leading to a low phase shift between adjacent elements. This state corresponds to the

relaxation waves that were introduced in section 5.3. In the homoclinic regime chains exhibit a strong alteration of the oscillation period similar to single half-sarcomeres. The chain is also excitable for parameter values that give rise to the canard phenomenon in half-sarcomere elements.

Chains of half-sarcomere elements self-organize into states of spontaneous wave patterns. Waves are a mode of chains triggered by pulse coupling. The mode is excitable and can vary vastly in its oscillation frequency. Dynamical effects spontaneously break the symmetries of half-sarcomere elements and chains of elements and permit for wave dynamics. In the following chapter symmetries that are spontaneously broken will allow a conceptual design of a microscopic swimmer to self-organize into directed motion. The swimmer is driven by microscopic force generators and restores its shape via elastic elements.

Chapter 7 A simple self-organized microscopic swimmer

Swimming within fluids is an important aspect of the life of micro-organisms. In search for food and partners for mating, active controlled motion enhances the chance of success. Some micro-organisms use flagella and cilia to move within fluids. Autonomous swimming is driven by molecular motors that act as force generators. Even though, owing to the complicated structure of the filament-motor assemblies that are responsible for self-propelled beating patterns, swimming of micro-organisms is not very well understood. Beside the works of TAYLOR, PURCELL, SHAPER and WILCZEK, microscopic swimmers have only recently attracted attention. Mechanisms that generate the beating patterns of micro-swimmers eventually leading to swimming have mostly been disregarded.

This chapter tries to open a door by providing a conceptual study of a self-propelling swimmer. Mechanisms will be suggested, which produce motion that self-organizes into swimming states. The minimal demands for self-propelled swimming without external influences for this conceptual swimmer will be exposed.

Microscopic objects moving in simple fluids have a different experience of the physical laws than humans have. Their life at low REYNOLDS number will initiate this chapter. Strategies that allow for swimming under these conditions will be discussed thereafter. A short introduction to fluid hydrodynamic of spherical objects and geometrical implications will open the stage for a simple swimmer. The swimmer is self-propelling and is driven by the self-organized collective action of molecular force generators.

7.1 Physical aspects of low Reynolds number swimming

Life at low REYNOLDS number is different from human's everyday experiences [174, 175]. Swimming is also different. Swimming is a repetitive self-generated motion, i.e. a cyclic deformation of a body, in order to propel in a fluid by natural means. For the purpose of providing an intuitive explanation what so different is, I recall the definition of the REYNOLDS number from the beginning of chapter 5,

$$\text{Re} \sim \frac{\text{inertia forces}}{\text{friction forces}} . \quad (7.1)$$

Humans that swim in water have $\text{Re} \approx 10^4$, fish have $\text{Re} \approx 10^2$ and micro-organisms have $\text{Re} \approx 10^{-4}$. Humans can push against water and wait. Momentum transfer between the water and the body is significant enough to overcome friction, at least for a while, and a human will have propagated some distance. Thereby, the speed and the pattern of the human's stroke in the water accounts for the propelled distance. Humans can even use reciprocal motion to swim. A forward stroke is followed by the same stroke backwards, but at a different speed. Since the fluid equations are time dependent, a complete stroke results in a net motion. Micro-organisms can push against water and wait, too. Nothing will happen. The motion is so weak that the organism's momentum transfer to the water is negligible. For humans, the swimming of micro-organisms may best be compared with humans trying to move within quick sand or in swamp. Reciprocal motion of micro-organisms would lead to a certain displacement during the forward stroke. During the backward stroke exactly the same displacement, but in the opposite direction, will bring the micro-organism back to its starting point. The possibly different speeds of the strokes do not matter since the fluid equations are independent of time in the low REYNOLDS number regime, which illustrates nicely PURCELL's scallop theorem [175]: At low REYNOLDS number, displacements through swimming strokes are independent of time.

How do micro-organisms swim? Overcoming both, the lack of a relevant fluid inertia and the time invariance of displacements through swimming strokes is possible. Nature elegantly takes possession of the friction itself, for swimming. Thereby hydrodynamic interactions are of great importance.

7.2 Swimming strategies

Swimming of microscopic objects in aqueous environments has to deal with two concerns: The object's shape has to change and a mechanism that drives the shape changes is needed. This section concentrates on the former aspect.

Microscopic swimming relies on sequences of geometrical shape changes [174, 176]. Due to the lack of fluid inertia, swimming requires at least two degrees of freedom for shape alterations [175]. A proposal of a simple swimmer consists of three rods, which are connected by two hinges. Non-reciprocal changes of the relative angle between the rods allow for swimming [175]. Another proposal consist of two spheres that are connected by a linker, which periodically changes its length. For swimming the *pushmepullyou* swimmer needs to cyclically resize the spheres' radius [177].

Another sphere based swimmer with constant radius of the spheres has been proposed: The swimmer consists of three identical rigid spheres, which are aligned along the x -axis, see figure 7.1. Adjacent spheres exert forces on each other, which are generated within the linkers. The linkers periodically change their length [178–181]. Correspondingly, the three-sphere swimmer is symmetric with respect to exchange of left and right, i. e. space inversion.

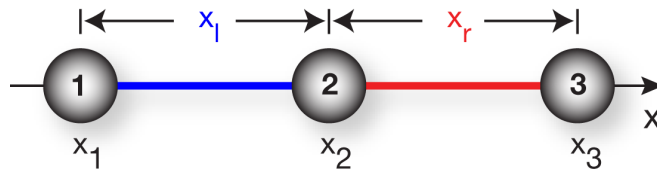


Figure 7.1 Three-sphere swimmer introduced in [178]. Three rigid spheres are connected by linkers. The length of the left and the right linker x_l and x_r , respectively, can change periodically. For certain sequences the center of mass $(x_1 + x_2 + x_3)/3$ propagates.

In addition, concepts of butterfly swimmer [182], toroidal swimmer [175, 183, 184], as well as swimmers that are driven by rotating elastic rods [185] have been proposed, see also [186, and references therein]. Some ideas suggest to use fluctuations on the microscale like a swimming ratchet [187]. Swimmers performing reciprocal motion can propel as well as long as they interact with each other [188, 189] or use their body's inertia [190] to swim.

Micro-organisms in nature often use cilia and flagella [16, 191] for swimming. Eucaryotic cells autonomously move through the action of molecular motors within the cellular appendages. Attempts to incorporate mechanisms that drive

the shape changes of conceptual designs of swimmers are restricted to cilia and flagella [100, 101]. Currently none of the artificial swimmers introduced above provide a driving mechanism. Experimentally realized micro-swimmers also rely on external alternating magnetic fields [192–194].

In order to conceptually assemble a simple self-driven and self-organized swimmer it is necessary to have a short excursion into hydrodynamic interactions. Starting from the NAVIER-STOKES equation the motion of rigid spheres, which move in a simple newtonian fluid, will be derived. For review see [195].

7.3 Hydrodynamic interactions

The fundamental equation of fluid motion, the NAVIER-STOKES equation, for an incompressible fluid with $\nabla \cdot \mathbf{u} = 0$ reads [196],

$$\eta \nabla^2 \mathbf{u} - \nabla p + \mathbf{f} = \rho [\partial_t \mathbf{u} + (\mathbf{u} \cdot \nabla) \mathbf{u}] \quad , \quad (7.2)$$

with the fluids flow field $\mathbf{u}(\mathbf{r}, t)$ at position \mathbf{r} and time t , the pressure $p(\mathbf{r}, t)$ and the force density $\mathbf{f}(\mathbf{r}, t)$, while η is the fluid's viscosity and ρ its mass density. In the limit of low REYNOLDS number equation 7.2 reduces to the linear STOKES (creeping flow) equation [197, 198],

$$\eta \nabla^2 \mathbf{u} - \nabla p + \mathbf{f} = 0 \quad . \quad (7.3)$$

A GREEN's function for this problem is provided by the OSEEN tensor $\mathbf{H}(\mathbf{r})$. This tensor gives a solution for the STOKES equation in the case of a vanishing flow at infinity, $\lim_{r \rightarrow \infty} \mathbf{u}(\mathbf{r}, t) = 0$, so that

$$\mathbf{u}(\mathbf{r}, t) = \int d^3 r' \mathbf{H}(\mathbf{r} - \mathbf{r}') \cdot \mathbf{f}(\mathbf{r}', t) \quad . \quad (7.4)$$

In the case of an infinitely large fluid without boundaries the OSEEN tensor is given by

$$\mathbf{H}(\mathbf{r}) = \frac{1}{8\pi\eta} \left(\frac{\mathbf{I}}{r} + \frac{\mathbf{r}\mathbf{r}}{r^3} \right) \quad , \quad (7.5)$$

This GREEN's function is known as a *stokeslet*.

In 1922, FAXÉN related the velocity \mathbf{v} of a sphere with radius R to the force \mathbf{f} and the external flow \mathbf{u} acting on the sphere, which is immersed in a fluid. Assuming no slip boundary conditions¹ on the spheres surface while

¹No slip on the body's surface guarantees that the body is force and torque free.

neglecting the (counter-) flow field induced by the motion of the sphere and in combination with the *stokeslet approximation*, which allows only point forces so that $\mathbf{f}(\mathbf{r}, t) = \mathbf{f}(t) \cdot \delta(\mathbf{r})$, FAXÉNS first law [197] states that

$$\mathbf{v} = \frac{1}{6\pi\eta R} \cdot \mathbf{f} + \mathbf{u} + \frac{R^2}{6} \nabla^2 \mathbf{u} \quad . \quad (7.6)$$

In this case equation (7.4) reduces to $\mathbf{u}(\mathbf{r}, t) = \mathbf{H}(\mathbf{r}) \cdot \mathbf{f}$. At large distances $r \gg R$, the last term in equation (7.6) can be ignored since the flow field appears nearly uniform. Thus, the sphere is simply advected by the external flow for vanishing forces on the sphere: $\mathbf{v} = \mathbf{u}$.

In a colloidal suspension the motion of a sphere influences the other spheres. If the fluid field that is experienced by a sphere i at position \mathbf{r}_i is generated only by the motion of the other spheres j , which are subject to forces \mathbf{f}_j , the sphere's velocity is given by the force acting on the sphere and by a superposition of the flow fields [198] so that

$$\frac{d\mathbf{r}_i}{dt} \equiv \dot{\mathbf{r}}_i = \sum_j \mathcal{M}_{ij} \mathbf{f}_j \quad . \quad (7.7)$$

The mobility tensor \mathcal{M} is symmetric, $\mathcal{M}_{ij} = \mathcal{M}_{ji}$, and depends on the distance of the spheres $|\mathbf{r}_{ij}|$ with $\mathbf{r}_{ij} = \mathbf{r}_i - \mathbf{r}_j$, the spheres' radius R and the fluid's viscosity η ,

$$\mathcal{M}_{ij} = \begin{cases} (6\pi\eta R)^{-1} \cdot \mathbf{I} & : i = j \\ \mathbf{H}_{ij} & : i \neq j \end{cases} \quad . \quad (7.8)$$

Neglecting the OSEEN tensor's contribution, $\mathbf{H}_{ij} \equiv 0$, equation (7.7) corresponds to the STOKES friction for a sphere. Including hydrodynamic interactions via \mathbf{H}_{ij} gives a contribution to a sphere's motion by the motion of other spheres. The contribution is mediated by the fluid flow, which is generated by the movement of other particles in the fluid. The OSEEN tensor \mathbf{H}_{ij} for spheres emerged in a fluid is given by [199]

$$\mathbf{H}_{ij} = \frac{1}{4\pi\eta R} \left[\left(\frac{R}{r_{ij}} + \mathcal{O}(r_{ij}^{-3}) \right) \cdot \mathbf{e}_{ij}^{\parallel} + \left(\frac{1}{2} \frac{R}{r_{ij}} + \mathcal{O}(r_{ij}^{-3}) \right) \cdot \mathbf{e}_{ij}^{\perp} \right] \quad , \quad (7.9)$$

with the unit vectors $\mathbf{e}_{ij}^{\parallel}$ along and \mathbf{e}_{ij}^{\perp} perpendicular to the sphere's distance r_{ij} . Note that the approximations above are only valid for distances between spheres that are large in comparison to the sphere radius, $r_{ij} \gg R$.

The motion of rigid spheres, which are immersed in a fluid, is governed by equation (7.7). Forces that induce the colloids' motion, can be externally applied to the colloidal particles or internally generated through interaction of the particles. A self-propelling swimmer implies forces that are internally generated. Internal forces, per definition, balance so that $\sum_j \mathbf{f}_j = 0$. A swimming ensemble that is composed of identical spheres changes its center of mass like $\sum_i \dot{\mathbf{r}}_i$. Neglecting hydrodynamic interactions, $\mathbf{H}_{ij} = 0$, in this case cannot result in a net motion of the ensemble, according to equation (7.7). For self-generated motion for the purpose of swimming hydrodynamic interactions are essential. In terms of conservation laws is swimming based on momentum conservation between the swimmer and the surrounding fluid. The transfer of momentum induces a fluid flow by an object's motion. Without hydrodynamic interactions the fluid flow is neglected.

From a different perspective this result reappears from a purely geometrical point of view. The creeping flow, see equation (7.3), is independent of time. A swimmer's propagation depends only on the pattern of its shape changes. Swimming at low REYNOLDS number can be reduced to a purely geometrical problem. This idea will be clarified by means of the three-sphere swimmer in the following section.

7.4 Geometrical aspects of the three-sphere swimmer

SHAPER and WILCZEK proposed a purely geometrical analysis of swimming of microscopic organisms [176]. Patterns of shape changes govern a swimmer's propulsion.

In the three-sphere swimmer, see figure 7.1, each sphere i with radius R is located at position x_i . The swimmer has two degrees of freedom, namely the sphere's left and right distances $x_l \equiv x_2 - x_1$ and $x_r \equiv x_3 - x_2$. The distances vary cyclically with period T upon periodically varying forces $f_i(t) = f_i(t + T)$ that act on sphere i . Forces are produced internally within the linkers between two adjacent spheres so that both attached spheres are exposed to the same force but with different sign. Correspondingly, in the absence of external forces on the swimmer all internal forces balance. The swimmers center of mass x_s is given by $x_s = (x_1 + x_2 + x_3)/3$. Under these circumstances the displacement of

the swimmer after one cycle \bar{x}_s implies

$$\bar{x}_s = \int_0^T \dot{x}_s dt \quad . \quad (7.10)$$

The displacement can be rewritten, see appendix D, as an integral over the oriented surface O encircled in the (x_l, x_r) -plane during one cycle of the periodic motion, see figure 7.2,

$$\bar{x}_s = \oint_O C(x_l, x_r) dx_l \wedge dx_r \quad . \quad (7.11)$$

The field C is symmetric with respect to space inversion $C(x_l, x_r) = C(x_r, x_l)$ and depends only on the mobility tensor \mathcal{M}_{ij} . C varies directly with R and scales inversely as a square of the distance of the spheres. Finally, the swimmer's velocity v_s is determined by the surface in the (x_l, x_r) -plane of the shape changes and the oscillation period with $v_s = \bar{x}_s/T$.

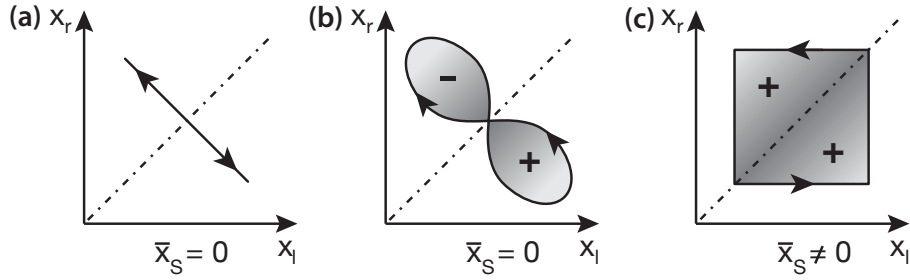


Figure 7.2 Schematic representation of the three-sphere swimmer's possible motions. (a) Reciprocal motion without net displacement. (b) Non-reciprocal motion with a vanishing displacement after one cycle. (c) Motion that allows for swimming as originally suggested by [178].

Exchange of the left and right sides of the swimmer, i.e. space inversion, inverts the swimming direction $\bar{x}_s \rightarrow -\bar{x}_s$. The orientation dependence in the integral in equation (7.11) emerges through the property of differential forms, which is $dx_l \wedge dx_r = -dx_r \wedge dx_l$. In the approximation (7.9) for the OSEEN tensor, the field C is independent of the fluid's viscosity. Any viscosity dependence of the swimmer's speed v_s is only mediated via shape changes in the (x_l, x_r) space or alterations of the swimming cycle's period T .

When does a sequence of shape changes lead to a net propagation? First of all, the field C must be nonzero. Neglecting hydrodynamic interactions, i.e. $\mathbf{H}_{ij} = 0$, yields $C = 0$. Any motion that considers local friction only can not lead to a net locomotion. Yet, for $C \neq 0$ a swimmer's displacement per cycle can vanish. Figure 7.2 illustrates several situations: A trivial case is any kind of reciprocal motion, whose path retraces itself in the (x_l, x_r) -plane, see figure 7.2a. Such motion illustrates PURCELL's scallop theorem. Paths encircling an oriented surface, which is unchanged upon space inversion so that x_l and x_r exchanges, would also not lead to a net motion, compare with figure 7.2b. This corresponds to situations in which the path is split up into two halves by the $x_l = x_r$ line while each half is a mirror image of the other. If the mirror images have different orientations, the swimmer's shape changes lead to net locomotion, see figure 7.2c. Any motion that is symmetric under space inversion in combination with time reversal ($t \rightarrow -t$) allows for swimming. For all paths that are not symmetric according to space inversion only the evaluation of the surface integral in expression (7.11) gives the amount of the net displacement per cycle.

In summary, swimming is possible for motion that is symmetric under a combined space and time inversion or for motion that breaks space inversion symmetry. The latter case can have a vanishing displacement per cycle. That far, the swimming motion inducing forces are imposed. Self-propulsion demands for forces that are generated internally. Any micro-swimmer in nature and any future microscopic man-made swimmer needs a force generating mechanism. The following section proposes a self-propelled and self-organized swimmer. Forces are generated locally within the linker according to mechanisms that generate forces in muscles. Elastic elements in combination with force generators, such as molecular motors, can drive spontaneous swimming motion of the three-sphere swimmer.

7.5 Simple swimmer driven by molecular motors

The self-propelled swimmer consists of three identical spheres and two identical elements linking the spheres. Linkers actively change their length and thereby exert forces on the attached spheres. Internally, a linker consists of molecular motors, which collectively act against elastic elements. The composition of each linker is identical to the model of a half-sarcomere, which was introduced in chapter 5, see figure 7.3. The structures have been shown to oscillate spontaneously in length. This section will adapt the equations of motion from



Figure 7.3 Self-propelled swimmer with force generating linkers, which resemble muscle half-sarcomeres.

section 5.3 for two coupled half-sarcomeres to the swimmer case, where hydrodynamic interactions are taken into account. Thereupon the swimmer's possible dynamics will be analyzed and will be related to its swimming behaviour.

Motor and elastic forces balance through equation (7.7) with $f_1 = -f_1^m - f_1^e$, $f_2 = -f_1 - f_3$ and $f_3 = f_r^m + f_r^e$. The subscripts l and r distinguish the left and right linker, respectively. The three-sphere model swimmer is treated one-dimensionally, hence, hydrodynamic interactions are restricted along the swimmer's axis. The mobility tensor reduces to $\mathcal{M}_{ii} = \zeta^{-1}$ for $i = 1, 2, 3$, $\mathcal{M}_{12} = (2\zeta/3)^{-1} \cdot R/x_l$, $\mathcal{M}_{13} = (2\zeta/3)^{-1} \cdot R/(x_l + x_r)$ and $\mathcal{M}_{23} = (2\zeta/3)^{-1} \cdot R/x_r$ with $\zeta = 6\pi\eta R$. Finally, the dimensionless force balance equation yields

$$\begin{aligned} \zeta \dot{x}_{l,r} &= \left\{ \frac{3R_l}{x_{l,r}} - 2 \right\} \cdot F(x_{l,r}, Q_{l,r}, y_{l,r}) \\ &+ \left\{ \frac{3R_l}{2} \left(\frac{1}{x_l + x_r} - \frac{1}{x_l} - \frac{1}{x_r} \right) + 1 \right\} \cdot F(x_{r,l}, Q_{r,l}, y_{r,l}) \quad , \end{aligned} \quad (7.12)$$

with dimensionless x , Q and y , see section 6.1, $R_l = R/\ell_0$ and

$$F(x, Q, y) = \left(\frac{L}{L_0} + 1 - x \right) \frac{Qy}{\kappa} + x - 1 \quad . \quad (7.13)$$

In combination with equation (5.7) and (5.8) the variable reduction procedure introduced in appendix C.2 for coupled half-sarcomeres, can be carried out to obtain the dimensionless equation of motion for the variables $Q_{l,r}$ and $y_{l,r}$. Note, the equations of motion are unchanged upon exchange of left and right, reflecting the swimmer's intrinsic space inversion symmetry. Equation (7.12) is identical to the equations of motion of a sarcomere for $R_l \rightarrow 0$. In general, the dynamics of the swimmer is similar to the dynamics of a sarcomere element. The hydrodynamic interaction terms do not alter qualitatively the dynamic behaviour. The implications of spontaneous symmetry breaking, however, are much more dramatic for the swimmer.

The swimmer is able to oscillate spontaneously. Figure 7.4a summarizes the swimmer's states as a function of the parameter² ζ . The same situation

²Other parameters can induce spontaneous oscillations or break space inversion symmetry

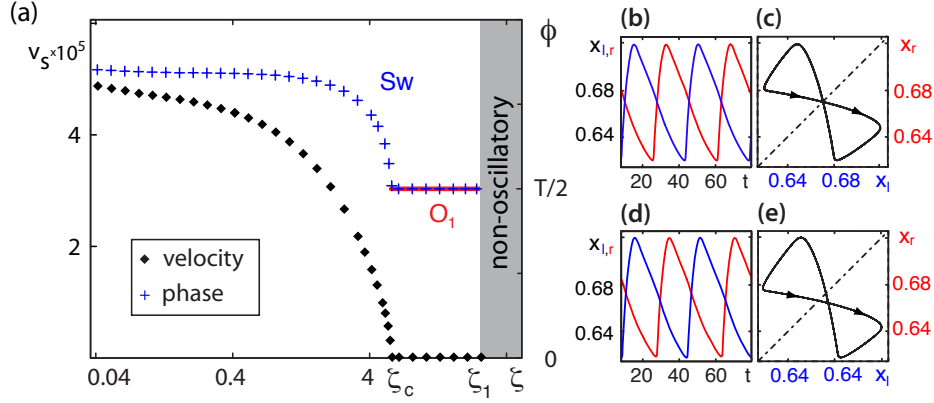


Figure 7.4 (a) Swimming velocity as function of ζ . The swimmer's linkers start to oscillate for $\zeta = \zeta_1$. However, the swimmer does not advance in average, compare with b) and c). For $\zeta = \zeta_c$ the linkers relative phase starts to deviate from half of the oscillatory period and the swimmer starts to propagate, compare with d) and e). (b,c) Linker length oscillations versus time and in the (x_l, x_r) -plane for $\zeta \gtrsim \zeta_c$. The state is non-swimming. (d,e) Linker length oscillatory state for $\zeta \lesssim \zeta_c$ allows for swimming. The swimmer speeds up to $v_s \approx 1 \mu\text{m}/\text{min}$. For parameter values see appendix A.2.

for a sarcomere was already discussed qualitatively in section 5.3.1 and more profound in section 6.2. The parameter ζ can be changed by varying ζ or the binding rate ω_b . Here, $R_l = 0.08$ that correspond to a reasonable large distance of adjacent spheres allowing for the usage of the approximations in section 7.3 for hydrodynamic interactions.

For $\zeta < \zeta_1$ the system is stationary. Decreasing ζ , the swimmer's linkers start to oscillate spontaneously with identical elongation but are phase shifted by half a period. The swimmer, however, does not stir away in average. The oscillatory state \mathbf{O}_1 is symmetric with respect to space inversion, thus non-swimming. The encircled surface in the (x_l, x_r) -plane vanishes, see figure 7.4b,c. Decreasing ζ further, for $\zeta < \zeta_c$ the swimmer spontaneously propagates. Neither the amplitude nor the oscillatory shape change at the critical value. The relative phase shift ϕ between the two linkers deviates from half a period. This deviation spontaneously breaks the motion's space inversion symmetry and the swimmer propagates, see figure 7.4d,e. Decreasing ζ further speeds up the swimmer due to larger displacements per cycle.

being in the oscillatory regime. Only ζ allows for both symmetry breaking.

7.5 Simple swimmer driven by molecular motors

There is another way that spontaneously breaks space inversion symmetry: An anti-gluing bifurcation of cycles. In section 6.2.3 the possibility of the gluing of cycles was examined. Figure 7.5 shows the gluing transition again. A glued cycle is symmetric with respect to space inversion. The swimmer is oscillating but not propagating. Anti-gluing of the cycles spontaneously breaks this symmetry and the swimmer starts to propagate. Even though the gluing induced swimming transition appears as a discontinuous jump in the swimmer's displacement \bar{x}_s , its velocity is continuously increasing. A gluing transition is an infinite period bifurcation, where T is infinite at the transition point. Correspondingly, the speed changes with parameter values qualitatively similar to figure 7.4a. In section 6.2.3 it was mentioned that gluing transitions are barely measurable in sarcomeres. In a sarcomere like swimmer a gluing transition discriminates between swimming and not swimming, which is measurable.

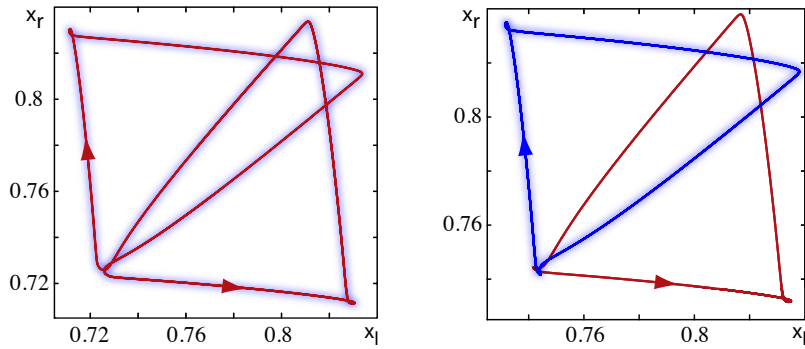


Figure 7.5 Recall of figure 6.11 in section 6.2.3. Phase space projections of the (x_1, x_r) -plane of (a) glued cycles (b) non-glued cycles. The motion with glued cycles in a) is symmetric with respect to space inversion, thus non-swimming. The two non-glued cycles in b) allow for swimming, where each state corresponds to a different swimming direction.

By the space inversion symmetry of the swimmer, for each motion, which spontaneously breaks this symmetry leading to propagation in one direction exists the space inverted motion propagating in the opposite direction. In a non deterministic realization, the swimmer would stochastically switch swimming direction, see figure 7.6. With spheres of radius $R = 0.1 \mu\text{m}$ the predicted swimming speed is of the order of $v_s \approx 1 \mu\text{m}/\text{min}$. Diffusion and noise is immanent to microscopic objects. A sphere's diffusion constant in water at room temperature reaches $D \approx 2 \mu\text{m}^2/\text{s}$. On distances comparable to the swimmers size $L_s \approx 3 \mu\text{m}$, diffusion dominates the swimmer's motion, since

$L_s v_s / D = 0.025$. Optimization could start in the increase of the swimmer's speed. This is possible by increasing the linkers' oscillating frequencies or amplitudes, see section 5.2.3. However, even a diffusion dominated swimmer would exhibit diffusion constants, which are larger than for a comparable passive system.

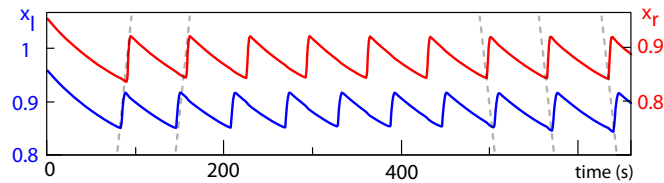


Figure 7.6 Stochastic switching of swimming states (without hydrodynamic interactions). At the beginning the swimmer has a different swimming direction than at the end of the switching process.

A swimmer that is composed of three spheres can self-organize into directed motion by the action of molecular motors. The motors collectively exert forces and spontaneously break the space-inversion symmetry. An experimental realization has overcome first obstacles. In a recent experiment the three-sphere swimmer was realized in a setup with three optical beads whose distance variation was imposed externally [200]. Measuring the flow field approved the predictions for the imposed motion. A next step could couple polar filaments to the beads within a bath of motor filaments. The optical beads can provide elastic restoring forces via feedback circuits. For myosin filaments, which cannot flow away upon detachment, such a setup can measure properties of the self-organized three-sphere swimmer. It is not out of reach. Far from it, such a setup can serve as an experimental setup to understand muscle oscillations on a (half-)sarcomere level, since the hydrodynamic interactions do not alter qualitatively the dynamics in theory. In a further step one could examine the interplay of several swimmers through their hydrodynamic interactions.

Chapter 8 Conclusions and perspectives

Life is a self-sustained complex system. Different life-forms exist in spite of the adversities of the environment. They adapt themselves to the environment without a master plan. In order to do so cells are very likely organized in a non-central way. There is evidence for self-organization of subsets of cell constituents whereas the subsets interact with each other. Especially in the cytoskeleton of cells self-organizing principles presumably play an important role. In order to multiply the evidence for such principles two directions of experiments are carried out. First, within biomimetic assays that contain purified proteins in solution, situations are adjusted *in vitro*. Second, whole functional structures are isolated from living cells. In this study I focused on a set of experiments that isolated the cytoskeleton of muscle cells. For chemical environments that correspond to a partial activation of muscles the isolated cytoskeleton shows spontaneous oscillations in length. The cytoskeleton cyclically shortens and lengthens with distinct time scales. Wave phenomena are observed in homogeneous cytoskeletal structures. Waves nucleate at random with in the cytoskeleton and travel some distance.

In order to describe these phenomena as self-organized processes I used distinct techniques: Muscles' cytoskeletal structures were described as active gels, as chains of microscopic contractile units and as a continuous medium. The description of myofibrils as an active non-polar one-component gel is based on symmetry considerations and conservation laws. The gel cannot show wave phenomena. Waves are based on a non-hydrodynamic mode that is not incorporated within the gel's description. A microscopic model of a half-sarcomere treated the active components of the muscle cell's cytoskeleton as force generators. They exert forces on filaments and act against elastic elements. The force generators themselves depend on the forces that act upon them. Collective action of the active components spontaneously breaks the symmetries of the system and allows for spontaneous oscillations in half-sarcomeric elements. Cyclic contractions and relaxations have distinct time scales. The elements' dynamics is remarkably similar to the dynamics that are found in the experiments. The system is excitable

and shows homoclinic behaviour. Chains of half-sarcomeric elements resemble the structure of muscle myofibrils. Spontaneous waves form within the chains. Waves are a dynamic mode of the chains, not synchronization effects. The wave patterns are similar to the patterns found in the experiments. A continuous description of myofibrils also allows for wave phenomena. The description incorporated basic mechanisms that allowed for spontaneous oscillations at the microscopic level. In the continuous description a non-hydrodynamic mode could be identified. This mode cannot be associated with a conservation law and is necessary for the wave phenomena in myofibrils. The coefficients of the phenomenological description can directly be related to the microscopic's model parameters.

There is evidence that the wave behaviour could play a role in cyclic muscle contractions under physiological conditions, especially in heart muscles. Physiological muscle oscillations likely result from a superposition of different mechanisms. Nature has a tendency for robust fail-safe designs, which means that the possible weight of the microscopic mechanism that was suggested here has to be probed. Precise experiments could reveal the physiological relevance of the dynamical effects that are possible within the microscopic description. In principle, the structural composition of half-sarcomeric elements can be adjusted *in vitro* and the theory's predictions could be probed experimentally.

Dynamically broken symmetries provide a way to drive microscopic swimmers. In this study I suggested a conceptual design of an autonomous self-organized swimmer. It is composed of three spheres in a row that are linked by force generating elements. The whole swimmer is symmetric with respect to space-inversion. The collective action of force generators and elastic elements within the linkers can spontaneously break the space inversion symmetry of the swimmer's shape changes. In this case the swimmer undergoes directed movement. It would be interesting to investigate the interactions of several autonomous swimmers. This would help to understand pattern formation mechanisms in colonies of swimming micro-organisms. The influence of surfaces could be probed as well as the details of the hydrodynamic interactions. This swimmer could be realized experimentally and provide a clearly defined experimental environment for the study of the swimming of micro-organisms.

Appendix

Appendix A Parameter

A.1 Parameter set I

In distinct kinds of experiments the parameter values naturally differ. Instead of concentrating to a particular experiment, I will give average parameter values, which are related to experiments on partially activated myofibrils.

Muscle geometries differ in distinct muscle types. Typical lengths for actin filaments are $\ell_p = 0.6 \mu\text{m}$ and for the bipolar myosin filaments $2 \cdot \ell_m = 1.5 \mu\text{m}$. Myosin filaments consists of about 300 myosin-II motors [15, 20, 201–204]. Hence, the average distance between motors is $d = 5 \text{ nm}$. Inactive sarcomeres have a typical resting length of $2 \cdot \ell_0 = 2.5 \mu\text{m}$. Sarcomere's elastic component in the absence of motors is hard to measure. It is strongly non-linear [36, 41] and depends on the initial stretch of the muscle in the experiments. However, I choose $k = 0.5 \text{ pN nm}^{-1}$. Experiments on the elasticity of single myosin-II motors suggests $K = 4 \text{ pN nm}^{-1}$ [20, 205]. For the motor I choose a stall force of $f_0 = 4 \text{ pN}$ and a load free velocity under partial activation of $v_0 = 0.4 \mu\text{m/s}$. Single motors are bound to actin filaments in average for 5 ms [206]. Following the line of partial activation I choose 30 ms, which defines the load free unbinding rate of single motors $1/\omega_{\text{off}}^0 = 30 \text{ ms}$. With an average duty ratio of 0.09, see [20], the binding rate is $1/\omega_{\text{on}} = 3 \text{ ms}$. The microscopic length scale a is unknown, but must be of molecular dimension. Here, I choose $a = 3 \text{ nm}$. Since experiments are realized at room temperature $k_B T = 4 \text{ pN nm}$. The effective friction coefficient cannot be measured either. Here I use $\zeta = 10 \text{ pN s } \mu\text{m}^{-1}$, which corresponds to a surrounding fluid with a viscosity of ten times the viscosity of water. Finally, M has to be determined. This parameter cannot be measured directly. A reasonable choice is $M = 100$, see [139].

A.2 Parameter set II

The parameter values here slightly differ from the experimentally motivated values given in section A.1. Unmentioned parameter are unaltered. Hence, $v_0 = 2 \mu\text{m/s}$, $d = 50 \text{ nm}$, $k = 0.01 \text{ pN nm}^{-1}$, $\zeta = 0.5 \text{ pN s } \mu\text{m}^{-1}$, $M = 10$, $\omega_{\text{off}}^0 = 1/50 \text{ ms}$ and $\omega_{\text{on}} = 1/5 \text{ ms}$. In addition the swimmer's sphere radius is $R = 0.1 \mu\text{m}$. Dimensionless parameter values are derived from these values.

Appendix B Half-sarcomere element

B.1 Fokker-Planck dynamics

Binding and unbinding dynamics of molecular motors is a stochastic process that is subject to BROWNIAN motion. Eventually, for a two state system this process can be modelled by means of coupled FOKKER-PLANCK equations. Denoting the probability densities for the bound and unbound states P_b and P_u and the currents by J_b and J_u , respectively, the equations reads

$$\partial_t P_b + \partial_y J_b = \omega_b P_u - \omega_u P_b \quad (\text{B.1})$$

$$\partial_t P_u + \partial_y J_u = -\omega_b P_u + \omega_u P_b \quad . \quad (\text{B.2})$$

The distributions are normalized so that $\int_{-\infty}^{+\infty} (P_b + P_u) dy = 1$ while the currents are given by

$$J_b = \dot{y} P_b - D_b \partial_y P_b \quad (\text{B.3})$$

$$J_u = -\nu y P_u - D_u \partial_y P_u \quad . \quad (\text{B.4})$$

The currents of motor bound on the polar filament emerge via active motion of bound motors mediated by \dot{y} as well as diffusion on the polar filament, which is characterized by its diffusion coefficient D_b . Unbound motors diffuse as well with diffusion coefficient D_u and are subject to fast relaxation in its spring potential, characterized by the relaxation rate ν . Fast relaxation means that unbound motors are assumed to be immediately after detachment in their equilibrium distribution, which is a GAUSSIAN distribution in FOKKER-PLANCK processes, see [126]. Therefor the ansatz is used

$$P_u(y,t) = (1 - Q(t)) \cdot A \exp \left\{ -\frac{Ky^2}{2k_B T} \right\} \quad (\text{B.5})$$

with normalization $A = \sqrt{K/(2\pi k_B T)}$. Neglecting fluctuations of the motors' spring extensions is taken into account through

$$P_b(y,t) = Q(t) \cdot \delta(y - y_i) \quad . \quad (\text{B.6})$$

Integration over y of equation (B.2) and using probability conservation as well as $\int_{-\infty}^{\infty} \partial_y J_u dy = 0$, the fraction of bound motors changes accordingly [126]

$$\dot{Q} = (1 - Q) \cdot \omega_b - Q \cdot \omega_u \quad . \quad (\text{B.7})$$

B.2 Reduced equations of motion

The equations of motion (5.7), (5.8) and (5.11) read,

$$\xi \dot{x} = x \cdot \left(\frac{QKy}{d} - k \right) - (\ell_p + \ell_m) \frac{QKy}{d} + k\ell_0 + f_{\text{ext}} \quad (\text{B.8})$$

$$\dot{Q} = (1 - Q) \cdot \omega_b - Q \cdot \omega_u \quad (\text{B.9})$$

$$\dot{x} = y [\omega_u(y) + Kv_0/f_0] - v_0 \equiv g(y) \quad (\text{B.10})$$

It is possible to unfold this problem into a set of equations of motion in the variables Q and y while x is given by an algebraic expression $x = x(Q, y)$ of the dynamical variables. By replacing \dot{x} in equation (B.8) through (B.10) one obtains

$$d\xi g(y) = x \cdot (QKy - dk) - (\ell_p + \ell_m) QKy + dk\ell_0 + df_{\text{ext}} \quad . \quad (\text{B.11})$$

The derivative of equation (B.11) with respect to time is multiplied with the term $(QKy - dk)$ and the \dot{x} term can be replaced by equation (B.10) while $x \cdot (QKy - dk)$ is replaced by equation (B.11). This procedure finally leads to the reduced equations of motion

$$\dot{Q} = (1 - Q) \cdot \omega_b - Q \cdot \omega_u \quad (\text{B.12})$$

$$\dot{y} = \frac{g(y)(QKy - dk)^2/d - \dot{Q}Ky [k(\ell_0 - \ell_p - \ell_m) - \xi g(y) + f_{\text{ext}}]}{\xi(QKy - dk)g'(y) + KQ [k(\ell_0 - \ell_p - \ell_m) - \xi g(y) + f_{\text{ext}}]} \quad , \quad (\text{B.13})$$

while x can be obtained from equation (B.11) in the case $QKy \neq dk$ so that

$$x(Q, y) = \ell_0 - \frac{(\ell_p + \ell_m - \ell_0) QKy - df_{\text{ext}} + d\xi g(y)}{dk - QKy} \quad . \quad (\text{B.14})$$

While in the case $QKy = dk$ the equations of motions are still well defined, it is not possible to obtain x in an algebraic way. In this situation the dynamics of the element becomes independent of the elements length, see equation (B.8), and therefore is obtained by directly integrating equation (B.8). For appropriate initial conditions $x(t_0)$, $x(t)$ reads

$$x(t) = x(t_0) + \xi^{-1} (f_{\text{ext}} - (\ell_p + \ell_m - \ell_0)k) \cdot t \quad . \quad (\text{B.15})$$

B.3 Oscillatory instability

The jacobian of the linearized system of equations of motion of the half-sarcomeric element, see equation (5.12) and (5.13) has two conjugate-complex eigenvalues for the stationary state. Oscillatory dynamics requires a non-vanishing imaginary part of the eigenvalues, which lead to

$$0 > \left[\zeta d (\omega_b + \omega_u(y)) + dk - QKy + \frac{k(\ell_p + \ell_m - \ell_0) - f_{\text{ext}}}{dk - QKy} QK g'(y)^{-1} d (\omega_b + \omega_u(y) - y \omega'_u(y)) \right]^2 - 4 [dk - QKy] [\omega_b + \omega_u(y)] \left[\zeta d + N(x) QK g'(y)^{-1} d \right]. \quad (\text{B.16})$$

with $N(x) = (\ell_p + \ell_m - x)/d$ while $x(Q, y)$ is given by equation (B.14) and (B.15). Condition (B.16) can only be satisfied iff $dk > QKy$. An oscillatory instability further requires a positive real part of the eigenvalues, which results in

$$0 \geq \zeta d (\omega_b + \omega_u(y)) + dk - QKy + \frac{k(\ell_p + \ell_m - \ell_0) - f_{\text{ext}}}{dk - QKy} QK g'(y)^{-1} d (\omega_b + \omega_u(y) - y \omega'_u(y)). \quad (\text{B.17})$$

This expression necessarily implies $\omega_b + \omega_u(y) < y \omega'_u(y)$. In all expressions Q and y are taken in the stationary state.

B.4 Critical frequency at the oscillatory instability

At the oscillatory instability the critical frequency f_c of oscillations is given by the imaginary part of the eigenvalues restricted to their vanishing real part, thus leading to

$$f_c = \frac{1}{2\pi} \sqrt{\frac{(\omega_b + \omega_u(y)) \cdot (dk - QKy)^2}{\zeta d (dk - QKy) + (k(\ell_p + \ell_m - \ell_0) - f_{\text{ext}}) QK g'(y)^{-1} d}}. \quad (\text{B.18})$$

B.5 Stochastic simulations

Binding and unbinding of molecular motors to a filament is an inherent noisy process due to brownian motion. Here I use the GILLESPIE algorithm [207] to simulate a half-sarcomere's dynamics as a stochastic process. At each time step

Appendix B Half-sarcomere element

dt each bound motor i can unbind with probability $\omega_u(y_i) \cdot dt$. Unbound motors in the overlap region of motor and polar filament can bind with probability $\omega_b \cdot dt$. In the bound state the motors' spring elongations are distributed as shown in figure 5.8. Unbinding of motors is accompanied with fast ($\tau \ll dt$) relaxation into their equilibrium distribution. Correspondingly, during binding a motor's spring elongation is drawn from a GAUSSIAN distribution with zero mean and standard deviation $\sqrt{k_B T/K}$. In the same time step each bound motors actuates along the polar filament by

$$\Delta y_i^t \equiv v \left(y_i^{t-dt} \right) \cdot dt \quad , \quad (\text{B.19})$$

see section 5.2.1. Time is indicated with the superscript. The updated motor induced tension in the half-sarcomeric element sums up to $K \cdot \sum_{i=1}^N \Delta y_i^t \equiv K \cdot Y$. Increased tension induces a change in length of the element, taking friction and the elastic restoring force according to the force balance equation (5.11) into account ($f_{\text{ext}} = 0$ case):

$$-\tilde{\zeta} \frac{x^t - x^{t-dt}}{dt} - k(x^t - \ell_0) - K \cdot Y = 0 \quad . \quad (\text{B.20})$$

The collective action of motors changes the elements length to x^t and alters at the same time the individual motor spring extension, resulting in $y_i^t = y_i^{t-dt} + \Delta y_i^t + x^t - x^{t-dt}$.

Appendix C Chain of elements

C.1 Linear stability for a simple homogeneous chain.

The equations of motion derived in section 5.1 read

$$\dot{x}_1 = -2f(x_1) + f(x_2) \quad (\text{C.1})$$

$$\dot{x}_j = -2f(x_j) + f(x_{j-1}) + f(x_{j+1}) \quad \text{with } j = 2, \dots, n-1 \quad (\text{C.2})$$

$$\dot{x}_n = -2f(x_n) + f(x_{n-1}) \quad , \quad (\text{C.3})$$

while the constant friction coefficient ζ has been set to 1. There exists only one stationary state, which is $x^* = x_i^* = f^{-1}(0)$ for $i = 1, \dots, n$. This corresponds to a chain whose elements are of equal length in stationary state. The linearization of the equations around the stationary state reads $\dot{x} = J \cdot x$ with $x = (x_1, \dots, x_n)$ and the jacobian J ,

$$J = \begin{pmatrix} -2f'(x^*) & f'(x^*) & 0 & 0 & \dots \\ f'(x^*) & -2f'(x^*) & f'(x^*) & 0 & \dots \\ & \ddots & \ddots & \ddots & \\ \dots & 0 & f'(x^*) & -2f'(x^*) & f'(x^*) \\ \dots & 0 & 0 & f'(x^*) & -2f'(x^*) \end{pmatrix} . \quad (\text{C.4})$$

The jacobian is symmetric $J_{ij} = J_{ji}$. Thus, eigenvalues are real and no oscillations can emerge in this simple myofibrillar model. Further, all eigenvectors are orthogonal towards each other. The eigenvalues λ_j and eigenvectors v_j of J are given by

$$\lambda_j = -2f'(x^*) + 2|f'(x^*)| \cos(z) \quad (\text{C.5})$$

$$v_j = (\sin(z), \sin(2z), \dots, \sin(nz))^T \quad \text{with } z = \frac{j\pi}{n+1} . \quad (\text{C.6})$$

Due to the nature of the eigenvalues there are growing modes (positive λ) beside decaying modes (negative λ) of perturbations of the stationary state.

Perturbations evolve according to $x(t) = \sum_{i=1}^n c_i \exp(\lambda_i t) v_i$ with $c_i = \text{const.}$, given through the initial conditions $x(t = t_0)$.

C.2 Reduced equations of motion for a chain of half-sarcomeric elements

The equations of motion are obtained similarly as for one half-sarcomere, see section B.2. The state of element i in a chain, which is composed of n elements, is described by

$$\dot{Q}_i = (1 - Q_i) \cdot \omega_b - Q_i \cdot \omega_u(y_i) \quad (\text{C.7})$$

$$\dot{y}_i = \left(A^{-1} \cdot (B \cdot c + C \cdot g / (d\zeta)) \right)_i, \quad (\text{C.8})$$

with $c = C^{-1} \cdot (d + g)$, while the elements lengths are obtained via

$$x_i = c_i + \ell_p + \ell_m, \quad (\text{C.9})$$

in the case that C is invertible or otherwise

$$x_i(t) = x_i(t_0) - (d\zeta)^{-1} d_i \cdot t. \quad (\text{C.10})$$

In the latter case $\dot{y}_i = 0$. The tensor components are given by

$$A_{1,1} = g'_1 - (1 + b_d) Q_1 K c_1 \quad (\text{C.11})$$

$$A_{1,2} = Q_2 K c_2 \quad (\text{C.12})$$

$$A_{i,i-1} = Q_{i-1} K c_{i-1} \quad (\text{C.13})$$

$$A_{i,i} = g'_i - 2Q_i K c_i \quad (\text{C.14})$$

$$A_{i,i+1} = Q_{i+1} K c_{i+1} \quad (\text{C.15})$$

$$A_{n,n-1} = Q_{n-1} K c_{n-1} \quad (\text{C.16})$$

$$A_{n,n} = g'_n - 2Q_n K c_n, \quad (\text{C.17})$$

for $i = 2 \dots n - 1$.

$$B_{1,1} = (1 + b_d) \dot{Q}_1 K y_1 \quad (\text{C.18})$$

$$B_{1,2} = -\dot{Q}_2 K y_2 \quad (\text{C.19})$$

$$B_{i,i-1} = -\dot{Q}_{i-1} K y_{i-1} \quad (\text{C.20})$$

$$B_{i,i} = 2\dot{Q}_i K y_i \quad (\text{C.21})$$

$$B_{i,i+1} = -\dot{Q}_{i+1} K y_{i+1} \quad (\text{C.22})$$

$$B_{n,n-1} = -\dot{Q}_{n-1} K y_{n-1} \quad (\text{C.23})$$

$$B_{n,n} = 2\dot{Q}_n K y_n, \quad (\text{C.24})$$

$$C_{1,1} = (1 + b_d)(Q_1Ky_1 - dk) \quad (C.25)$$

$$C_{1,2} = -(Q_2Ky_2 - dk) \quad (C.26)$$

$$C_{i,i-1} = -(Q_{i-1}Ky_{i-1} - dk) \quad (C.27)$$

$$C_{i,i} = 2(Q_iKy_i - dk) \quad (C.28)$$

$$C_{i,i+1} = -(Q_{i+1}Ky_{i+1} - dk) \quad (C.29)$$

$$C_{n,n-1} = -(Q_{n-1}Ky_{n-1} - dk) \quad (C.30)$$

$$C_{n,n} = 2(Q_nKy_n - dk) \quad (C.31)$$

All other components vanish.

$$d_1 = b_d dk(\ell_p + \ell_m - \ell_0) \quad (C.32)$$

$$d_i = 0 \quad (C.33)$$

$$d_n = dk(\ell_p + \ell_m - \ell_0) - (1 - b_d)df_{\text{ext}} \quad (C.34)$$

$$g_1 = d\tilde{\zeta}g(y_1) \quad (C.35)$$

$$g_i = d\tilde{\zeta}g(y_i) \quad (C.36)$$

$$g_n = d\tilde{\zeta}g(y_n) \quad (C.37)$$

Unfortunately, the reduced equations of motion (C.7) and (C.8) for chains with more than one element $n \geq 1$ are numerically unstable. For numerical solution I suggest to use the equations above with $c_i = x_i - l$ and to obtain the elements length via

$$d\tilde{\zeta}x_i = (\mathbf{C} \cdot \mathbf{c} - \mathbf{d})_i \quad (C.38)$$

Dimensionless reduced equations of motion

The dimensionless equations of motion of a chain of half-sarcomeric elements reads,

$$\dot{Q}_i = (1 - Q_i) - Q_i \cdot \omega(y_i) \quad (C.39)$$

$$\dot{y}_i = \gamma^{-1} \left(\mathbf{A}^{-1} \cdot (\mathbf{B} \cdot \mathbf{c} + \mathbf{C} \cdot \mathbf{g} / (\kappa\tilde{\zeta})) \right)_i \quad (C.40)$$

with $\mathbf{c} = \mathbf{C}^{-1} \cdot (\mathbf{d} + \mathbf{g})$.

$$x_i = L_0^{-1}(\mathbf{c}_i + L + L_0) \quad (C.41)$$

in the case that \mathbf{C} is invertible or otherwise

$$x_i(t) = x_i(t_0) - (\kappa\tilde{\zeta}L_0)^{-1} \mathbf{d}_i \cdot t \quad (C.42)$$

Appendix C Chain of elements

The tensor components are given by

$$A_{1,1} = g'_1/\gamma - (1 + b_d)Q_1c_1 \quad (C.43)$$

$$A_{1,2} = Q_2c_2 \quad (C.44)$$

$$A_{i,i-1} = Q_{i-1}c_{i-1} \quad (C.45)$$

$$A_{i,i} = g'_i/\gamma - 2Q_i c_i \quad (C.46)$$

$$A_{i,i+1} = Q_{i+1}c_{i+1} \quad (C.47)$$

$$A_{n,n-1} = Q_{n-1}c_{n-1} \quad (C.48)$$

$$A_{n,n} = g'_n/\gamma - 2Q_n c_n \quad , \quad (C.49)$$

for $i = 2 \dots n - 1$.

$$B_{1,1} = (1 + b_d)\dot{Q}_1 y_1 \quad (C.50)$$

$$B_{1,2} = -\dot{Q}_2 y_2 \quad (C.51)$$

$$B_{i,i-1} = -\dot{Q}_{i-1} y_{i-1} \quad (C.52)$$

$$B_{i,i} = 2\dot{Q}_i y_i \quad (C.53)$$

$$B_{i,i+1} = -\dot{Q}_{i+1} y_{i+1} \quad (C.54)$$

$$B_{n,n-1} = -\dot{Q}_{n-1} y_{n-1} \quad (C.55)$$

$$B_{n,n} = 2\dot{Q}_n y_n \quad , \quad (C.56)$$

$$C_{1,1} = (1 + b_d)(Q_1 y_1 - \kappa) \quad (C.57)$$

$$C_{1,2} = -(Q_2 y_2 - \kappa) \quad (C.58)$$

$$C_{i,i-1} = -(Q_{i-1} y_{i-1} - \kappa) \quad (C.59)$$

$$C_{i,i} = 2(Q_i y_i - \kappa) \quad (C.60)$$

$$C_{i,i+1} = -(Q_{i+1} y_{i+1} - \kappa) \quad (C.61)$$

$$C_{n,n-1} = -(Q_{n-1} y_{n-1} - \kappa) \quad (C.62)$$

$$C_{n,n} = 2(Q_n y_n - \kappa) \quad . \quad (C.63)$$

All other components vanish.

$$d_1 = b_d \kappa L \quad (C.64)$$

$$d_i = 0 \quad (C.65)$$

$$d_n = \kappa L - (1 - b_d)\kappa \tilde{f}_{\text{ext}} \quad , \quad (C.66)$$

$$g_1 = \kappa \zeta \tilde{g}(y_1) \quad (C.67)$$

$$g_i = \kappa \zeta \tilde{g}(y_i) \quad (C.68)$$

$$g_n = \kappa \zeta \tilde{g}(y_n) \quad , \quad (C.69)$$

with $\omega(y) = \omega_u(y)/\omega_b$ and $\tilde{g}(y) = y(\gamma\omega(y) + 1) - 1$.

C.3 Stationary states of a chain

According to the equations (C.7) and (C.8) the chain is in steady state for $0 = g$, if C is invertible, since B vanishes in steady state. In steady state the chain decouples and each element appears like one single half-sarcomere that is in the state with $g(y) = 0$. For the only non-invertible case $C = 0$, the chain's steady state decouples and resembles the case $QKy = dk$ for each element. Correspondingly, the chains element lengths are all equal.

C.4 Continuum limit

In a force free chain of infinite many half-sarcomere elements, element j is described by its equations of motion through equations (5.7), (5.8) and (5.21)–(5.23). In order to obtain a continuum limit all nonlinear terms are rejected. A linear expansion around the chain's stationary state (x_j^*, Q_j^*, y_j^*) with $x_j = x^* + x_j^1$, $Q_j = Q^* + Q_j^1$ and $y_j = y^* + y_j^1$ yields

$$\dot{x}_j^1 = y_j^1 \cdot [\omega'_u(y^*)y^* + \omega_u(y^*) + Kv_0/f_0] \quad (\text{C.70})$$

$$\dot{Q}_j^1 = -y_j^1 \cdot Q^* \omega'_u(y^*) - Q_j^1 \cdot (\omega_b + \omega_u(y^*)) \quad (\text{C.71})$$

$$\begin{aligned} \zeta \dot{x}_j = & N(x^*)Ky^* \cdot (2Q_j^1 - Q_{j-1}^1 - Q_{j+1}^1) \\ & + N(x^*)KQ^* \cdot (2y_j^1 - y_{j-1}^1 - y_{j+1}^1) \\ & + (k - Q^*Ky^*/d) \cdot (2x_j^1 - x_{j-1}^1 - x_{j+1}^1) \quad . \end{aligned} \quad (\text{C.72})$$

According to section 6.3, all elements within a chain have identical stationary states $(x_j^*, Q_j^*, y_j^*) = (x^*, Q^*, y^*)$, $\forall j$. Defining a muscle tissue density ρ through the distance of adjacent Z-discs, the elements' lengths are related to the density via

$$x_j = x^* \cdot (1 - \rho/\rho^*) \equiv x \quad . \quad (\text{C.73})$$

I approximate $2x_j - x_{j-1} - x_{j+1} = -(x^*)^2 \partial_z^2 x$ and replace x by the density ρ via equation (C.73). Here, z is the coordinate along the chain. Repeating the later limit for Q and y , but replacing y by equation (C.70) and relating any length variables x to the tissue's density by equation (C.73) reveal the continuous equations

$$\zeta \partial_t \rho = c_1 \partial_z^2 \rho + c_2 \partial_t \partial_z^2 \rho - c_3 \partial_z^2 Q \quad (\text{C.74})$$

$$\partial_t Q = c_4 \partial_t \rho - c_5 Q \quad , \quad (\text{C.75})$$

The coefficients are given by

$$c_1 = [Q^*Ky^*/d - k](x^*)^2 \quad (C.76)$$

$$c_2 = -(x^*)^2 \cdot N(x^*)Q^*K/[\omega'_u(y^*)y^* + \omega_u(y^*) + Kv_0/f_0] \quad (C.77)$$

$$c_3 = -\rho^*x^* \cdot N(x^*)Ky^* \quad (C.78)$$

$$c_4 = x^* \cdot Q^*\omega'_u(y^*)/\{\rho^*[\omega'_u(y^*)y^* + \omega_u(y^*) + Kv_0/f_0]\} \quad (C.79)$$

$$c_5 = \omega_b + \omega_u(y^*) \quad (C.80)$$

A final remark to the density definition in equation (C.73) shall be made. This relation can be derived using the approximation $z_j - z_{j-1} \simeq x^*\partial_z x$, where z_j denotes the position of the right end of element j , compare with figure 5.11. Since the gradients in x corresponds to the strain in the chain, a chain's density can be linked to the expression by considering a section of length Λ of the chain. By changing the density from its stationary value ρ^* to ρ the density changes like $\int_{\Lambda}(\rho^* - \rho)dz$. Likewise, alteration of the density changes by variations of the distances between the elements and yields $\rho^*[x(z_{j+\Lambda}) - x(z_j)] = \rho^* \int_{\Lambda} \partial_z x dz$. A comparison yields $\partial_z x = 1 - \rho/\rho^*$.

C.5 Stochastic simulations

Stochastic simulations of a chain of n half-sarcomere elements extend the scheme introduced in appendix B.5 only by one aspect. Alteration of the elements' lengths change according to the force balance equation for a chain, see equations (5.21)—(5.23). In the force free case of an unfortified chain ($f_{\text{ext}} = 0$) the modified length of element j is given by the equations

$$-\zeta \frac{x_j^t - x_j^{t-dt}}{dt} - 2f_j + f_{j-1} + f_{j+1} = 0 \quad , \quad (C.81)$$

with $f_j = k(x_j^t - \ell_0) + K \cdot Y_j$ and $f_0 = f_{n+1} = 0$. Fixation of the chains first element demands for a replacement of the term $2f_1$ by f_1 .

In the simulation in figure 5.15 a high number of motors is used. Simulations with the same number of motors like in the mean-field description are too noisy for the formation of wave trains. Noisy means that the distribution of oscillation periods is not very sharp. This indicates that cooperative mechanisms of motor binding and unbinding might be important in noisy systems.

Appendix D Swimmer displacement by distance variations

It is possible to express the forces f_i as functions of \dot{x}_l and \dot{x}_r using equation (7.7) and global force balance $\sum_j f_j = 0$. Replacing a single spheres' velocities \dot{x}_i in expression (7.10) with the help of equation (7.7) and the emerging forces by \dot{x}_l and \dot{x}_r yields the expression

$$\bar{x}_s = \int_0^T (A_1(x_l, x_r) \dot{x}_l + A_2(x_l, x_r) \dot{x}_r) dt = \oint_O C(x_l, x_r) dx_l \wedge dx_r \quad , \quad (\text{D.1})$$

where the STOKES relation is used for rewriting \bar{x}_s as a surface integral in the (x_l, x_r) -plane with

$$C(x_l, x_r) = \frac{\partial A_2}{\partial x_l} - \frac{\partial A_1}{\partial x_r} \quad . \quad (\text{D.2})$$

The functions A_i depend only on the mobility tensor \mathcal{M}_{ij} . Without hydrodynamic interactions ($\mathcal{M}_{ij} = 0, \forall i \neq j$) the field vanishes, so that $C = 0$.

Appendix D Swimmer displacement

Bibliography

- [1] G. WÖHRLE: Einleitung. *Biologie*. F. Steiner, Stuttgart (1999).
- [2] E. KARSENTI: Self-organization in cell biology: A brief history. *Nat Rev Mol Cell Biol* **9**(3), p. 255–262 (2008).
- [3] E. SCHRÖDINGER: *What is life? The physical aspect of the living cell*. Cambridge University Press, Cambridge; New York, USA (1945).
- [4] M. EIGEN: Wie entsteht Information? - Prinzipien der Selbstorganisation. *Berichte der Bunsen-Gesellschaft für Physikalische Chemie*, p. 1059–1074 (1976).
- [5] I. PRIGOGINE and I. STENGERS: *Dialog mit der Natur: Neue Wege naturwissenschaftlichen Denkens*. Piper, Munich (1981).
- [6] D. E. CLAPHAM: Calcium signaling. *Cell* **131**(6), p. 1047–1058 (2007).
- [7] H. BÉNARD: Les tourbillons cellulaires dans une nappe liquide. *Rev Gen Sci Pure Appl* **11**, p. 1261–1271 (1900).
- [8] L. RAYLEIGH: On convection currents in a horizontal layer of fluid when the higher temperature is on the other side. *Philos Mag* **32**, p. 529–543 (1916).
- [9] B. P. BELOUSOV: A periodic reaction and its mechanism. *Collection of short papers on radiation medicine for 1958*. Med. Publ., Moscow (1959).
- [10] A. M. ZHABOTINSKY: Periodical oxidation of malonic acid in solution (a study of the Belousov reaction kinetics). *Biofizika* **9**, p. 306–311 (1964).
- [11] G. NICOLIS and I. PRIGOGINE: *Self-organization in nonequilibrium systems: From dissipative structures to order through fluctuations*. Wiley, New York (1977).
- [12] A. M. TURING: The Chemical Basis of Morphogenesis. *Philos Trans R Soc Lond B* **237**(641), p. 37–72 (1952).

Bibliography

- [13] M. LOOSE, E. FISCHER-FRIEDRICH, J. RIES, K. KRUSE and P. SCHWILLE: Spatial regulators for bacterial cell division self-organize into surface waves in vitro. *Science* **320**(5877), p. 789–792 (2008).
- [14] G. MEACCI: *Physical aspects of min oscillations in Escherichia coli*. Ph.D. thesis, Technical University Dresden (2006).
- [15] B. ALBERTS, A. JOHNSON, J. LEWIS, M. RAFF, K. ROBERTS and P. WALTER: *Molecular biology of the cell*. Garland Science, New York (2008).
- [16] D. BRAY: *Cell movements: From molecules to motility*. Garland Pub., New York (2001).
- [17] S. ASAKURA and F. OOSAWA: Dephosphorylation of adenosine triphosphate in actin solutions at low concentrations of magnesium. *Arch Biochem Biophys* **87**, p. 273–280 (1960).
- [18] The myosin home page. URL <http://www.mrc-lmb.cam.ac.uk/myosin/myosin.html> (2009-06-20).
- [19] J. A. SPUDICH: The myosin swinging cross-bridge model. *Nat Rev Mol Cell Biol* **2**(5), p. 387–92 (2001).
- [20] J. HOWARD: *Mechanics of motor proteins and the cytoskeleton*. Sinauer Associates, Sunderland, Mass. (2001).
- [21] F. JÜLICHER, A. AJDARI and J. PROST: Modeling molecular motors. *Rev Mod Phys* **69**(4), p. 1269–1281 (1997).
- [22] P. REIMANN: Brownian motors: Noisy transport far from equilibrium. *Phys Rep* **361**(2-4), p. 57–265 (2002).
- [23] F. JÜLICHER and J. PROST: Spontaneous oscillations of collective molecular motors. *Phys Rev Lett* **78**(23), p. 4510–4513 (1997).
- [24] F. NÉDELÉC, T. SURREY and A. C. MAGGS: Dynamic concentration of motors in microtubule arrays. *Phys Rev Lett* **86**(14), p. 3192–5 (2001).
- [25] S. W. GRILL, K. KRUSE and F. JÜLICHER: Theory of mitotic spindle oscillations. *Phys Rev Lett* **94**(10), p. 108104 (2005).
- [26] K. KRUSE, J. F. JOANNY, F. JÜLICHER, J. PROST and K. SEKIMOTO: Generic theory of active polar gels: A paradigm for cytoskeletal dynamics. *Eur Phys J E* **16**, p. 078101 (2005).

- [27] F. J. NÉDELÉC, T. SURREY, A. C. MAGGS and S. LEIBLER: Self-organization of microtubules and motors. *Nature* **389**(6648), p. 305–8 (1997).
- [28] T. SVITKINA, A. VERKHOVSKY, K. MCQUADE and G. BORISY: Analysis of the actin-myosin II system in fish epidermal keratocytes: Mechanism of cell body translocation. *J Cell Biol* **139**(2), p. 397–415 (1997).
- [29] T. KILLICH, P. PLATH, X. WEI, H. BULTMANN, L. RENSING and M. VICKER: The locomotion, shape and pseudopodial dynamics of unstimulated dictyostelium cells are not random. *J Cell Sci* **106**, p. 1005–1013 (1993).
- [30] O. WEINER, W. MARGANSKI, L. WU, S. ALTSCHULER and M. KIRSCHNER: An actin-based wave generator organizes cell motility. *PLoS Biol* **5**(9), p. 2053–2063 (2007).
- [31] K. DOUBROVINSKI: *Physical Approaches to Cytoskeletal Self-Organization*. Ph.D. thesis, Saarland University (2008).
- [32] U. ALON: *An introduction to systems biology*. Chapman & Hall (2007).
- [33] D. M. NEEDHAM: *Machina carnis: The biochemistry of muscular contraction in its historical development*. Cambridge University Press, Cambridge; New York, USA (2009).
- [34] C. R. BAGSHAW: *Muscle contraction*. Kluwer, Dordrecht (1999).
- [35] J. AUBER: Myofibrillogenesis of striated muscle. 1. Insects. *J Microsc-Paris* **8**(2), p. 197 (1969).
- [36] L. TSKHOVREBOVA and J. TRINICK: Titin: Properties and family relationships. *Nat Rev Mol Cell Biol* **4**(9), p. 679–89 (2003).
- [37] A. F. HUXLEY: Muscle structure and theories of contraction. *Prog Biophys Biophys Chem* **7**, p. 255–318 (1957).
- [38] T. L. HILL: Theoretical formalism for the sliding filament model of contraction of striated muscle. *Prog Biophys Mol Biol* **28**, p. 267–340 (1974).
- [39] T. L. HILL: Theoretical formalism for the sliding filament model of contraction of striated muscle. Part II. *Prog Biophys Mol Biol* **29**(2), p. 105–59 (1975).
- [40] A. F. HUXLEY: Cross-bridge action: Present views, prospects, and unknowns. *J Biomech* **33**(10), p. 1189–95 (2000).

Bibliography

- [41] A. F. HUXLEY and R. M. SIMMONS: Proposed mechanism of force generation in striated muscle. *Nature* **233**(5321), p. 533–538 (1971).
- [42] S. EBASHI and M. ENDO: Calcium ion and muscle contraction. *Prog Biophys Mol Biol* **18**, p. 123–183 (1968).
- [43] A. WEBER and J. M. MURRAY: Molecular control mechanisms in muscle contraction. *Physiol Rev* **53**(3), p. 612–673 (1973 Jul).
- [44] L. TSKHOVREBOVA and J. TRINICK: Giant Proteins: Sensing tension with titin kinase. *Curr Biol* **18**(24), p. R1141–R1142 (2008).
- [45] J. A. FAULKNER: Terminology for contractions of muscles during shortening, while isometric, and during lengthening. *J Appl Physiol* **95**(2), p. 455–9 (2003).
- [46] A. F. HUXLEY and R. NIEDERGERKE: Structural changes in muscle during contraction - interference microscopy of living muscle fibres. *Nature* **173**(4412), p. 971–973 (1954).
- [47] H. E. HUXLEY and J. HANSON: Changes in the cross-striations of muscle during contraction and stretch and their structural interpretation. *Nature* **173**(4412), p. 973–976 (1954).
- [48] L. LORAND and C. MOOS: Auto-oscillations in extracted muscle fibre systems. *Nature* **177**(4522), p. 1239 (1956).
- [49] M. C. GOODALL: Auto-oscillations in extracted muscle fibre systems. *Nature* **177**(4522), p. 1238–1239 (1956).
- [50] C. F. ARMSTRON, A. F. HUXLEY and F. J. JULIAN: Oscillatory responses in frog skeletal muscle fibres. *J Physiol* **186**(1), p. P26 (1966).
- [51] A. FABIATO and F. FABIATO: Contractions induced by a calcium-triggered release of calcium from the sarcoplasmic reticulum of single skinned cardiac cells. *J Physiol* **249**(3), p. 469–495 (1975).
- [52] B. BRENNER: An indirect proof of stretch-induced Ca⁺⁺ release from the sarcoplasmic reticulum in glycerinated skeletal and heart muscle preparations. *Basic Res Cardiol* **74**(2), p. 177–202 (1979).
- [53] G. RIESER, R. SABBADINI, P. PAOLINI, M. FRY and G. INESI: Sarcomere motion in isolated cardiac cells. *Am J Physiol* **236**(1), p. C70–7 (1979).

- [54] D. L. LAPPE and E. G. LAKATTA: Intensity fluctuation spectroscopy monitors contractile activation in "resting" cardiac muscle. *Science* **207**(4437), p. 1369–1371 (1980 Mar 21).
- [55] A. A. KORT, M. C. CAPOGROSSI and E. G. LAKATTA: Frequency, amplitude, and propagation velocity of spontaneous Ca^{++} -dependent contractile waves in intact adult rat cardiac muscle and isolated myocytes. *Circ Res* **57**(6), p. 844–855 (1985).
- [56] R. W. TSIEN and R. Y. TSIEN: Calcium channels, stores, and oscillations. *Annu Rev Cell Biol* **6**, p. 715–760 (1990).
- [57] M. FALCKE: On the role of stochastic channel behavior in intracellular Ca^{2+} dynamics. *Biophys J* **84**(1), p. 42–56 (2003).
- [58] A. FABIATO: Calcium-induced release of calcium from the cardiac sarcoplasmic reticulum. *Am J Physiol* **245**(1), p. C1–14 (1983).
- [59] M. M. PRATT, M. S. MOOSEKER, D. P. KIEHART and R. E. STEPHENS: Cyclic contraction and relaxation of glycerinated myofibrils isolated from skeletal muscle. *Biol Bull* **151**, p. 426 (1976).
- [60] M. S. MOOSEKER, M. PRATT, D. P. KIEHART and R. E. STEPHENS: Cyclic contraction and relaxation of sarcomers in isolated myofibrils. *Biophys J* **17**, p. 173a (1977).
- [61] A. FABIATO and F. FABIATO: Myofilament-generated tension oscillations during partial calcium activation and activation dependence of the sarcomere length-tension relation of skinned cardiac cells. *J Gen Physiol* **72**(5), p. 667–99 (1978).
- [62] D. G. STEPHENSON and D. A. WILLIAMS: Calcium-activated force responses in fast- and slow-twitch skinned muscle fibres of the rat at different temperatures. *J Physiol* **317**, p. 281–302 (1981).
- [63] T. IWAZUMI and G. H. POLLACK: The effect of sarcomere non-uniformity on the sarcomere length-tension relationship of skinned fibers. *J Cell Physiol* **106**(3), p. 321–337 (1981).
- [64] D. G. STEPHENSON and D. A. WILLIAMS: Effects of sarcomere length on the force-pCa relation in fast- and slow-twitch skinned muscle fibres from the rat. *J Physiol* **333**, p. 637–653 (1982).

Bibliography

- [65] N. K. SWEITZER and R. L. MOSS: The effect of altered temperature on Ca²⁺(+)-sensitive force in permeabilized myocardium and skeletal muscle. Evidence for force dependence of thin filament activation. *J Gen Physiol* **96**(6), p. 1221–1245 (1990).
- [66] W. A. LINKE, M. L. BARTOO and G. H. POLLACK: Spontaneous sarcomeric oscillations at intermediate activation levels in single isolated cardiac myofibrils. *Circ Res* **73**(4), p. 724–734 (1993).
- [67] R. K. JOSEPHSON, J. G. MALAMUD and D. R. STOKES: Asynchronous muscle: A primer. *J Exp Biol* **203**(18), p. 2713–2722 (2000).
- [68] S. ISHIWATA, T. ANAZAWA, T. FUJITA, N. FUKUDA, H. SHIMIZU and K. YASUDA: Spontaneous tension oscillation (spoc) of muscle fibers and myofibrils minimum requirements for spoc. *Adv Exp Med Biol* **332**(0065-2598), p. 545–56 (1993).
- [69] S. ISHIWATA and K. YASUDA: Mechano-chemical coupling in spontaneous oscillatory contraction of muscle. *Phase Transitions* **45**(105) (1993).
- [70] N. FUKUDA, H. FUJITA, T. FUJITA and S. ISHIWATA: Spontaneous tension oscillation in skinned bovine cardiac muscle. *Pflugers Arch* **433**(1-2), p. 1–8 (1996).
- [71] N. FUKUDA, H. FUJITA, T. FUJITA and S. ISHIWATA: Regulatory roles of MgADP and calcium in tension development of skinned cardiac muscle. *J Muscle Res Cell Motil* **19**(8), p. 909–921 (1998).
- [72] D. SASAKI, H. FUJITA, N. FUKUDA, S. KURIHARA and S. ISHIWATA: Auto-oscillations of skinned myocardium correlating with heartbeat. *J Muscle Res Cell Motil* **26**(2-3), p. 93–101 (2005).
- [73] D. SASAKI, N. FUKUDA and S. ISHIWATA: Myocardial sarcomeres spontaneously oscillate with the period of heartbeat under physiological conditions. *Biochem Biophys Res Commun* **343**(4), p. 1146–52 (2006).
- [74] S. ISHIWATA, Y. SHIMAMOTO, M. SUZUKI and D. SASAKI: Regulation of muscle contraction by Ca²⁺ and ADP: Focusing on the auto-oscillation (SPOC). *Adv Exp Med Biol* **592**, p. 341–358 (2007).
- [75] Y. SHIMAMOTO, M. SUZUKI and S. ISHIWATA: Length-dependent activation and auto-oscillation in skeletal myofibrils at partial activation by Ca²⁺. *Biochem Biophys Res Commun* **366**(1), p. 233–238 (2008).

- [76] R. H. ABBOTT and P. E. CAGE: A possible mechanism of length activation in insect fibrillar flight muscle. *J Muscle Res Cell Motil* **5**(4), p. 387–397 (1984).
- [77] J. W. S. PRINGLE: The mechanical characteristics of insect fibrillar muscle. R. T. TREGAR (ed.) *Insect Flight Muscle*, p. 177. North-Holland, Amsterdam (1977).
- [78] J. W. PRINGLE: The croonian lecture, 1977. Stretch activation of muscle: Function and mechanism. *Proc R Soc Lond B* **201**(1143), p. 107–30 (1978).
- [79] C. POGGESI, C. TESI and R. STEHLE: Sarcomeric determinants of striated muscle relaxation kinetics. *Pflugers Arch* **449**(6), p. 505–517 (2005).
- [80] R. STEHLE, M. KRUGER and G. PFITZER: Force kinetics and individual sarcomere dynamics in cardiac myofibrils after rapid Ca(2+) changes. *Biophys J* **83**(4), p. 2152–2161 (2002).
- [81] C. TESI, N. PIRODDI, F. COLOMO and C. POGGESI: Relaxation kinetics following sudden Ca(2+) reduction in single myofibrils from skeletal muscle. *Biophys J* **83**(4), p. 2142–2151 (2002).
- [82] I. A. TELLEY, J. DENOTH, E. STUSSI, G. PFITZER and R. STEHLE: Half-sarcomere dynamics in myofibrils during activation and relaxation studied by tracking fluorescent markers. *Biophys J* **90**(2), p. 514–530 (2006).
- [83] N. ONODERA and Y. UMAZUME: Periodic contraction of skinned muscle fiber under high pH. *Biophys (Jpn)* **24**(S84) (1984).
- [84] N. ONODERA: *Jikeikai Med J* **37**, p. 447 (1990).
- [85] N. FUKUDA and S. ISHIWATA: Effects of pH on spontaneous tension oscillation in skinned bovine cardiac muscle. *Pflugers Arch* **438**(2), p. 125–132 (1999).
- [86] N. OKAMURA and S. ISHIWATA: Spontaneous oscillatory contraction of sarcomeres in skeletal myofibrils. *J Muscle Res Cell Motil* **9**(2), p. 111–9 (1988).
- [87] S. ISHIWATA, N. OKAMURA, H. SHIMIZU, T. ANAZAWA and K. YASUDA: Spontaneous oscillatory contraction (SPOC) of sarcomeres in skeletal muscle. *Adv Biophys* **27**, p. 227–235 (1991).

Bibliography

- [88] T. ANAZAWA, K. YASUDA and S. ISHIWATA: Spontaneous oscillation of tension and sarcomere length in skeletal myofibrils. Microscopic measurement and analysis. *Biophys J* **61**(5), p. 1099–108 (1992).
- [89] H. SHIMIZU, T. FUJITA and S. ISHIWATA: Regulation of tension development by MgADP and Pi without Ca²⁺. Role in spontaneous tension oscillation of skeletal muscle. *Biophys J* **61**(5), p. 1087–98 (1992).
- [90] K. YASUDA, Y. SHINDO and S. ISHIWATA: Synchronous behavior of spontaneous oscillations of sarcomeres in skeletal myofibrils under isotonic conditions. *Biophys J* **70**(4), p. 1823–9 (1996).
- [91] H. FUJITA and S. ISHIWATA: Spontaneous oscillatory contraction without regulatory proteins in actin filament-reconstituted fibers. *Biophys J* **75**(3), p. 1439–45 (1998).
- [92] Y. SHIMAMOTO, F. KONO, M. SUZUKI and S. ISHIWATA: Nonlinear force-length relationship in the ADP-induced contraction of skeletal myofibrils. *Biophys J* **93**(12), p. 4330–4341 (2007).
- [93] V. A. GOLOVINA, L. V. ROZENSHTRAUKH, B. S. SOLOV'EV, A. I. UNDOVINAS and G. G. CHERNAIA: Wave-like spontaneous contractions of isolated cardiomyocytes. *Biofizika* **31**(2), p. 283–289 (1986).
- [94] A. LUNDBLAD, H. GONZALEZ-SERRATOS, G. INESI, J. SWANSON and P. PAOLINI: Patterns of sarcomere activation, temperature dependence, and effect of ryanodine in chemically skinned cardiac fibers. *J Gen Physiol* **87**(6), p. 885–905 (1986).
- [95] B. J. MULDER, P. P. DE TOMBE and H. E. TER KEURS: Spontaneous and propagated contractions in rat cardiac trabeculae. *J Gen Physiol* **93**(5), p. 943–961 (1989).
- [96] M. D. STERN: Theory of excitation-contraction coupling in cardiac muscle. *Biophys J* **63**(2), p. 497–517 (1992).
- [97] K. KRUSE and F. JÜLICHER: Oscillations in cell biology. *Curr Opin Cell Biol* **17**(1), p. 20–26 (2005).
- [98] J. D. MURRAY: *Mathematical biology. I, An introduction*. Springer, New York (2002).
- [99] C. J. BROKAW: Molecular mechanism for oscillation in flagella and muscle. *Proc Natl Acad Sci USA* **72**(8), p. 3102–6 (1975).

-
- [100] S. CAMALET, F. JÜLICHER and J. PROST: Self-organized beating and swimming of internally driven filaments. *Phys Rev Lett* **82**, p. 1590 (1999).
- [101] S. CAMALET and F. JÜLICHER: Generic aspects of axonemal beating. *New J Phys* **2**, p. 24.1–24.23 (2000).
- [102] M. MURASE, H. TANAKA, K. NISHIYAMA and H. SHIMIZU: A three-state model for oscillation in muscle: Sinusoidal analysis. *J Muscle Res Cell Motil* **7**(1), p. 2–10 (1986).
- [103] W. S. GUO, L. F. LUO and Q. Z. LI: A chemical kinetic theory on muscle contraction and spontaneous oscillation. *Chem Phys Lett* **363**(5-6), p. 471–478 (2002).
- [104] A. VILFAN and T. DUKE: Synchronization of active mechanical oscillators by an inertial load. *Phys Rev Lett* **91**(11), p. 114101 (2003).
- [105] D. A. SMITH and D. G. STEPHENSON: Theory and observation of spontaneous oscillatory contractions in skeletal myofibrils. *J Muscle Res Cell Motil* **15**, p. 369 (1994).
- [106] K. KRUSE, J. F. JOANNY, F. JÜLICHER, J. PROST and K. SEKIMOTO: Asters, vortices, and rotating spirals in active gels of polar filaments. *Phys Rev Lett* **92**(7) (2004).
- [107] J. F. JOANNY and J. PROST: Active gels as a description of the actin-myosin cytoskeleton. *HFSP Journal* **3**(2), p. 94–104 (2009).
- [108] J. WILHELM and E. FREY: Elasticity of stiff polymer networks. *Phys Rev Lett* **91**(10) (2003).
- [109] D. HEAD, A. LEVINE and F. MACKINTOSH: Deformation of cross-linked semiflexible polymer networks. *Phys Rev Lett* **91**(10) (2003).
- [110] P. C. MARTIN, O. PARODI and P. S. PERSHAN: Unified hydrodynamic theory for crystals, liquid-crystals, and normal fluids. *Phys Rev A* **6**(6), p. 2401 (1972).
- [111] P. DE GENNES: *Scaling concepts in polymer physics*. Cornell University Press, Ithaca, N.Y. (1979).
- [112] J. F. JOANNY, F. JÜLICHER, K. KRUSE and J. PROST: Hydrodynamic theory for multi-component active polar gels. *New J Phys* **9**(11), p. 422 (2007).

Bibliography

- [113] A. BASU, J. F. JOANNY, F. JÜLICHER and J. PROST: Thermal and non-thermal fluctuations in active polar gels. *Eur Phys J E* **27**(2), p. 149–160 (2008).
- [114] S. R. DE GROOT and P. MAZUR: *Non-equilibrium thermodynamics*. Dover, New York (1984).
- [115] P. M. CHAIKIN and T. C. LUBENSKY: *Principles of condensed matter physics*. Cambridge University Press, Cambridge; New York, USA (1995).
- [116] K. TAWADA and K. SEKIMOTO: Protein friction exerted by motor enzymes through a weak-binding interaction. *J Theor Biol* **150**(2), p. 193–200 (1991).
- [117] K. TAWADA and K. SEKIMOTO: A physical model of ATP-induced actin-myosin movement in vitro. *Biophys J* **59**(2), p. 343–56 (1991).
- [118] B. N. J. PERSSON: *Sliding friction: Physical principles and applications*. Springer, Berlin; New York (1998).
- [119] C. W. GARDINER: *Handbook of stochastic methods for physics, chemistry and the natural sciences*. London, Berlin (1997).
- [120] T. NISHIZAKA, R. SEO, H. TADAKUMA, K. J. KINOSITA and S. ISHIWATA: Characterization of single actomyosin rigor bonds: Load dependence of lifetime and mechanical properties. *Biophys J* **79**(2), p. 962–74 (2000).
- [121] J. T. FINER, R. M. SIMMONS and J. A. SPUDICH: Single myosin molecule mechanics: Piconewton forces and nanometer steps. *Nature* **368**(6467), p. 113–9 (1994).
- [122] T. A. DUKE: Molecular model of muscle contraction. *Proc Natl Acad Sci USA* **96**(6), p. 2770–5 (1999).
- [123] K. SVOBODA and S. M. BLOCK: Force and velocity measured for single kinesin molecules. *Cell* **77**(5), p. 773–84 (1994).
- [124] A. J. v. D. SCHAFT and J. M. SCHUMACHER: *An introduction to hybrid dynamical systems*. Springer, London; New York (2000).
- [125] S. KLUMPP and R. LIPOWSKY: Cooperative cargo transport by several molecular motors. *Proc Natl Acad Sci USA* **102**(48), p. 17284–9 (2005).
- [126] S. GÜNTHER: *Oszillationen, Synchronisation und Fortbewegung von Sarkomeren*. Master's thesis, Technical University Dresden (2005).

- [127] S. H. STROGATZ: *Nonlinear dynamics and Chaos: With applications to physics, biology, chemistry, and engineering*. Addison-Wesley Pub., Reading, Mass. (1994).
- [128] S. WIGGINS: *Introduction to applied nonlinear dynamical systems and chaos*. Springer (2003).
- [129] Y. A. KUZNETSOV: *Elements of applied bifurcation theory*. Springer (1998).
- [130] E. F. MISHCHENKO and N. K. ROZOV: *Differential equations with small parameters and relaxation oscillations*. Plenum Press, New York (1980).
- [131] J. GRASMAN: *Asymptotic methods for relaxation oscillations and applications*. Springer-Verlag, New York (1987).
- [132] J. D. MURRAY: *Mathematical biology. II Spatial models and biomedical applications*. Springer, New York (2003).
- [133] T. A. McMAHON: *Muscles, reflexes, and locomotion*. Princeton University Press, Princeton, N. J. (1984).
- [134] N. A. SINITSYN: The stochastic pump effect and geometric phases in dissipative and stochastic systems. *J Phys A-Math Theor* **42**(19), p. 193001 (2009).
- [135] S. GÜNTHER, L. M. BEIDOKHTI and K. KRUSE: Cyclic muscle activity without pacemaker (unpublished) (2009).
- [136] M. LINARI, M. REEDY, M. REEDY, V. LOMBARDI and G. PIAZZESI: Ca-activation and stretch-activation in insect flight muscle. *Biophys J* **87**(2), p. 1101–1111 (2004).
- [137] J. C. RUEGG, G. J. STEIGER and M. SCHADLER: Mechanical activation of the contractile system in skeletal muscle. *Pflugers Arch* **319**(2), p. 139–145 (1970).
- [138] M. ENDO: Stretch-induced increase in activation of skinned muscle fibers by calcium. *Nature-New Biol* **237**(76), p. 211 (1972).
- [139] S. GÜNTHER and K. KRUSE: Spontaneous waves in muscle fibres. *New J Phys* **9**, p. 417 (2007).
- [140] N. FUKUDA and S. ISHIWATA: Standard SPOC. URL <http://www.ishiwata.phys.waseda.ac.jp/movies/SPOC.htm> (2009-05-30).

Bibliography

- [141] B. ERMENTROUT: *Simulating, analyzing, and animating dynamical systems*. Siam (2002).
- [142] E. DOEDEL: AUTO - Software for continuation and bifurcation problems in ordinary differential equations. URL <http://indy.cs.concordia.ca/auto/> (2009-06-28).
- [143] S. WOLFRAM: Mathematica. URL <http://www.wolfram.com> (2009-06-28).
- [144] E. BENOIT, J. L. CALLOT, F. DIENER and M. DIENER: Chasse au canard. *Collect Math* **32**, p. 37 (1981).
- [145] W. ECKHAUS: Relaxation oscillations including a standard chase on French ducks. *Lect Notes Math* **985**, p. 449–494 (1983).
- [146] M. KRUPA and P. SZMOLYAN: Relaxation oscillation and canard explosion. *J Differ Equations* **174**(2), p. 312–368 (2001).
- [147] R. FITZHUGH: Thresholds and plateaus in the Hodgkin-Huxley nerve equations. *J Gen Physiol* **43**(5), p. 867–896 (1960).
- [148] R. FITZHUGH: Impulses and physiological states in theoretical models of nerve membrane. *Biophys J* **1**(6), p. 445 (1961).
- [149] J. NAGUMO, S. ARIMOTO and S. YOSHIZAWA: Active pulse transmission line simulating nerve axon. *P IRE* **50**(10), p. 2061–& (1962).
- [150] A. L. HODGKIN and A. F. HUXLEY: A quantitative description of membrane current and its application to conduction and excitation in nerve. *J Physiol* **117**(4), p. 500–544 (1952).
- [151] J. GUCKENHEIMER, K. HOFFMAN and W. WECKESSER: Numerical computation of canards. *Int J Bifurcat Chaos* **10**(12), p. 2669 – 2687 (2000).
- [152] P. SZMOLYAN and M. WECHSELBERGER: Canards in \mathbb{R}^3 . *J Differ Equations* **177**(2), p. 419–453 (2001).
- [153] M. WECHSELBERGER: Existence and bifurcation of canards in \mathbb{R}^3 in the case of a folded node. *SIAM J Appl Dyn Syst* **4**(1), p. 101–139 (2005).
- [154] J. RUBIN and M. WECHSELBERGER: Giant squid-hidden canard: The 3D geometry of the Hodgkin-Huxley model. *Biological Cybernetics* **97**(1), p. 5–32 (2007).

-
- [155] M. BROENS and K. BAR-ELI: Canard explosion and excitation in a model of the Belousov-Zhabotinskii reaction. *J Phys Chem* (1991).
- [156] Scholarpedia. URL <http://www.scholarpedia.org> (2009-15-08).
- [157] T. RISLER, J. PROST and F. JÜLICHER: Universal critical behavior of noisy coupled oscillators. *Phys Rev Lett* **93**(17) (2004).
- [158] S. GÜNTHER and K. KRUSE: A simple self-organized swimmer driven by molecular motors. *Europhys Lett* **84**(6), p. 68002 (2008).
- [159] A. PIKOVSKY, M. ROSENBLUM and J. KURTHS: *Synchronization: A universal concept in nonlinear sciences*. Cambridge University Press, Cambridge; New York, USA (2001).
- [160] A. PIKOVSKY: Private communication. (2006).
- [161] J. P. VAN DER WEELE and E. J. BANNING: Mode interaction in horses, tea, and other nonlinear oscillators: The universal role of symmetry. *Am J Phys* **69**, p. 953 (2001).
- [162] J. D. CRAWFORD, E. KNOBLOCH and H. RIECKE: Mode interactions and symmetry. S. PNEVMATIKOS, T. BOUNTIS and S. PNEUVMATIKOS (eds.) *Singular Behavior and Nonlinear Dynamics*, vol. 1, p. 277–297. World Scientific, Samos, Greece (1988).
- [163] J. D. CRAWFORD, E. KNOBLOCH and H. RIECKE: Period-doubling mode interactions with circular symmetry. *Physica D* **44**, p. 340 (1990).
- [164] C. VAN VREESWIJK, L. F. ABBOTT and G. B. ERMENTROUT: When inhibition not excitation synchronizes neural firing. *J Comput Neurosci* **1**(4), p. 313–21 (1994).
- [165] L. F. ABBOTT and C. VAN VREESWIJK: Asynchronous states in networks of pulse-coupled oscillators. *Phys Rev E* **48**(2), p. 1483–1490 (1993).
- [166] M. TIMME: Private communication. (2008).
- [167] P. COULLET, J. M. GAMBAUDO and C. TRESSER: A new bifurcation of codimension 2 - the gluing of cycles. *C R Acad Sci I* **299**(7), p. 253–256 (1984).
- [168] P. GLENDINNING, J. ABSHAGEN and T. MULLIN: Imperfect homoclinic bifurcations. *Phys Rev E* **64**(3) (2001).

Bibliography

- [169] J. M. GAMBAUDO, P. GLENDINNING and C. TRESSER: The gluing bifurcation: I. Symbolic dynamics of the closed curves. *Nonlinearity* **1**(1), p. 203–214 (1988).
- [170] E. NICOLA: Private communication. (2006).
- [171] H. G. SCHUSTER and W. JUST: *Deterministic chaos*. Wiley (2005).
- [172] A. MILIK, P. SZMOLYAN, H. LOFFELMANN and E. GROLLER: Geometry of mixed-mode oscillations in the 3-D autocatalator. *Int J Bifurcat Chaos* **8**(3), p. 505–519 (1998).
- [173] M. BRONS, M. KRUPA and M. WECHSELBERGER: Mixed mode oscillations due to the generalized canard phenomenon. *Fields Inst Commun* **49** (2006).
- [174] G. I. TAYLOR: Analysis of the swimming of microscopic organisms. *Proc R Soc Lond A* **209**, p. 447 (1951).
- [175] E. M. PURCELL: Life at low Reynolds number. *Am J Phys* **45**(1), p. 3–11 (1977).
- [176] A. SHAPER and F. WILCZEK: Self-Propulsion at low Reynolds number. *Phys Rev Lett* **58**(20), p. 2051–2054 (1987).
- [177] J. E. AVRON, O. KENNETH and D. H. OAKNIN: Pushmepullyou: An efficient micro-swimmer. *New J Phys* **7**, p. 234 (2005).
- [178] A. NAJAFI and R. GOLESTANIAN: Simple swimmer at low Reynolds number: Three linked spheres. *Phys Rev E* **69**(6 Pt 1), p. 062901 (2004).
- [179] R. GOLESTANIAN and A. AJDARI: Analytic results for the three-sphere swimmer at low Reynolds number. *Phys Rev E* **77**, p. 036308 (2008).
- [180] R. GOLESTANIAN and A. AJDARI: Mechanical response of a small swimmer driven by conformational transitions. *Phys Rev Lett* **100**(3), p. 038101 (2008).
- [181] R. GOLESTANIAN: Three-sphere low-Reynolds-number swimmer with a cargo container. *Eur Phys J E* **25**(1), p. 1–4 (2008).
- [182] M. IIMA and A. S. MIKHAILOV: Propulsion hydrodynamics of a butterfly micro-swimmer. *Europhys Lett* **85**(4) (2009).
- [183] A. M. LESHANSKY and O. KENNETH: Surface tank treading: Propulsion of Purcell’s toroidal swimmer. *Phys Fluids* **20** (2008).

- [184] J. YANG, C. W. WOLGEMUTH and G. HUBER: Kinematics of the swimming of spiroplasma. *Phys Rev Lett* **102**(21), p. 218102–4 (2009).
- [185] B. QIAN, T. R. POWERS and K. S. BREUER: Shape transition and propulsive force of an elastic rod rotating in a viscous fluid. *Phys Rev Lett* **100**(7), p. 078101 (2008).
- [186] P. GARSTECKI and M. CIEPLAK: Swimming at low Reynolds numbers - motility of micro-organisms. *J Phys-Condens Mat* **21**(20) (2009).
- [187] R. GOLESTANIAN and A. AJDARI: Stochastic low Reynolds number swimmers. *J Phys-Condens Mat* **21**(20) (2009).
- [188] E. LAUGA and D. BARTOLO: No many-scallop theorem: Collective locomotion of reciprocal swimmers. *Phys Rev E* **78**(3), p. 030901 (2008).
- [189] G. P. ALEXANDER and J. M. YEOMANS: Dumb-bell swimmers. *Europhys Lett* **83**(3), p. 34006 (2008).
- [190] D. GONZALEZ-RODRIGUEZ and E. LAUGA: Reciprocal locomotion of dense swimmers in Stokes flow. *J Phys-Condens Mat* **21**(20) (2009).
- [191] E. M. PURCELL: The efficiency of propulsion by a rotating flagellum. *Proc Natl Acad Sci USA* **94**(21), p. 11307–11 (1997).
- [192] R. DREYFUS, J. BAUDRY, M. L. ROPER, M. FERMIGIER, H. A. STONE and J. BIBETTE: Microscopic artificial swimmers. *Nature* **437**(7060), p. 862–5 (2005).
- [193] E. GAUGER and H. STARK: Numerical study of a microscopic artificial swimmer. *Phys Rev E* **74**(2), p. 021907 (2006).
- [194] F. Y. OGRIN, P. G. PETROV and C. P. WINLOVE: Ferromagnetic Microswimmers. *Phys Rev Lett* **100**(21), p. 218102 (2008).
- [195] J. VEYSEY and I. N. GOLDENFELD: Simple viscous flows: From boundary layers to the renormalization group. *Rev Mod Phys* **79**(3), p. 883 (2007).
- [196] L. D. LANDAU, E. M. LIFSCHITZ and W. WELLER: *Lehrbuch der theoretischen Physik 6 - Hydrodynamik*. Deutsch (Harri), Berlin (1991).
- [197] J. HAPPEL and H. BRENNER: *Low Reynolds number hydrodynamics with special applications to particulate media*. Martinus Nijhoff Publishers, The Hague, The Netherlands (1973).

Bibliography

- [198] G. K. BATCHELOR: *An introduction to fluid dynamics*. Cambridge University Press, Cambridge; New York, USA (2002).
- [199] G. K. BATCHELOR: Brownian diffusion of particles with hydrodynamic interaction. *J Fluid Mech* **74**(01), p. 1 (1976).
- [200] M. LEONI, J. KOTAR, B. BASSETTI, P. CICUTA and M. LAGOMARSINO: A basic swimmer at low Reynolds number. *Soft Matter* **5**(2), p. 472–476 (2008).
- [201] R. CRAIG and G. OFFER: Axial arrangement of crossbridges in thick filaments of vertebrate skeletal muscle. *J Mol Biol* **102**(2), p. 325–32 (1976).
- [202] M. SJOSTROM and J. M. SQUIRE: Fine structure of the a-band in cryosections. The structure of the a-band of human skeletal muscle fibres from ultra-thin cryo-sections negatively stained. *J Mol Biol* **109**(1), p. 49–68 (1977).
- [203] Y. AU: The muscle ultrastructure: A structural perspective of the sarcomere. *Cell Mol Life Sci* **61**(24), p. 3016–33 (2004).
- [204] J. S. DAVIS: Assembly processes in vertebrate skeletal thick filament formation. *Annu Rev Biophys Biophys Chem* **17**(0883-9182), p. 217–39 (1988).
- [205] I. SCHWAIGER, C. SATTLER, D. R. HOSTETTER and M. RIEF: The myosin coiled-coil is a truly elastic protein structure. *Nat Mater* **1**(4), p. 232–5 (2002).
- [206] C. RUEGG, C. VEIGEL, J. E. MOLLOY, S. SCHMITZ, J. C. SPARROW and R. H. A. FINK: Molecular motors: Force and movement generated by single myosin ii molecules. *News Physiol Sci* **17**(0886-1714), p. 213–8 (2002).
- [207] D. T. GILLESPIE: A General Method for Numerically Simulating the Stochastic Time Evolution of Coupled Chemical Reactions. *J Comput Phys* **22**(4), p. 403–434 (1976).

Eidesstattliche Versicherung

Hiermit versichere ich an Eides statt, dass ich die vorliegende Arbeit selbstständig und ohne Benutzung anderer als der angegebenen Hilfsmittel angefertigt habe. Die aus anderen Quellen oder indirekt übernommenen Daten und Konzepte sind unter Angabe der Quelle gekennzeichnet. Die Arbeit wurde bisher weder im In- noch im Ausland in gleicher oder ähnlicher Form in einem Verfahren zur Erlangung eines akademischen Grades vorgelegt.

Saarbrücken, 21. Juli 2009

STEFAN GÜNTHER